

The ribosome-SecYEG complex in the membrane environment



Jens Frauenfeld
aus Mannheim

München, 2010

Erklärung

Diese Dissertation wurde im Sinne von § 13 Abs. 3 bzw. 4 der Promotionsordnung vom 29. Januar 1998 von Herrn Prof. Dr. Roland Beckmann betreut.

Ehrenwörtliche Versicherung

Diese Dissertation wurde selbstständig, ohne unerlaubte Hilfe erarbeitet.

München, am 20.04.2010

Jens Frauenfeld

Dissertation eingereicht am: 20.04.2010

1. Gutachter: Herr Prof. Dr. Roland Beckmann

2. Gutachter: Herr Prof. Dr. Karl-Peter Hopfner

Mündliche Prüfung am: 27.05.2010

Table of Contents

1. Introduction	7
1.1 Co-translational targeting via SRP and FtsY	9
1.2 FtsQ as a model for membrane-protein type II insertion	11
1.3 Ribosome binding and EM-data	12
1.4 Architecture of the PCC	14
1.5 Membrane proteins in the lipid environment	16
1.6 Nanodiscs	19
1.7 Aim of this study	21
2 Materials and Methods	23
2.1 Media and supplements	23
2.2 PCR	23
2.3 Agarose gel electrophoresis	23
2.4 Transformation of <i>E. coli</i> and Isolation of Plasmid DNA	23
2.5 Protein separation by SDS-PAGE	24
2.6 TCA precipitation	24
2.7 SYPRO orange staining	24
2.8 Western Blotting	25
2.9 Expression and Purification of Apo-A1	25
2.10 Preparation of Lipid/Cholate stock solution	26
2.11 Expression of SecYEG	26
2.12 Preparation of SecYEG-IMVs	27
2.13 Purification of SecYEG	27
2.14 Generation of Nanodisc-SecYEG	28
2.15 Binding assays of FtsY to Nanodiscs (Nd-E, Nd-SecYEG)	28
2.16 Purification of <i>E. coli</i> 70S RNCs	29
2.17 Reconstitution of <i>E. coli</i> 70S RNC-Nd-SecYEG complexes	30
2.18 Reconstitution of targeting complexes	30
2.19 Negative stain electron microscopy	31
2.20 Cryo-EM	31
2.21 Image processing	31
2.22 Alignment and initial 3D-reconstruction	32
2.23 Refinement and sorting	33
2.24 Modeling and MDFF	33

2.25 Fitting of SecYE and nascent FtsQ	34
2.26 Model and fitting of the Nanodisc	34
2.27 Figures	35
2.28 Simulations	35
3. Results	37
3.1 Purification of Apo-A1	37
3.2 Purification of SecYEG	38
3.3 Nanodisc assembly	40
3.4 Incorporation of SecYEG into Nanodiscs	42
3.5 Binding studies of Nanodiscs	44
3.5.1 Binding of FtsY to Nd-E	44
3.5.2 Binding of FtsY to Nd-SecYEG	45
3.6 Purification of ribosome-nascent-chain complexes	46
3.7 Binding assays of RNCs	48
3.8 Targeting complex formation	49
3.9 Reconstitution of a RNC-Nd-SecYEG complex	51
3.10 Cryo-EM reconstruction of the 70S-RNC-Nd-SecYEG complex	53
3.11 Structure of the Nanodisc	55
3.12 Canonical binding mode	57
3.13 Model for the <i>E. coli</i> SecYE complex	58
3.14 Ribosome-SecYE contacts	64
3.15 Ribosome-lipid interactions	64
3.16 Ribosome-Membrane-SecYE interactions	66
3.17 Path of the nascent chain within the ribosomal exit tunnel	67
4 Discussion	79
4.1 Generating Nanodiscs	79
4.2 Incorporation of SecYEG into Nanodiscs	81
4.3 Membrane and SecYEG interaction of FtsY	81
4.4 SA-dependent interaction of 70S ribosomes with Nd-SecYEG	82
4.4 SecYEG-dependent interaction of RNCs with Nanodiscs	83
4.5 SecYEG triggers GTP hydrolysis in FtsY	83
4.6 Visualization of transmembrane helices within the lipid bilayer	86
4.7 Structure of nascent discoidal HDL	87

4.7 The ribosome-membrane junction	89
4.8 The canonical binding mode of ribosome-PCC complexes	91
4.9 L6/7 acts as a sensor within the tunnel	93
4.10 Conformational changes of L23 and L24	94
4.11 Open structure of SecYEG and path of the nascent chain	95
4.12 Path of the nascent FtsQ within SecY	96
4.13 Position of the signal anchor	98
4.13 H59 modulates the lipid bilayer	99
4.14 Double role of H59	100
5. Summary	104
6. References	107
7. Appendix	116
Supplementary Table 1: Ribosome-SecY interactions	117
Supplementary Table 2: Ribosome-SecE interactions	118
Supplementary Table 3: NC-ribosome-SecY interactions	119
Supplementary Table 4: NC-SecY interactions	120
Supplementary Table 5: SA-SecY interactions	121
8. Acknowledgements	122
9. Curriculum vitae Jens Frauenfeld	124

1. Introduction

The vast majority of proteins designated to be secreted or to be integrated into the membrane has to pass the ubiquitous protein-conducting channel (PCC), termed Sec61 complex in eukaryotes or SecYEG in prokaryotes (Rapoport, 2007). In the co-translational mode, the hydrophobic signal sequence or signal anchor (SA) of a nascent polypeptide chain emerges from the ribosome and the ribosome-nascent chain complex (RNC) is targeted to the membrane by the signal recognition particle (SRP) and the SRP-receptor (SR) (Figure 1). After transfer from the SRP system to the PCC, the ribosome continues translation and the nascent polypeptide is directly guided from the ribosomal exit tunnel into the ribosome-bound SecY/61 complex for membrane translocation or integration.

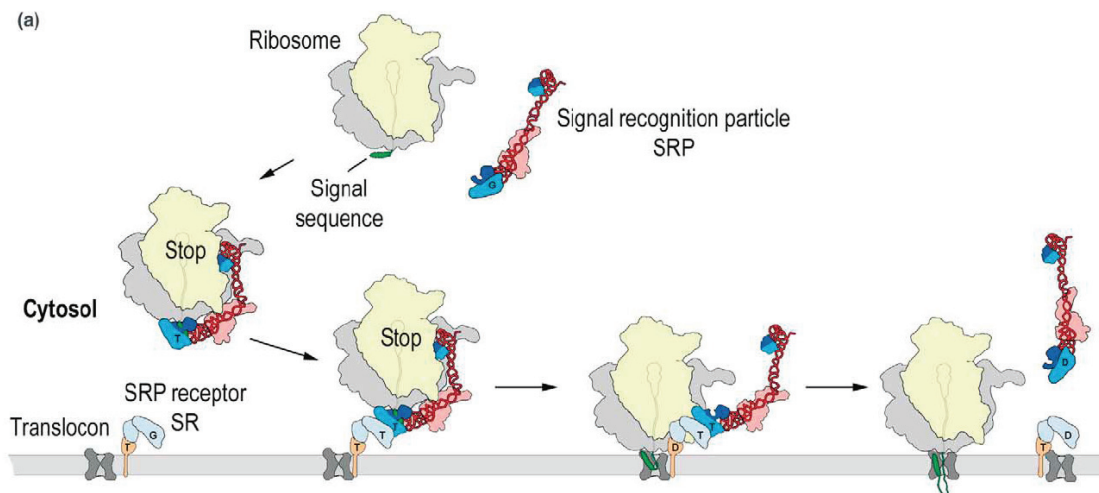


Figure 1: Model of co-translational protein translocation | Schematic overview of the co-translational targeting of proteins destined for secretion or membrane insertion (SRP cycle). SRP interacts with the signal sequence as soon as it emerges from the ribosomal polypeptide exit tunnel. Peptide elongation is retarded in eukaryotes upon SRP–RNC complex formation. The complex is targeted to the ER membrane by the interaction of SRP with the SR, for which GTP binding to both SRP and SR is a prerequisite. The RNC is then transferred to the protein-conducting channel in the membrane (the translocon) and, triggered by GTP hydrolysis in SRP and SR, the SRP–SR complex dissociates.

The evolutionary conserved protein conducting channel serves to translocate proteins (Simon and Blobel, 1991) across or into cellular membranes. It can open in two directions, perpendicular to the plane of the membrane for protein translocation and laterally for the insertion of transmembrane segments of proteins into the lipid bilayer.

While soluble proteins cross the membrane completely and contain a cleavable signal sequence, membrane proteins show different topologies, ranging from 1 – 20 transmembrane (TM) domains, with each of them composed of approximately 20 hydrophobic amino acids.

The protein conducting channel is a heterotrimeric protein complex (Table 1). The Sec61 α subunit is the largest protein of the trimeric complex, containing 10 TM helices, with both N- and C-termini localized in the cytosol. The core of the protein-conducting channel is composed of both the Sec61 α and Sec61 γ subunits. These subunits are essential for viability in yeast and eubacteria and show a high degree of sequence similarity amongst all species. In contrast, the Sec61 β subunit is not essential for eubacteria and yeast. Furthermore, only between eukaryotes and archaea sequence similarity for this subunit is found, which is not the case for eubacteria.

Table 1: Overview of protein conducting channel terms in eukaryotes, eubacteria and archaea

eukaryotes		eubacteria	archaea
mammals	<i>S. cerevisiae</i>		
Sec61	Sec61 Ssh1 for cotranslational transport	Sec YEG	Sec YEG
Sec61 α 10 TM helices	Sec61p 10 TM helices	Sec Y 10 TM helices	Sec Y 10 TM helices
Sec61 β 1 TM helix	Sbh1p 1 TM helix	Sec G 2 TM helices	Sec β 1 TM helix
Sec61 γ 1 TM helix	Sss1p 1 TM helix	Sec E 3 TM helix	Sec E 1 TM helix

The indication that the Sec-complex is the only membrane component required for protein translocation was validated by experiments where purified heterotrimeric complexes were reconstituted into proteoliposomes (Akimaru et al., 1991; Brundage et al., 1990; Gorlich and Rapoport, 1993; Panzner et al., 1995). Systematic cross-linking experiments showed that the nascent protein chain is only encompassed by the α -subunit of the complex (Martoglio et al., 1995).

In general, the PCC has three modes of translocation:

(i) The conserved mechanism of cotranslational translocation that occurs in all species, with the ribosome as the major channel partner. This is also the general way

of integrating transmembrane domains of proteins into phospholipid bilayers. As soon as a nascent peptide chain emerges from the ribosome, the signal recognition particle (SRP) binds to the hydrophobic signal sequence and directs it via the SRP receptor to the Sec-complex (Halic and Beckmann, 2005).

(ii) The second mode of protein translocation occurs only in eukaryotes and is termed posttranslational translocation. Hereby, proteins are transported after completion of their synthesis. These proteins contain a less hydrophobic sequence, thus the SRP is not directed to the RNC, protein synthesis may be completed in the cytosol (Ng et al., 1996)

(iii) The third mode of protein translocation that occurs only in eubacteria is posttranslationally as well. In this case, fully synthesized proteins are kept in an unfolded state by the molecular chaperone SecB. SecB directs the preprotein to SecYEG bound SecA, a peripheral ATPase (de Keyzer et al., 2003). Conformational changes due to the ATPase activity of SecA allow the translocation of the protein through the PCC.

1.1 Co-translational targeting via SRP and FtsY

The signal recognition particle (SRP) is a ubiquitous ribonucleotide particle found in all domains of life (review: (Grudnik et al., 2009; Halic and Beckmann, 2005; Luirink et al., 2005). It binds to the nascent hydrophobic signal sequence of proteins designated for co-translational protein translocation (Figure 2). Together with its membrane-associated receptor FtsY, SRP connects the hydrophobic signal sequence with the membrane embedded translocon SecYEG. *E. coli* SRP is composed of one protein subunit termed Ffh (fifty-four homologue) and a 4.5 S RNA component. Ffh consists of an N-terminal NG domain that harbours a conserved GTPase subdomain and a C-terminal M domain which is responsible for binding of the hydrophobic signal sequence and the 4.5 S RNA.

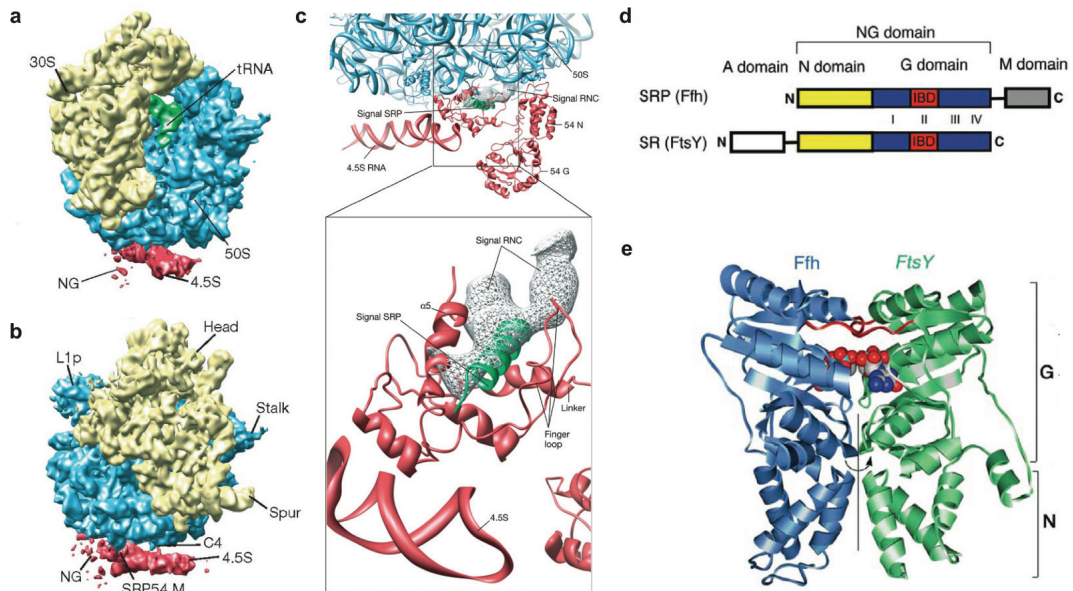


Figure 2: SRP and FtsY | (a) Cryo-EM density map of an *E. coli* 70S RNC–SRP complex with SRP. (b) View onto the back of the 30S subunit. (c) Transfer of the signal sequence from ribosome to SRP. Lower panel, close-up with the density of the signal sequence bound to the ribosome shown as a white mesh. (d) Domain organization of Ffh and FtsY. I–IV represents the conserved GTPase sequence motifs and IBD represent the insertion box domain unique to the SRP-type GTPases. (e) Crystal structure of the Ffh · FtsY NG domain complex. Ffh and FtsY are shown as blue and green ribbons, respectively, and the two nucleotides are shown as space-filled models (adapted from: (Halic et al., 2006; Shan and Walter, 2005))

At the membrane, the NG domain of SRP interacts with the homologous NG domain of FtsY. In addition to its conserved NG domain with GTPase activity, *E. coli* FtsY contains an acidic A domain which is believed to be important for membrane association and a putative interaction site for SecY (Angelini et al., 2006; Angelini et al., 2005; Braig et al., 2009; Weiche et al., 2008). Thus, FtsY exhibits two functions: (i) it senses both the membrane and the presence of a translocon and (ii) reacts to the presence of RNC-SRP complexes. These functions are regulated by the GTPase activity of FtsY. For the interaction of FtsY with the membrane, the presence of anionic lipids is crucial (de Leeuw et al., 2000). Recently it has been shown that FtsY binds preferably to phosphatidyl glycerol (Braig et al., 2009). Parlitz et al. identified an amphipathic helix at the N-terminus of the NG domain that is responsible for membrane association (Parlitz et al., 2007). Protein targeting via SRP and FtsY is tightly coupled to GTP binding. The transfer of the nascent signal sequence to SecY leads to GTP-hydrolysis of the corresponding GTPase domains of FtsY and SRP. Subsequently, the targeting complex dissociates while the membrane protein is

inserted into the membrane upon the GTPase activity of ribosomal co-factors such as EF-G.

1.2 FtsQ as a model for membrane-protein type II insertion

Type-II membrane proteins contain a single transmembrane helix, the signal anchor (SA), with the N-terminus of the protein facing the cytosol (Figure 3a). A well-characterized membrane-protein that displays type II orientation is FtsQ, a protein required for cell division in *E. coli*, which contains a signal anchor helix between residues 24 and 49. It has been used as a model substrate to investigate the stages of inner membrane protein insertion in vitro (Figure 3b).

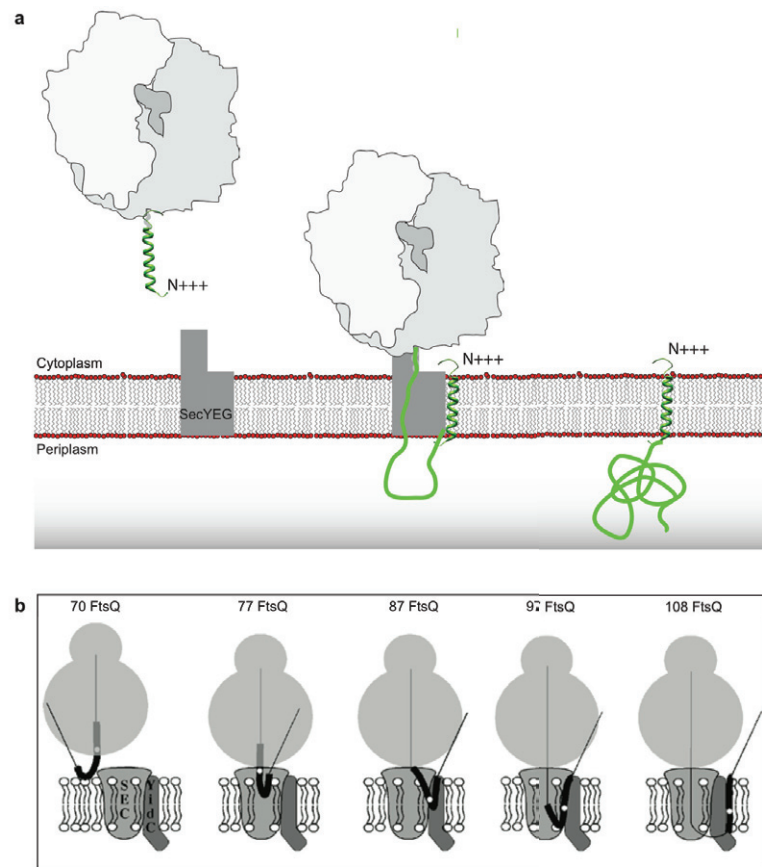


Figure 3: Membrane protein type-II insertion | (a) The positively charged N-terminus of an emerging membrane protein remains within the cytoplasm, the TM helix spans the membrane once and the C-terminal part is translocated via an intermediate loop into the periplasm (b) Model for the membrane insertion of short nascent FtsQ. Nascent FtsQ with varying lengths as indicated were used in a cross-linking study by Urbanus et al. The TM region is represented as a thick line with a white dot at the position of the photo-crosslink sites (Urbanus et al., 2001)

The insertion pathway of this 276-residue-long protein was explored by cross-linking approaches (review: (Dalbey and Chen, 2004). Previously it has been shown that FtsQ integrates into membranes via SecYEG (Scotti et al., 2000) and that the nascent FtsQ inserts into the membrane close to SecY and lipids (Urbanus et al., 2001).

Upon chain elongation, it moves to a combined YidC/lipid environment. It was shown that SecA is needed for the translocation of the large C-terminal domain of FtsQ (Scotti et al., 2000; Urbanus et al., 2001). The signal anchor of FtsQ interacts first with SecY and then with YidC. It remains in a YidC/phospholipid environment during further protein synthesis. The lateral transfer of the transmembrane domain requires both SecA and YidC and suggests a crucial role for YidC to mediate the TM release into the lipid bilayer.

In contrast, Driessen et al. showed that YidC is not required for insertion of FtsQ (van der Laan et al., 2004), but could play a kinetic role for the lateral release of the TMS from the translocon. Furthermore, it was shown ribosome-bound nascent FtsQ inserts into SecYEG proteoliposomes in the absence of a proton motive force (PMF), while the complete translocation of the hydrophilic C-terminal part of the protein requires a PMF. Taken together, FtsQ is one of the most intensively studied membrane proteins regarding insertion into the lipid bilayer.

1.3 Ribosome binding and EM-data

Early cryo-EM reconstructions of ribosomes bound to purified Sec complexes in detergent micelles and biochemical data lead to contradictory results regarding the oligomeric state of the Sec-complex that interacts with the ribosome.

In eukaryotes, early reconstructions of ribosome-Sec61 complexes displayed a donut-like structure beneath the ribosome (Beckmann et al., 1997; Menetret et al., 2000) (Figure 4a). Based on the volume of these donut-like structures, it was suggested that three or four copies of the Sec61 complex are bound to the ribosome. Moreover, three or four connections were observed between the ribosome and the channel density, presumably indicating the presence of Sec61 oligomers.

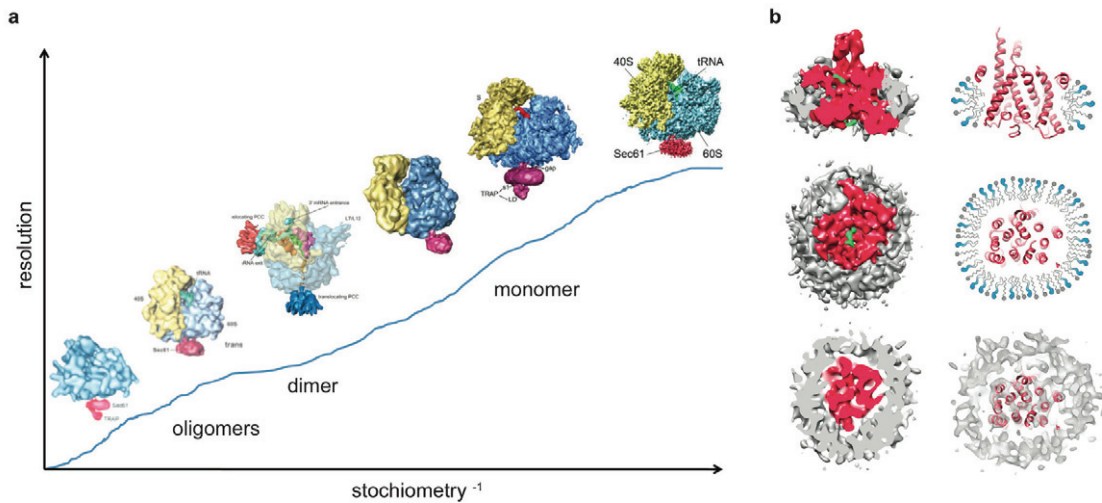


Figure 4: Detergent-solubilized Sec-complexes bound to ribosomes | (a) Scheme with cryo-EM structures of ribosomes bound to donut-shaped Sec-complexes. From left to right: Oligomer (Beckmann et al., 1997), Trimer (Beckmann et al., 2001), Dimer (Mitra et al., 2005), Monomer (Becker et al., 2009; Menetret et al., 2007; Menetret et al., 2008). (b) The RNC-bound mammalian Sec61 complex is a monomer surrounded by a micelle. Upper left section: side view cut perpendicular to the plane of the membrane of the isolated densities for the Sec61 complex (red), the surrounding mixed micelle (grey) and the nascent DP120 polypeptide chain and/or the signal anchor sequence (green). Right: Schematic drawing of the mixed micelle of phospholipids (grey) and detergent molecules (blue) surrounding the PCC (red ribbons). Middle section: Isolated densities and schematic drawing as in upper section in a top view (left) or sliced within the plane of the membrane (right). Lower section: Sliced top views, represented as in middle section (left) or as red ribbons for the Sec61 model and transparent mesh for the electron density (right) (adapted from Becker et al., 2009)

Yet, at the resolution of these maps, it is difficult to distinguish between density contributed by detergent, lipid or protein. With increasing resolution, the apparent oligomeric state of Sec-complexes bound to ribosomes decreased: The structure of a translating *E. coli* ribosome bound to a detergent-solubilized SecYEG complex at 15 Å resolution was interpreted to be composed of a dimer of Sec-complexes arranged in a front-to-front orientation, i.e. with the lateral gates of the Sec-complexes facing towards each other (Mitra et al., 2005).

However, a more recent cryo-EM reconstruction of nontranslating ribosome exhibited density beneath the ribosomal exit tunnel that was composed of a monomeric SecYEG complex (Menetret et al., 2007). This is in agreement with more recent biochemical, structural, and molecular dynamics simulation data, showing that a single copy of the Sec complex is most likely forming the active PCC (Becker et al.,

2009; Gumbart et al., 2009; Kalies et al., 2008; Menetret et al., 2007; Menetret et al., 2008).

In addition, the donut-like shape of Sec-complexes bound to ribosomes could be explained: the two recent cryo-EM reconstructions of eukaryotic ribosomes bound to detergent-solubilized Sec61 structurally revealed the detergent micelle surrounding Sec-complex (Becker et al., 2009; Menetret et al., 2008) (Figure 4b). Thus, it appears likely that previous cryo-EM structures represented single copies of the Sec complex in micelles of varying sizes.

1.4 Architecture of the PCC

Van den Berg et al. solved the crystal structure of a detergent-solubilized archaeal SecYEG complex to 3.2 Å (Van den Berg et al., 2004). A model has been proposed in which the functional protein-conducting channel is made up of only one copy of the heterotrimeric complex (Figure 5a,b). The α -subunit of the complex displays pseudosymmetry with two linked halves, namely TM1-TM5 (N-terminus) and TM6-TM10 (C-terminus). The corresponding γ -subunit is believed to function as a brace, serving to prevent separation of the two halves. The β -subunit contacts only the periphery of the α -subunit.

The α -subunit TM helices form an hourglass-shaped pore that displays a cytoplasmic and a periplasmic funnel, with the central constriction located in the middle of the membrane surface. Interestingly, in the inactive state of SecY the periplasmic funnel is blocked by the so-called plug-helix. The central constriction is made up of six hydrophobic residues and referred to as the “pore ring”.

Regarding the domain organization of the α -subunit, together with the presence of the β - and γ -subunit in the periphery of the complex, a model was proposed in which a monomeric SecYEG complex would suffice to translocate proteins across or to integrate proteins into the membrane bilayer (Figure 5c,d). In all cases of translocation, the hydrophobic segment of a signal anchor or signal sequence is thought to intercalate into the “lateral-gate” of the Sec-complex, situated between TM2b and TM7 (Osborne and Rapoport, 2007). The insertion of a SS or SA would

require the two clam shell-like halves of SecY to open in order to provide enough space within the lateral gate for the accommodation of the signal sequence or the SA.

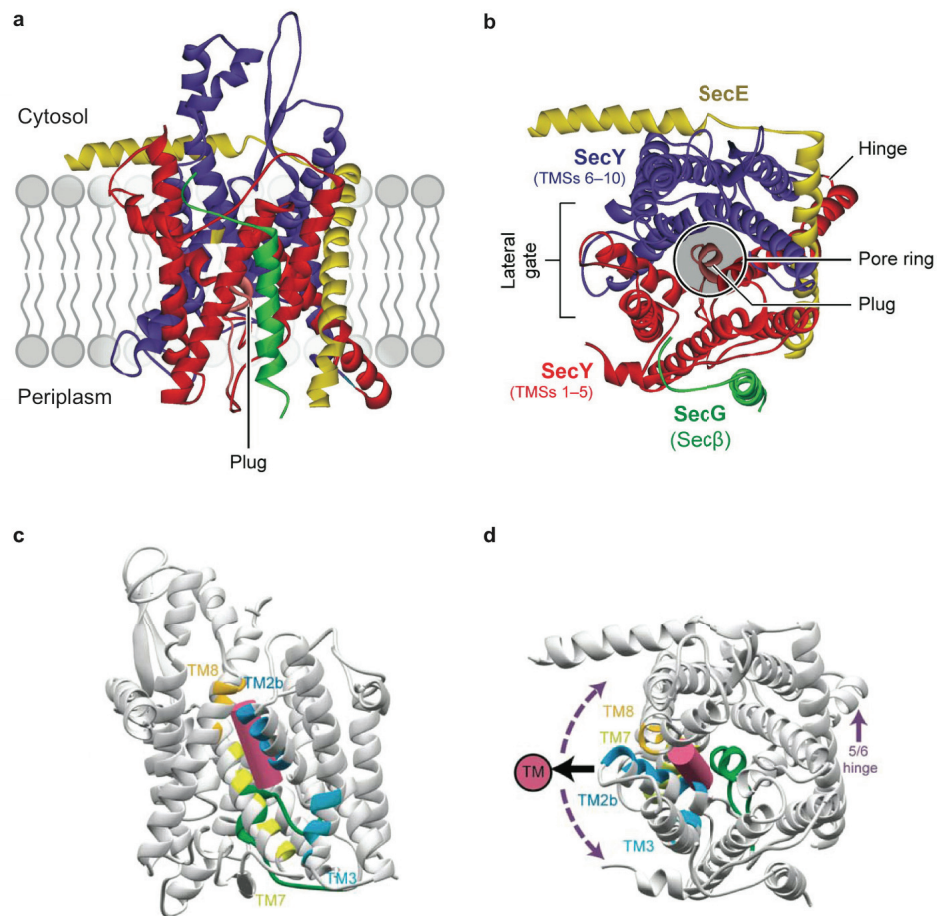


Figure 5: Structure of the protein-conducting channel | (a) Membrane cross section and (b) a cytosolic view of the structure of the *M. jannaschii* SecYE β (pdb: 1RHZ). The protein-conducting channel consists of three subunits: the SecY (Sec61 α) that is embraced by the SecE (Sec61 γ) subunit and the peripherally bound SecG (Sec61 β) protein. The two halves of the clamshell-like structure of SecY are indicated as TM1–5 and TM6–10 and are connected by a hinge region. The clamshell opening in the front may form a lateral gate to the lipid bilayer. (c), (d) View from the front (c) and from the top (d) of the signal-sequence-binding site and lateral gate. The hydrophobic core of the signal sequence probably forms an α -helix, modelled as a magenta cylinder, which intercalates between TM2b (blue) and TM7 (yellow) above the plug. Intercalation requires opening the front surface, as indicated by the broken arrows. A solid arrow pointing to the magenta circle in the top view indicates schematically how a TM of a nascent membrane protein would exit the channel into the lipid bilayer (adapted from: (Driessen and Nouwen, 2008; Van den Berg et al., 2004)

Consistent with this idea, two recent crystal structures of SecYE bound to SecA or a Fab fragment show a partial opening of the lateral gate (Figure 6). Apparently, the binding of either a Fab fragment or SecA to the cytosolic loops of SecY lead to a conformational change of the PCC. Hereby, the opening of the lateral gate appears to be initiated by a rigid-body movement of the C-terminal part of SecY (Tsukazaki et al., 2008; Zimmer et al., 2008)

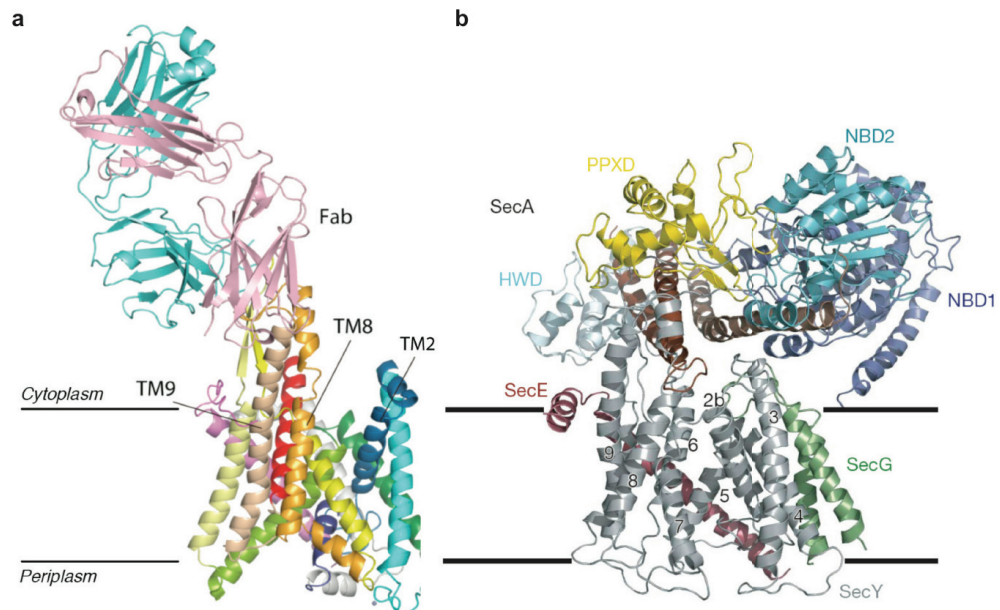


Figure 6: Architectures of pre-open PCCs | Structure of the *T. maritima* SecA–SecYEG complex. (a) Cartoon of the complex viewed from the side. The lines indicate the membrane boundaries. (b) X-ray structure of the Fab-bound *T. thermophilus* SecYE viewed from the front side (adapted from Tsukazaki et al., 2008 and Zimmer et al., 2008).

After the gating event, the polypeptide is thought to use the central hourglass-shaped aqueous vestibule of the Sec complex as a conduit for translocation.

1.5 Membrane proteins in the lipid environment

All structures obtained so far have a common feature: Sec-complexes used in these studies are surrounded by a detergent micelle. It has long been observed that, once exposed to detergents, most membrane proteins rapidly lose their functionality (for an example among hundreds of studies, see e.g. (Breyton et al., 1997)).

Several molecular dynamics studies revealed conformational differences of transmembrane proteins embedded in a membrane and a detergent micelle, highlighting the importance of the lipid scaffold for the correct orientation of transmembrane helices and the interaction of flanking residues of membrane proteins and lipids (Lerch-Bader et al., 2008; Patargias et al., 2005; Sansom et al., 2005) (Figure 7).

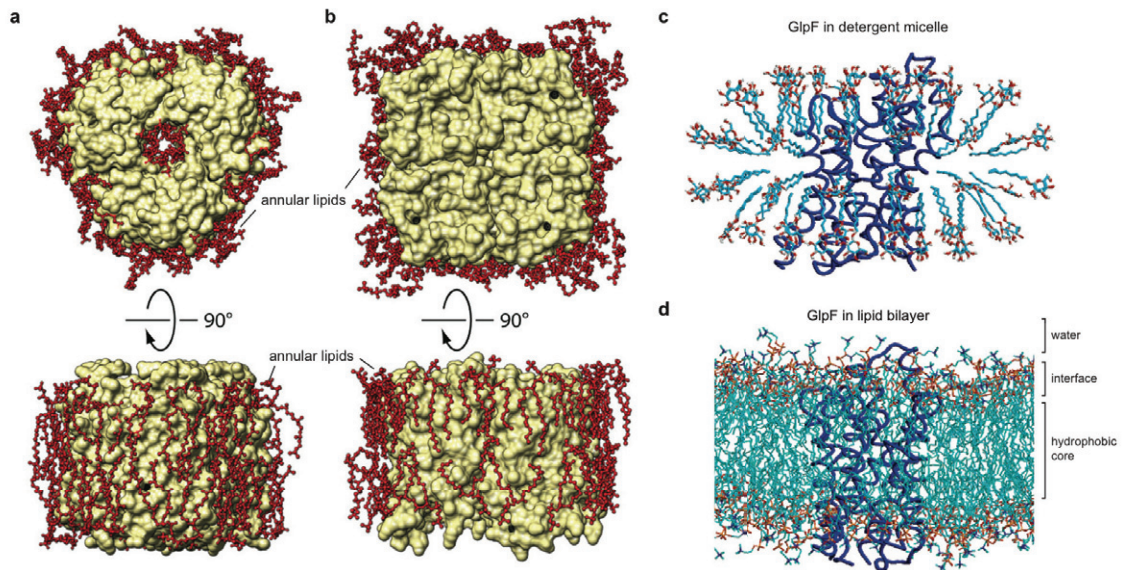


Figure 7: Membrane proteins in a lipid environment or in a detergent micelle | (a,b) Top (top panels) and side (bottom panels) views of annular lipids in membrane protein structures determined by electron crystallography. (a) Bacteriorhodopsin (PDB entry 2BRD). (b) Aquaporin-0 (PDB entry 2B6O). The proteins are shown in surface representation (yellow) and the lipid molecules are shown in ball-and-stick representation (red) (adapted from Raunser, Walz, 2009). (c) Molecular dynamics simulation of the membrane protein GlpF in a detergent micelle (octyl glucoside, OG) and (d) in a lipid bilayer (DMPC). In both diagrams the protein is shown as a CR trace (blue), and the detergent or lipid molecules are shown in bonds format with C atoms in cyan, oxygen atoms in red, etc. In (d) the location of the bulk water, interface, and hydrophobic core regions are indicated (adapted from Patargias et al., 2005).

Apart from its scaffolding function, the lipid membrane bilayer is more complex than just being a (semi-) fluid hydrophobic layer, since specific protein-lipid interactions may further influence the architecture of membrane proteins. It was suggested that phospholipids may work as chaperones in the assembly of membrane proteins (Bogdanov et al., 1996) and that the transmembrane domain orientation within some membrane proteins is dependent on membrane lipid composition (Bogdanov et al., 2009). Transmembrane helices tilt with respect to the membrane bilayer thickness to

achieve hydrophobic matching (White and von Heijne, 2008). The chain length of the lipid often modulates the function of integral transmembrane proteins. In numerous cases, the enzyme or transport activity reaches a maximum at a particular lipid chain length and is reduced in membranes with either shorter or longer lipid chains (Marsh, 2008). In general, some lipids specifically interact with the transmembrane core of the protein, as has been shown by co-crystallization of cytochrome c oxidase (Raunser and Walz, 2009). Beyond that, another layer of lipids surrounds the protein: lipids that are tightly associated with the membrane proteins and that form a shell around it are called annular lipids (Figure 7a,b). The tight interaction of these lipids with the hydrophobic surface of the protein is crucial to prevent leakage of solutes across the membrane. The interactions of membrane proteins with lipids is based (i) van der Waals interactions between the lipid tails and the hydrophobic intramembranous surface of the protein and (ii) ionic interactions of the charged lipid headgroups with the hydrophilic extramembranous surface of the protein (Raunser and Walz, 2009). Tryptophane residues have been shown to modulate electrostatic and hydrogen-bonding interactions between the positively charged lysine residues and the negatively charged headgroups of phosphatidylglycerol bilayers (review: White and von Heijne, 2005). Furthermore, lipid-protein interactions play an integral role in stabilizing the quaternary architecture of membrane proteins, since the oligomeric assembly of many membrane proteins is disrupted upon delipidation by detergent extraction (Reichow and Gonen, 2009). For the translocation of membrane proteins into the lipid bilayer it has to be noted that many components of the protein-translocating machineries interact with phospholipids during translocation (review: (Van Voorst and De Kruijff, 2000). These interactions are perturbed by a change of the phospholipid composition and compromise the whole machinery. It has been suggested that substantial conformational changes occur in the membrane during membrane protein integration, leading to a reduced lateral pressure from the lipid bilayer so that the insertion of a transmembrane segment into the membrane is facilitated. Furthermore, it has been shown that a physiological amount of the diacylglycerol is required to prevent spontaneous insertion of TM segments into the membrane (Nishiyama et al., 2006). Taken together, studying the process of protein translocation across or into the membrane should also involve one of the main actors: the lipid bilayer.

1.6 Nanodiscs

The visualization of membrane proteins within a lipid bilayer environment is one of the major challenges of structural biology. The lipid bilayer is a complex two-dimensional system and it has been proven to be difficult to obtain structural information from membrane proteins within a membrane. Attempts to do so involved 2D-electron crystallography (Raunser and Walz, 2009) and a single-particle cryo-EM approach called RSC (Wang and Sigworth, 2009). Yet, traditional 2D-electron crystallography is limited by the difficulty to generate 2D crystals and the visualization of putative hydrophilic loop regions is impossible. The RSC approach circumvents crystallization, yet it leads to only low-resolution information thus far, making it impossible to map details of TM interactions or protein-lipid interactions.

It is possible to integrate membrane proteins into a defined nano-scale phospholipid environment, termed Nanodiscs (Borch and Hamann, 2009). Nanodiscs represent the initial state of nascent discoidal high-density lipoprotein (HDL). Nanodiscs are small discoidal phospholipid bilayers that are surrounded by a protein belt of Apo-A1 (Nath et al., 2007). In contrast to liposomes or proteoliposomes, they present distinct advantages: they maintain their particle size and are robust over time. In addition, it has been shown that Nanodiscs better reflect the complex phase transition behaviour of biological membranes than model membranes like liposomes (Denisov et al., 2005). To date, a variety of different membrane proteins have been incorporated into Nanodiscs, such as cytochrome P450s, NADPH-cytochrome P450 reductase, bacteriorhodopsin, G protein-coupled receptors, a bacterial chemoreceptor, SecYEG (Alami et al., 2007) and recently, the anthrax toxin pore (Katayama et al., 2010).

As mentioned above, the *in vivo* function of Apo-A1 is reverse cholesterol transport, where accumulated cholesterol is transported from tissues to the liver (Ajees et al., 2006). Hereby, two monomers of Apo-A1 bind to serum phospholipids to form nascent discoidal HDL particles. Upon interaction with the ATP-binding cassette transporter A1, cholesterol is incorporated into the particles via esterification by the lecithin-cholesterol acyltransferase. Through the incorporation of increasing amounts of cholesteryl esters, the nascent discoidal HDL particles are transformed into mature spherical HDL particles.

Recently, the crystal structure of lipid-free full-length Apo-A1 has been solved (Ajees et al., 2006) and a truncated version lacking the N-terminal 43 amino acids which adopts a conformation in which the two Apo-A1 molecules form a cylindrical belt of amphipathic helices (Borhani et al., 1997). Interestingly, ApoA-I exists in multiple conformations, such as lipid-free/poor, partially lipidated, and fully lipidated states (Figure 8). The lipid-free form of ApoA-I is thermodynamically labile but gets rapidly lipidated.

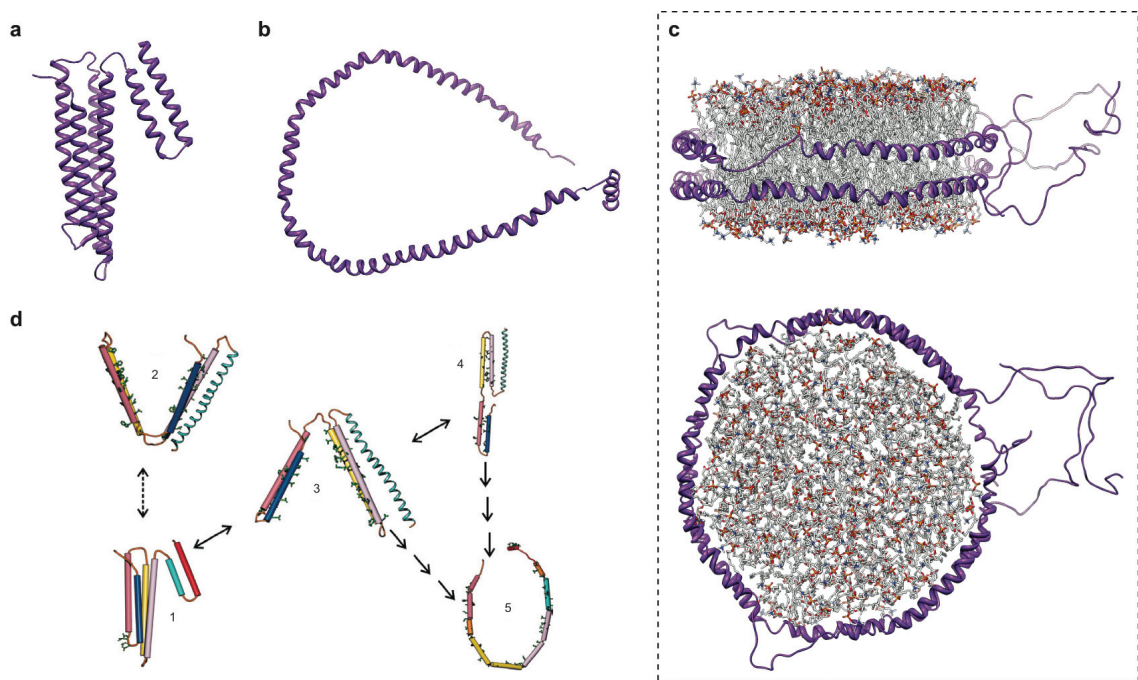


Figure 8: Conformations of Apolipoprotein-A1 | (a) X-ray structure of the lipid-free conformation of full-length Apo-A1 (pdb: 2A01). It displays a compact α -helical structure with an N-terminal four-helix bundle and two C-terminal helices. Lipid-free apoA-I displays a lower α -helical content in solution than that observed in this crystal structure, suggesting that the protein dynamically samples multiple conformations as shown in (d) (Ajees et al., 2006). (b) The N-terminal truncation Apo-A1 Δ [1-43] displays a cylindrical belt of amphipathic helices. In solution, this truncated protein resembles discoidal HDL in terms of α -helical content and proteolytic cleavage patterns (Nath et al., 2007) suggesting it is a good qualitative model for discoidal HDL particles. (c) Molecular model of nascent discoidal HDL, determined using hydrogen-deuterium exchange mass spectrometry. The model reveals two Apo-A1 molecules arranged in an antiparallel double-belt structure (model database accession number: PM0074956) in side view (upper panel) and top view (lower panel).

The crystal structure of human Apo-A1 consists of two helical domains: a four-helix antiparallel bundle formed by the N-terminal part of Apo-A1 and a two-helix bundle adopted by the C-terminal part of the molecule. The N-terminal domain of Apo-A1 stabilizes the lipid-free conformation. Upon removal of the first 43 N-terminal residues of Apo-A1, the protein adopts, even in the absence of lipid, an open and discoidal form whose structure was solved to 4 Å resolution (Borhani et al. 1997).

1.7 Aim of this study

The ubiquitous protein-conducting channel (PCC), termed the Sec61 complex in eukaryotes or the homologous SecYEG complex in both eubacteria and archaea, translocates nascent proteins across cellular membranes and serves to integrate transmembrane domains of proteins into lipid bilayers. Attempts to solve the structure of the protein-conducting channel have involved cryo-electron microscopy (cryo-EM) and X-ray techniques. Whereas these methods revealed new insights into the mechanism by which proteins may pass through the translocon, the structures also lead to apparently contradictory results regarding the oligomerization state and conformational arrangement of the active translocon. Furthermore, all 3D-structures of ribosomes bound to the translocon were obtained from detergent solubilized Sec-complexes. It is often criticised that the presence of a detergent micelle might induce conformational changes and lead to non-native associations of the Sec-complex. Thus, the conformation of the ribosome-Sec-complex in its natural environment remains to be elucidated. In addition, it is very likely that a lipid bilayer contributes to targeting, regulation and control of membrane integration.

Therefore, the main aim of this study is to establish the generation of Nanodiscs, followed by the incorporation of the *E. coli* SecYEG complex (Nd-SecYEG) (Figure 9a). Once this method is set up, *E. coli* ribosomes carrying the nascent chain of the well-characterized FtsQ membrane protein should be purified and used for the reconstitution with Nd-SecYEG (Figure 9b). If this proves to be successful, high resolution cryo-EM data of this reconstituted 70S-RNC-Nd-SecYEG complex should be obtained for a structural investigation of this complex.

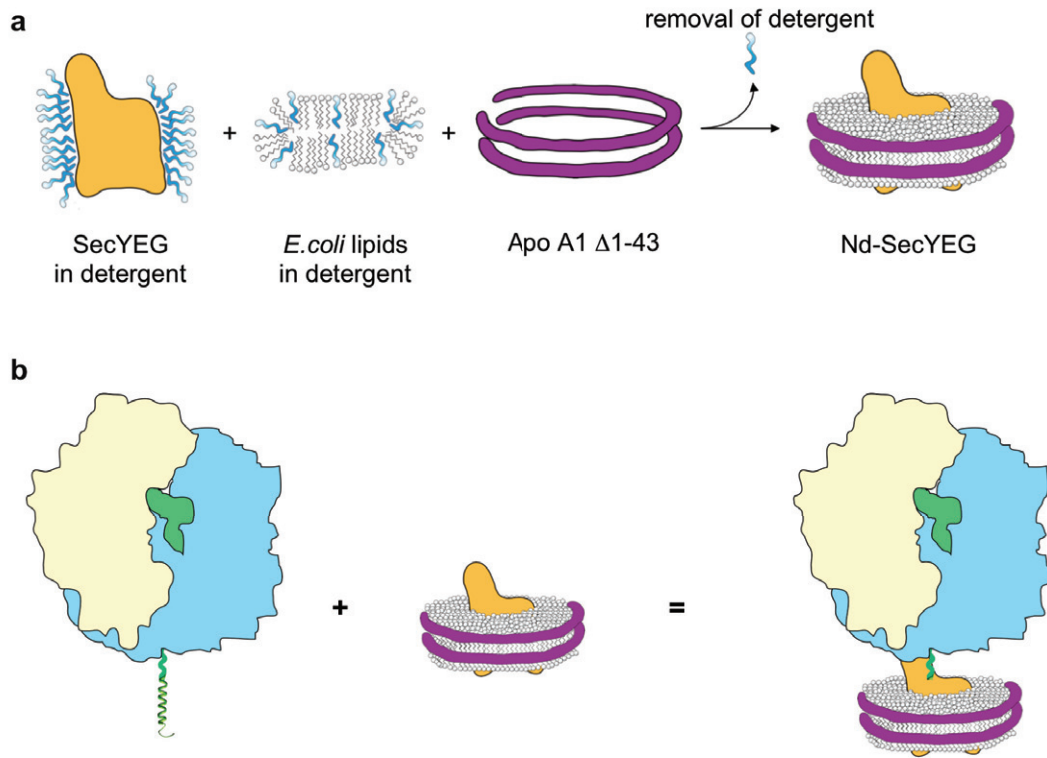


Figure 9: Approach | (a) Purified Apo-A1, phospholipids and solubilized SecYEG are mixed and incubated. The self-assembly of Nanodiscs-SecYEG (Nd-SecYEG) is initiated by removing detergent. (b) Reconstitution of the 70S-RNC-Nd-SecYEG complex.

2 Materials and Methods

2.1 Media and supplements

Terrific Broth (TB) and Luria Broth (LB) liquid media as well as LB Agar plates were prepared according to standard protocols (Sambrook and Russell, 2001). The media was supplemented with the respective antibiotics using stock solutions of ampicillin (100 mg/ml water; Roth), kanamycin (50 mg/ml water; Roth) and chloramphenicol (34 mg/ml ethanol; Roth).

2.2 PCR

The kit Phusion Flash High-Fidelity Master Mix (Finnzymes) was used as 20 μ l reaction, where only to 10 μ l of the 2x Master Mix, primers and template DNA was added, according to the manufacturer's protocol. Reactions were conducted using appropriate cycling programs. Samples were analyzed subsequently by agarose gel electrophoresis.

2.3 Agarose gel electrophoresis

Agarose gel electrophoresis was used to separate DNA and RNA according to their size. Gels were made with 1-2 % agarose (Invitrogen) in TAE buffer (40 mM Tris/HCl pH 8.0, 20 mM acetic acid, 2 mM EDTA) and run for 30 min at 50 V. DNA and RNA molecules were stained with SYBR Green I and II (Molecular Probes), respectively and visualized at a wavelength of 300 nm. DNA markers (Bio-Rad and NEB) were used as molecular weight standards.

2.4 Transformation of *E. coli* and Isolation of Plasmid DNA

Transformation of plasmid DNA into competent *E. coli* cells was performed by mixing 100 μ l of competent cells with 10 μ l of the ligation reaction or 1 μ l of purified plasmid DNA (40 ng/ μ l) and incubating on ice for 20 min. Cells were heat-shocked at 42°C for 45 sec and immediately afterwards chilled on ice. 1000 μ l of fresh LB medium was added, followed by incubation at 37°C for 45 min in a shaking

incubator. Cells were plated on LB agar plates containing the respective antibiotics and incubated at 37°C overnight. Plasmid DNA was isolated from a 5 ml overnight culture using the Plasmid Extraction Kit (Metabion, Matrnried, Germany). DNA-sequencing was performed by Eurofins MWG (Munich, Germany).

2.5 Protein separation by SDS-PAGE

Denaturing discontinuous SDS-PAGE (SDS polyacrylamide gel electrophoresis) was used to separate proteins according to their molecular size, using standard protocols (Laemmli, 1970). Samples were loaded on 15 % polyacrylamide gels. Electrophoresis was performed at constant voltage of 120-200 V in standard running buffer (25 mM Tris, 192 mM glycine, 0.1 % SDS) using Bio-Rad Mini-Protean II Electrophoresis cells (Biorad, Munich).

2.6 TCA precipitation

TCA precipitation was used prior to western blot analysis or reconstitution experiments, to concentrate proteins out of highly diluted reaction mixtures. To each reaction, 150-200 µl of 72 % trichlor acetic acid (TCA) and 0,15 % sodium desoxycholate (Roth) were added and the overall volume was adjusted to 1 ml with ddH₂O. Reactions were incubated overnight at -20°C, centrifuged, the resulting pellet was washed once with 100 % acetone p.a. (Roth) and finally 10 µl sample buffer was added to the dried pellet for SDS-PAGE.

2.7 SYPRO orange staining

The SDS gels were stained with SYPRO orange (Invitrogen) for detection of small amounts of proteins (< 100 ng per 0.5 cm lane), used in reconstitution assays. Gels were washed for 1 min in 7.5 % acetic acid (and stained in the dark for > 1 h at RT, in a solution of 1:5000 SYPRO orange in 7.5 % acetic acid (Roth). The gels were washed for 30 s in 7.5 % acetic acid and visualized at 480 nm excitation wavelength/ 580 nm emission filter/ 590 V sensitivity using a Typhoon scanner (Typhoon 9400, Amersham).

2.8 Western Blotting

Western blotting was used for the qualitative detection of tagged proteins. For HA- or His-tag detection, SDS gels were blotted for 45 min at 75 mA per gel, in blotting buffer (20% (v/v) methanol, 48 mM Tris, 39 mM glycine, 0,037% (w/v) SDS) on PVDF membranes, using a standard semi-dry blotting apparatus (Bio-Rad). Membranes were stained for 1 min in Amidoblack (0.1% (w/v) Naphtol Blue Black, 7.5% (v/v) acetic acid, 20% (v/v) methanol), digitized, destained and blocked with 2 % BSA (Roth) in 1x TBS buffer (200 mM Tris pH 7.6, 1.5 M NaCl). The primary antibody (HA-probe mouse AB, His-probe mouse AB, Santa Cruz Biotechnology) was used in a 1:1000 dilution in 2 % BSA/1x TBS and incubated overnight at 4°C. The membrane was washed three times for 10 min with 1x TBS-T buffer (200 mM Tris pH 7.6, 1.5 M NaCl, 1 % Tween) and the second antibody (goat anti-mouse antibody, Santa Cruz Biotechnology) was used in a 1:2000 dilution in 5 % milk in TBS and incubated for 1 h at RT. Membranes were washed three times with TBS-T buffer and signals detected by ECL reaction (Chemiluminescent Detection kit, AppliChem) and films (GE Healthcare).

2.9 Expression and Purification of Apo-A1

Protein expression was carried out using the pET28a plasmid and expressed using *E. coli* BL21 (DE3). Here, 5 ml LB medium containing 30 µg/ml kanamycin were inoculated with a single colony from a plate and grown overnight at 37°C with shaking. Subsequently, 45 ml of LB medium (30 µg/ml kanamycin) are inoculated with these 5 ml grown overnight. The next day, 3 l of TB medium (10 µg/ml kanamycin) are inoculated with 10 ml of the second overnight culture and induction with 1 mM IPTG (Roth) was performed when OD600 reached 0.8. One hour after induction, the temperature was lowered to 28 °C. Four hours after induction the cells were collected by centrifugation at 8000 g for 15 min and the supernatant discarded. The cell pellet was resuspended by adding 3 ml of residual supernatant and 2 ml glycerol, shock-frozen in liquid nitrogen and stored at – 80 °C.

For purification, the cell pellets were centrifuged at 8000 g at 15 min, the supernatant discarded and 10 g of cells were resuspended in apo-lysis-buffer (20 mM NaPO₄ pH 7.4, 1% Triton X-100, 1 mM PMSF). Cells were lysed by sonification on ice. The

lysate was cleared by centrifugation for 30 min at 30000 g at 4 °C. The cleared lysate was loaded onto an equilibrated 1 ml GE His-Trap column at 0.5 ml/min (Äkta Explorer, GE Healthcare). The column was washed with 25 column volumes of WB1 (40 mM Tris/HCl pH 8.0, 300 mM NaCl, 1% Triton X-100), 25 column volumes of WB2 (40 mM Tris/HCl pH 8.0, 300 mM NaCl, 50 mM cholate), 15 column volumes of WB3 (40 mM Tris/HCl pH 8.0, 300 mM NaCl) and 20 column volumes of WB4 (40 mM Tris/HCl pH 8.0, 300 mM NaCl, 50 mM imidazol). Apo-A1 was eluted with EB (40 mM Tris/HCl pH 8.0, 300 mM NaCl, 300 mM imidazol, 5 mM cholate, 5% glycerol) and fractions analyzed for purity by SDS-PAGE. Fractions containing pure Apo-A1 were collected, dialyzed against Apo-buffer (10 mM Tris/HCl pH 7.4, 100 mM NaCl, 5 mM cholate, 5% glycerol), shock-frozen in liquid nitrogen and stored at – 80 °C.

2.10 Preparation of Lipid/Cholate stock solution

E. coli phospholipids (Avanti Polar Lipids, *E. coli* total extract in chloroform) were dried under a stream of nitrogen and stored in a vacuum exsiccator overnight to remove residual solvent. Lipids were resuspended in cholate-buffer (20 mM Hepes pH 7.2, 100 mM KOAc, 6 mM Mg(OAc)₂, 1 mM DTT, 25 mg/ml cholate) to yield a final concentration of 20 mg/ml lipids. The suspension was vortexed, sonified and incubated at 37 °C for 30 min until a clear solution was obtained. Aliquots at 20 µl were shock-frozen in liquid nitrogen and stored at – 80 °C.

2.11 Expression of SecYEG

Protein expression of SecYEG was carried out using SF100 cells that were transformed with pEK20 (overexpression of SecYEG complex with a histidine tag at the amino terminus of the SecY subunit, cysteine less; (van der Sluis et al., 2002). 5 ml LB medium containing 100 µg/ml ampicillin and 0.5 % glucose were incubated at 37°C for 4h with shaking. Subsequently, 300 ml of LB medium (100 µg/ml ampicillin, 0.5 % glucose) were inoculated with these 5 ml and incubated at 37 °C overnight with shaking. The next day, 6x 2l of LB medium (100 µg/ml ampicillin) were each inoculated with 50 ml of the overnight culture. Induction with 1 mM IPTG was performed when OD600 reached 0.6 – 0.8. Two hours after induction the cells

were harvested by centrifugation at 8000 g for 10 min at 4 °C. Cell pellets were resuspended by adding 10 ml 50 mM Tris/HCl pH 8.0/ 20 % (w/v) sucrose, shock-frozen in liquid nitrogen and stored at – 80 °C.

2.12 Preparation of SecYEG-IMVs

The suspension was supplemented with 2 mM DTT, 0.5 mM PMSF and cells were lysed by French press (Microfluidizer, Microfluidics). Unbroken cells were removed by centrifugation (6000 g, 15 min), while the supernatant was subjected to an ultracentrifugation step for 60 min at 40000 rpm in a Ti45 rotor (Sorvall centrifuges). The membrane pellet was resuspended with 800 µl 50 mM Tris/HCl pH 8.0, 2 mM DTT and transferred into a potter-homogenizer and homogenized to viscosity. After full resuspension, the membrane pellet was applied to a sucrose step gradient in 50 mM Tris/HCl pH 8.0, 2 mM DTT with consecutive layers of each 5 ml of 55% - 50% - 45% - 40% -35% (w/v) sucrose. The gradient was spun for 17 h at 25000 rpm at 4 °C in a SW28 rotor. This led to a separation of vesicles of the inner membrane (upper layer) and the outer membrane. Vesicles of the inner membrane (IMVs) were collected with the help of a syringe, resuspended with 50 ml 50 mM Tris/HCl pH 8.0, 2 mM DTT and spun for 90 min at 4 °C and 40000 rpm in a Ti45 rotor. Each pellet was resuspended with 800 µl 50 mM Tris/HCl pH 8.0, 20 % glycerol, 2 mM DTT and homogenized to complete viscosity with the help of a potter-homogenizer. Homogenized IMVs were shock-frozen in liquid nitrogen and stored at -80 °C.

2.13 Purification of SecYEG

Inner membrane vesicles are solubilized at a protein concentration of 2 mg/ml (OD280) in sol-buffer (10 mM Tris/HCl pH 8.0, 20% glycerol, 2% DDM) for 1 h at 4 °C under gentle mixing. Non-solubilized material is removed by centrifugation for 30 min at 40000 rpm in a Ti45 rotor at 4 °C. The supernatant is loaded onto an equilibrated anion-exchange column (DEAE HiTrap Sepharose, 20 ml, GE Healthcare). The column is washed with one column volume of buffer A (10 mM Tris/HCl pH 8.0, 20% glycerol, 0.05% DDM) and bound protein is eluted in 150 ml of a linear gradient of 0-300 mM KCl in buffer B (10 mM Tris/HCl pH 8.0, 20% glycerol, 0.05% DDM, 1 M KCl). SecYEG elutes at a KCl concentration of about 100

mM KCl, fractions are analyzed by SDS-PAGE. Fractions containing SecYEG to a purity of 40 % are pooled, supplemented with an equal volume of buffer Ni-NTA buffer A (10 mM Tris/HCl pH 8.0, 20% glycerol, 0.05% DDM, 100 mM KCl, 10 mM imidazol) and loaded onto a Ni-NTA HiTrap column (1 ml, GE Healthcare). After washing with 5 column volumes of Ni-NTA buffer A, the SecYEG complex is eluted with Ni-NTA buffer B (10 mM Tris/HCl pH 8.0, 20% glycerol, 0.05% DDM, 100 mM KCl, 500 mM imidazol) and collected in fractions of 0.5 ml. Fractions are analyzed by SDS-PAGE, pooled, concentrated to a final volume of 500 μ l and subsequently subjected to a gel-filtration step using a Superdex S200 10/30 column and eluted with Sec-buffer (10 mM Tris-HCl pH 8.0, 20 % glycerol, 0.05 % DDM, 100 mM NaCl) The pooled fractions were concentrated to a final concentration of 2 mg/ml using Amicon Ultra Centrifugal Filter Devices 10K (Millipore).

2.14 Generation of Nanodisc-SecYEG

To reconstitute SecYEG into Nanodiscs, 600 μ g Apo-A1, 150 μ g SecYEG and 300 μ g lipids were mixed (mass-ratio 4:1:2), reconstitution buffer (20 mM Hepes (pH 7.2), 100 mM KOAc, 6 mM Mg(OAc)₂, 1 mM DTT, 0.1 % DDM) added and incubated at 37 °C for 1h. For the preparation of Nanodiscs without SecYEG, the reconstitution mixture contained an equivalent amount of Sec-buffer instead of SecYEG. Subsequently, detergent was removed with Biobeads (Bio-Rad) for 2h at room temperature. The reconstitution mixture was subjected to a gel-filtration step using a Superdex S200 10/30 column (GE Healthcare) and eluted with NDG-buffer (20 mM Hepes (pH 7.2), 100 mM KOAc, 6 mM Mg(OAc)₂, 1 mM DTT, 10% glycerol). Fractions containing Nanodiscs were pooled and concentrated to 8 pmol/ μ l.

2.15 Binding assays of FtsY to Nanodiscs (Nd-E, Nd-SecYEG)

Purified FtsY (NG+1) was kindly provided by AG Sinning, Heidelberg. For binding experiments, 140 pmol Nd-E and 520 pmol FtsY (NG+1) were mixed in a final volume of 15 μ l in NDG-buffer (20mM Hepes pH 7.2, 100 mM KOAc, 6 mM Mg(OAc)₂, 1 mM DTT, 10 % glycerol) in the presence of 2 mM GMPPnP and incubated for 15 min at 37 °C with shaking. Binding of FtsY (NG+1) to Nd-SecYEG was performed similarly. Here, 520 pmol FtsY (NG+1) were incubated with 140 pmol

Nanodiscs containing 60 pmol of SecYEG (Nd-SecYEG). After that, the sample was incubated for 1h on ice, subsequently loaded on a Superose-6 column (GE Healthcare) and eluted with NDG-buffer under a constant flow of 0.08 ml/min. The eluate is collected in fractions of 100 μ l. For analysis, fractions are subjected to TCA precipitation followed by Western Blotting.

2.16 Purification of *E. coli* 70S RNCs

70S RNCs carrying a nascent FtsQ polypeptide chain were generated using the *in vitro* *E. coli* T7 S30 Extract for Circular DNA (Promega). Ribosomes were programmed with truncated mRNA encoding the 102 N-terminal amino acid fragment of the *E. coli* membrane protein FtsQ with 16 additional C-terminal amino acids. RNCs were then purified using an additional N-terminal His-tag. The DNA encoding the FtsQ-fragment was amplified by PCR using genomic *E. coli* DNA as template and an extended forward primer for introducing a T7 promoter site followed by a high initiation efficiency 5'-untranslated region plus hexa-histidine and HA-tags. The reverse primer defined the length of the nascent chain to the first 102 amino acids of FtsQ and the additional 16 amino acids. mRNA was synthesized using the T7-MEGAShortscript Kit (Ambion) with the DNA-fragments as templates. For translation, two 400 μ l reactions were incubated at 30°C for 30 min. Translation was stopped by transferring the reaction to 4 °C. Each reaction was spun through 300 μ l of a high salt sucrose cushion (50 mM Tris/HCl pH 7.2, 500 mM KOAc, 25 mM Mg(OAc)₂, 5 mM 2-mercaptoethanol, 0.75 M sucrose, 0.1% Nikkol, 500 μ g/ml chloramphenicol, and 0.1% pill/ml [1 pill complete protease mix /ml H₂O, Roche Diagnostics GmbH) at 50000g for 178 min in a TLA 120.2 rotor. Each pellet was resuspended in 1 ml ice cold 250 buffer (50 mM Tris/HCl pH 7.2, 250 mM KOAc, 25 mM Mg(OAc)₂, 5 mM 2-mercaptoethanol, 250 mM sucrose, 0.1% Nikkol, 500 μ g/ml chloramphenicol, 0.2 U/ml RNAsin, 0.1% pill/ml, transferred on 750 μ l of Talon Metal Affinity Resin (BD) and incubated for 20 min at 4 °C. The resin was washed with 10 ml ice cold 250 buffer, and 3 ml 500 buffer (250 buffer but 500 mM KOAc). RNCs were eluted with 2.5 ml 250 buffer supplemented with 100 mM imidazol (pH 7.0). The eluted RNCs were spun through 200 μ l of a high salt sucrose cushion at 50000 g for 137 min in a TLA 100.4 rotor. After the last centrifugation step, the resulting pellet was resuspended slowly in grid buffer (20 mM Hepes (pH 7.2), 50

mM KOAc, 6 mM Mg(OAc)₂, 1 mM DTT, 500 µg ml⁻¹ chloramphenicol, 0.005% Nikkol, 0.5% pill ml⁻¹ and 125 mM sucrose), flash frozen and stored at -80 °C.

2.17 Reconstitution of *E. coli* 70S RNC-Nd-SecYEG complexes

For binding assays, RNC-Nd-SecYEG complexes were reconstituted by incubating 2 pmol RNCs with 20 pmol Nd-SecYEG for 15 min at 37°C in a final volume of 25 µl of buffer D (20 mM Hepes-KOH (pH 7.2), 100 mM KOAc, 10 mM Mg(OAc)₂, 1 mM DTT, 250 µg ml⁻¹ chloramphenicol, 0.5% pill ml⁻¹). Binding was tested by centrifugation through a sucrose cushion followed by SDS-PAGE and SYPRO-Orange stain.

For electron microscopy, RNC-Nd-SecYEG complexes were reconstituted by incubating 10 pmol RNCs with 80 pmol Nd-SecYEG for 15 min at 37°C in a final volume of 90 µl of buffer D (20 mM Hepes-KOH (pH 7.2), 100 mM KOAc, 10 mM Mg(OAc)₂, 1 mM DTT, 250 µg ml⁻¹ chloramphenicol, 0.5% pill ml⁻¹). To remove unbound Nd-SecYEG, the reconstitution mix was spun through a sucrose cushion (20 mM Hepes pH 7.2, 100 mM KOAc, 10 mM Mg(OAc)₂, 750 mM sucrose, 5 mM spermidine, 0.05 mM spermine, 0.5 mM PMSF, 1 mM DTT, 250 µg/ml chloramphenicol). The resulting pellet was resuspended slowly in grid buffer E (20 mM Hepes pH 7.2, 100 mM KOAc, 10 mM Mg(OAc)₂, 1 mM DTT, 250 µg/ml chloramphenicol, 0.5% pill/ml).

2.18 Reconstitution of targeting complexes

To reconstitute targeting complexes involving RNCs, ribosomes, SRP, FtsY and Nanodiscs, several binding assays were performed. Purified SRP and FtsY (wt) were kindly provided by AG Sinning, Heidelberg.

To mimic the targeting situation of ribosomes in the cytosol, 2 pmol of RNCs or ribosomes in reconstitution buffer (20 mM Hepes pH 7.2, 100 mM KOAc, 10 mM Mg(OAc)₂, 0.5 % pill/ml, 1 mM DTT, 250 µg/ml chloramphenicol) were incubated with 20 pmol of SRP in the presence of 2 mM GMPPnP/GTP/GDP or without nucleotide, respectively, for 10 min at 37 °C. To mimic the situation of targeting components located at the membrane, 45 pmol of FtsY were incubated with 60 pmol

Nd-E and Nd-SecYEG, respectively, using the same conditions as described above. Subsequently, RNCs/ribosomes with SRP and FtsY with Nd-E/Nd-SecYEG were combined and incubated for 15 min at 37 °C, followed by an incubation on ice for 30 min. Binding was tested by centrifugation through sucrose cushions (20 mM Hepes pH 7.2, 100 mM KOAc, 10 mM Mg(OAc)₂, 750 mM sucrose, 5 mM spermidine, 0.05 mM spermine, 0.5 mM PMSF, 1 mM DTT, 250 µg/ml chloramphenicol + 0.5 mM GMPPnP/GTP/GDP), followed by TCA-precipitation, SDS-PAGE and SYPRO-Orange staining.

2.19 Negative stain electron microscopy

Grid surfaces were cleaned with a plasma cleaner (Harrick Plasma, USA) at 0.22 Torr for 45 s and 3.5 µl were applied to the grid, incubated for 45 s and subsequently washed with five drops of water. Staining was performed by applying three drops of uranyl acetate (Ted Pella, Inc., USA) to the grid surface for 15 s, followed by the removal of excess staining solution by blotting paper. The grid was allowed to dry on blotting paper for 5 min. Negative stain data was analyzed using a Spirit microscope (FEI Tecnai G12 Spirit 120 kV cryo-microscope) or on a Morgagni microscope (100 kV FEI Morgagni electron microscope).

2.20 Cryo-EM

Samples were applied to carbon-coated holey grids according to standard methods (Wagenknecht et al., 1988). Micrographs were recorded under low-dose conditions on a Tecnai F30 field emission gun electron microscope at 300 kV under low dose conditions with $\sim 20 \text{ e}^-/\text{\AA}^2$ in a defocus range between 1.0 mm and 4.5 mm and scanned on a Heidelberg drum scanner with a pixel size of 1.23 Å on the object scale.

2.21 Image processing

Datasets of the Tecnai F30 microscope were pre-processed using the main SPIDER scripts (Frank et al., 1996). For the determination of the contrast transfer function (CTF) and the defocus values, the script `p_ctffind.nds` (`byteswap.sh`, `p_readmrc.py`, `ctffind.sh`) uses CTFFIND (Mindell and Grigorieff, 2003) was used, which prepares

an image for ctf determination, converts it into the .mrc file format and saved the defocus values for each micrograph in a document. The visual inspection of the power spectra was performed using WEB (Frank et al., 1996) and micrographs displaying bad power-spectra (high drift or astigmatism) were removed from the micsuse file.

Each micrograph contained up to thousands of single ribosomes that have to be selected. For the semi-automated screening for particles using SIGNATURE (Chen and Grigorieff, 2007), the script sig_decimate.nds generated micrographs that were two-fold decimated and converted to mrc format, followed by automated particle picking using the script sig_pick.nds. Screened micrographs were loaded in SIGNATURE and the coordinates for each particle of the micrograph were evaluated and saved. For the isolation of the selected particles, the script p_window.nds uses the determined coordinates and creates a box around the center of the particle with a given boxsize. In order to remove falsely selected particles from good particles by visual inspection with the program WEB, the particles are filtered and decimated using the script p_dcsflt.nds. Bad particles were retracted from the dataset and good particles renumbered by using the script p_copygood.nds. For this dataset, a total of 520 000 particles were selected and used for the reconstruction. A defocus-group document is created using p_makedefgrpfile.nds and micrographs are grouped into defocus-groups with similar defocus-values.

2.22 Alignment and initial 3D-reconstruction

During the first alignment step, three fold decimated particles were aligned using p_alidef.nds to projections of the reference volume of an empty E. coli 70S ribosome in 83 reference projection groups, corresponding to angular steps of 15 °. Here, a cross-correlation based projection matching technique (AP MQ command in SPIDER) was used. For each defocus group, the reference volume was distorted with the corresponding CTF function. Shifts in x and y directions were as large as possible to ensure the proper positioning of each particle. The resulting files contained the alignment information, i.e. best fitting projection group, CCC-values, and the in-plane rotation angles and x,y-shifts in pixels necessary to apply in order to match the projection. The resolution of each defocus group was calculated by comparing backprojected volumes of two random halfsets of each defocus-group. Here, the

Fourier shell correlation was calculated and a cut-off of 0.5 in the resulting curve is used for resolution determination. The final volume was generated by the sum of the CTF-corrected subvolumes of each defocus group, which was filtered to the corresponding resolution and used as an initial volume in the refinement procedure.

2.23 Refinement and sorting

In the refinement process, the particles were iteratively aligned to the new reference volume generated in the precedent alignment/refinement round. The resulting volume was masked, filtered and used as an input for the following round of refinement. During the refinement-process, a more accurate sampling of the projections was performed by decreasing the angular increments and restrictions, which results in an increasing number of possible angular projection groups and leads to improved resolution. Meanwhile, a variety of filter parameters and alignment algorithms were applied. Supervised sorting was used to sort for the presence of Nd-SecYEG. Here, a volume without Nanodisc was manually created by removing the Nanodisc-density. Thus, a volume with Nanodisc-density and a volume without Nanodisc-density were offered for alignment to the particles, leading to two different cross correlation coefficients for each particle. The cross correlation coefficients were compared and, dependent on the best match sorted into two subsets and back-projected separately. This procedure was repeated iteratively until particles stabilized in each subset. 85,664 particles from the *E. coli* RNC-Nd-SecYEG dataset were used for the final CTF-corrected reconstruction with the resolution of 7.1 Å based on the Fourier shell correlation with a cutoff value of 0.5. The dataset was processed on a high performance Intel/Opteron computer cluster comprising several hundred processors.

2.24 Modeling and MDFF

Models of the *E. coli* 70S structure and tRNA, obtained by X-ray (Berk et al., 2006) (PDB: 2I2V) and cryo-EM (Seidelt et al., 2009) (PDB: 2WWL, 2WWQ), were fitted into the density and refined by molecular dynamics flexible fitting (MDFF) (Trabuco et al., 2008). MDFF was performed in collaboration with James C. Gumbart from the Klaus Schulten Lab (University of Illinois, USA). MDFF is a method to flexibly fit atomic models into cryo-EM density maps while simultaneously preserving the

stereochemical accuracy of model. In MDFF, the atomic model is simulated using molecular dynamics in the presence of the cryo-EM density map, represented through an additional potential in the simulation. From this potential, forces proportional to the gradient of the cryo-EM density are derived that then drive atoms into high-density regions of the map. In addition, restraints are applied to maintain the secondary structure of protein and RNA molecules, which otherwise would distort or break under the forces required for fitting. Fitting of the 70S proceeded in stages and a total simulation time of 3.5 ns was used to fit the ribosome.

2.25 Fitting of SecYE and nascent FtsQ

Based on the structure of the *T. maritima* SecYEG (Zimmer et al., 2008) (PDB: 3DIN), an *E. coli* SecYE homology model was created using HHpred (Soding et al., 2005). Since α -helical secondary structures are resolved within the membrane environment, a highly reliable rigid body fit was obtained by aligning the model according to known ribosomal connections based on L8/9 and L6/7 of SecY and on characteristic secondary features of densities representing TM helices 6,8,9. Minor adjustments of the TM helices were carried out using Coot (Emsley and Cowtan, 2004). The N-terminal TM helices of SecE were placed into two additional rod-like densities, the position of which is in agreement with the 2D crystal structure of the SecYEG (Bostina et al., 2005; Breyton et al., 2002). These outlying helices have initially been attributed to SecG (Breyton et al., 2002), but in a later paper, after fitting the *M. jannaschii* structure into the map, reassigned as the two N-terminal TM helices of SecE (Bostina et al., 2005). An ab-initio model of the nascent chain was created using PyMol (<http://www.pymol.org>) and manually fitted into the cryo-EM density using Coot. The combined SecYE-nascent-chain model was refined using MDFF in the presence of the full ribosome, which was constrained during the fitting.

2.26 Model and fitting of the Nanodisc

A model of nascent discoidal HDL (Wu et al., 2007) was used as a template to generate a model for Nd-SecYEG containing 75 % phosphatidylethanolamine and 25 % phosphatidylglycerol.

In the model, non-structured elements of the so-called “solar-flares” were replaced by a corresponding α -helix with the same amino-acid-sequence. The Nanodisc model was manually fitted into the density. The lipid bilayer was added to the model with an initially flat profile. Lipids overlapping with SecYE were removed. No MDFF was performed for the Nanodisc proteins or lipid.

2.27 Figures

Densities for the large and small ribosomal subunit, the P-site tRNA, the nascent FtsQ-chain, the *E. coli* SecYE and the Nanodisc-Lipid-Bilayer were isolated using the color zone function of Chimera (Pettersen et al., 2004). A lower contour level of the ligand densities for surface representation was applied for some figures. This indicates that ligand densities are partially flexible or still under-represented because of incomplete removal of ligand-free ribosomal particles from the final particle subset.

2.28 Simulations

All MD simulations and MDFF were performed in collaboration by James C. Gumbart (University of Illinois) and carried out using NAMD 2.7b1 (Phillips et al., 2005) and the CHARMM27 force field with CMAP corrections (Foloppe et al., 2000; MacKerell et al., 1998; Mackerell et al., 2004). Simulation protocols, including multiple time-stepping and particle mesh Ewald, are identical to those used in Gumbart et al. (Gumbart et al., 2009). After completion of modeling and MDFF, the resulting ribosome-Nanodisc model was used for further equilibrium simulations. Water and ions were added in an iterative procedure using VMD (Humphrey et al., 1996). To reduce simulation complexity and to focus on the interactions between the ribosome and SecYE and Nanodisc, the ribosome and nascent chain were truncated just downstream of the L4/L22 constriction point. Any ribosomal backbone atoms within 5 Å of the truncation point were constrained. At the point of closest approach, SecYE was at least 25 Å away from the truncation point. While previous simulations of the ribosome-SecY complex required 2.7 million atoms (Gumbart et al., 2009), simulation of the truncated ribosome-Nanodisc complex required only 400,000 atoms.

Equilibration of the system occurred in stages. First, only the lipid tails were allowed to move, permitting them to “melt”, for 0.25 ns. Next, water and sidechains were released for an additional 2.25 ns. For the next 1.5 ns, only the encircling Apo A-1 proteins of the Nanodisc were constrained; the secondary structure of all proteins and RNA was also enforced during this time, and for a further 2 ns. Finally, after 6 ns of total simulation time, all restraints were released. At all times, a constant temperature of 310 K and a constant pressure of 1 atm were maintained.

3. Results

To visualize the SecYEG complex in its natural environment, it was crucial to establish the purification of SecYEG and Apo-A1. Subsequently, the conditions for the self-assembly of Nanodiscs with Apo-A1 and *E. coli* lipids had to be ascertained. These initial experiments would set up the basis for the incorporation of the SecYEG complex into the Nanodiscs.

3.1 Purification of Apo-A1

Two copies of Apo-A1 are believed to form a belt-like structure that wraps around a disk-like membrane bilayer, thus forming nascent discoidal HDL/ Nanodiscs. Overexpression and purification of Apo-A1 were essentially carried out as described before (Bayburt et al., 2002). After sonification of cells overexpressing Apo-A1, the cleared lysate was subjected to affinity chromatography (Figure 10a). Apo-A1 eluted as a sharp peak. Fractions containing Apo-A1 were pooled, dialyzed and subsequently analyzed by SDS-Page (Figure 10b). One liter of culture yielded about 20 mg of purified Apo-A1.

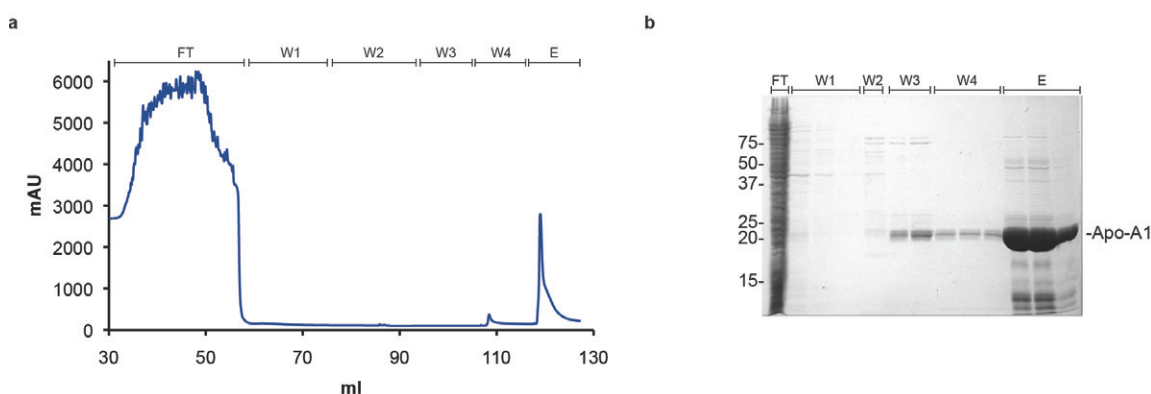


Figure 10: Purification of Apo-A1 | (a) Elution profile of the Ni-NTA affinity chromatography of Apo-A1. The various purification steps are indicated (FT: flowthrough, W1: wash1, W2: wash2, W3: wash3, W4: wash4, E: elution, see Material and Methods)

3.2 Purification of SecYEG

It is possible to overexpress SecYEG to approximately 20 % of the total inner membrane protein mass (van der Does et al., 2003). After solubilization from the membrane, nonsolubilized material was removed by centrifugation, whereas the supernatant was loaded on an anion-exchange column (Figure 11 a). After an initial washing step, the protein was gradually eluted by applying a linear gradient of 0 – 300 mM KCl. SecYEG started to elute at KCl concentration of 100 mM KCl, yet became highly impure starting at KCl concentrations around 200 mM (Figure 11b). Therefore, fractions in the range of 100 – 200 mM NaCl concentration were pooled and subsequently applied to NiNTA affinity purification.

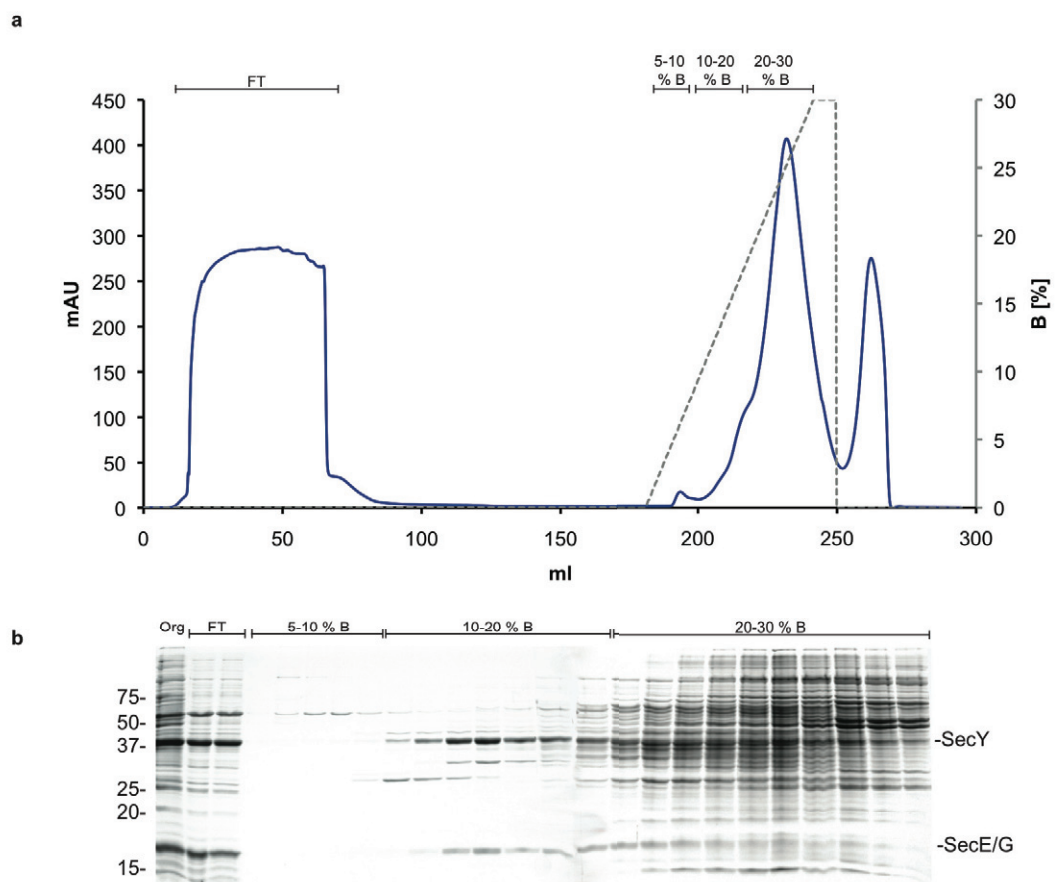


Figure 11: Purification of SecYEG, anion exchange chromatography | (a) Elution profile of the purification of SecYEG on a DEAE column. The concentration of buffer B is indicated on the y-axis on the right. (b) SDS-PAGE of the elution shown in (a).

The pooled fractions were loaded on a NiNTA affinity resin and eluted by applying a step gradient of 500 mM imidazol, leading to the elution of pure SecYEG (Figure 12a). Fractions containing SecYEG were pooled, concentrated and applied to a size-exclusion chromatography, eluting with a distinct peak at 13 ml elution volume, indicating a homogenous sample (Figure 12c,d). One liter of culture yielded about 0.25 mg of highly purified SecYEG.

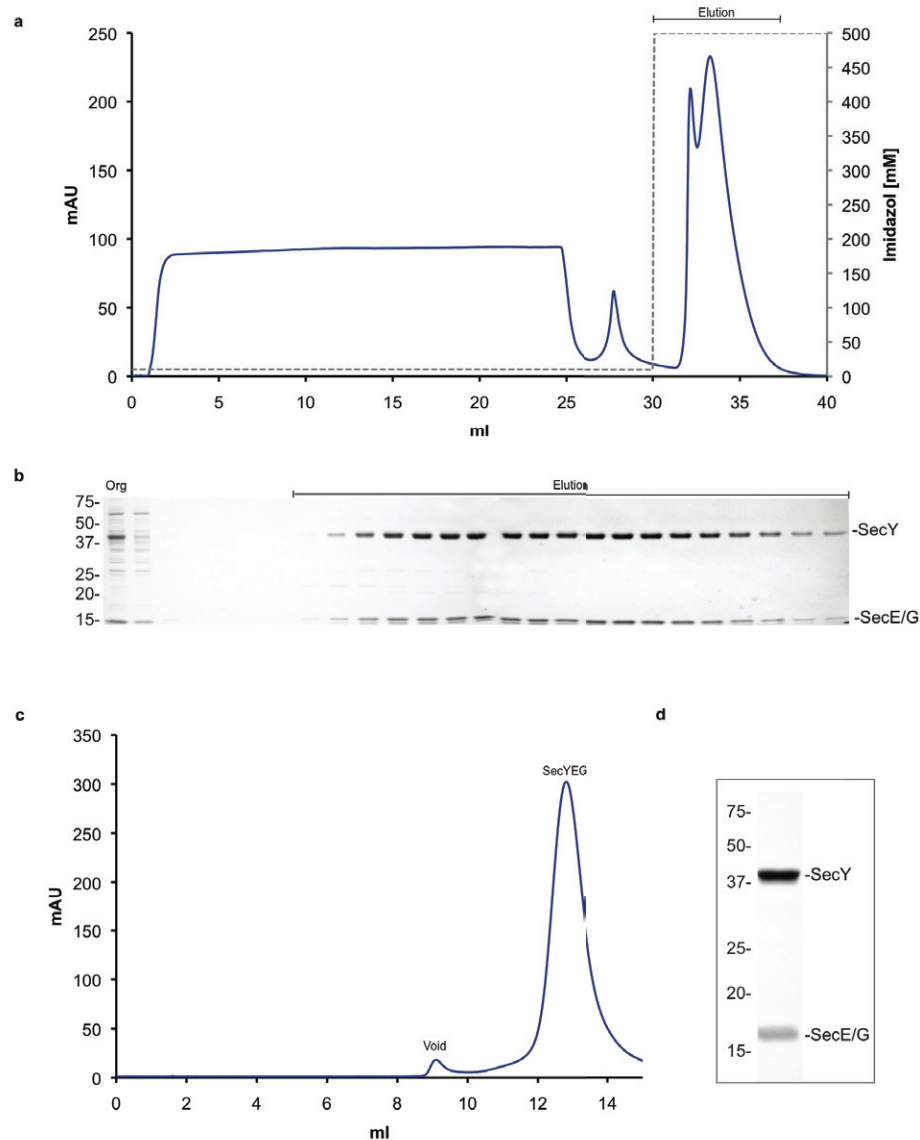


Figure 12: Affinity and size-exclusion chromatography of SecYEG. (a) Elution profile of the affinity chromatography with Imidazol concentrations on the y-axis on the right. (b) SDS-PAGE of the eluted fractions of the affinity chromatography. (c) Size-exclusion chromatography of the pooled fractions from affinity chromatography. (d) SDS-PAGE of the pooled fractions containing SecYEG from the size-exclusion chromatography.

3.3 Nanodisc assembly

Prior to incorporating SecYEG into Nanodiscs, the general assembly conditions had to be established. The few protocols for the generation of Nanodiscs published by the Sligar-Lab so far varied a lot within the conditions for the self-assembly of the Nanodiscs. Furthermore, all Nanodiscs reported to date had been composed of only one or two defined types of lipids. Since a more natural environment for the SecYEG complex was considered eligible, I used *E. coli* total lipid extract for the formation of Nanodiscs. Accordingly, a new protocol had to be established (see Material and Methods). Summarized briefly, for the generation of *E. coli* lipid Nanodiscs, 600 µg Apo-A1 and 300 µg lipids were mixed (mass-ratio 2:1), reconstitution buffer added and incubated at 37 °C for 1h. Subsequently, detergent was removed with Biobeads for 2h at room temperature. The reconstitution mixture was subjected to a gel-filtration step using a Superdex S200 10/30 column and eluted with NDG-buffer. Hereby, two main peaks were evident (Figure 13a,b). The Stokes diameters of the particles were estimated on a Superdex200 size-exclusion column calibrated with a standard set of globular proteins with known size (see Material and Methods). According to the calibration, the diameters of particles corresponding to the first peak at 11.5 ml elution volume was estimated to be around 11 nm, which is in agreement with previously reported elution behaviour and size of Nanodiscs. The second peak at 13.2 ml would correspond to particles with an estimated particle diameter of 8 nm. Negative stain images from particles of the first peak revealed discoidal particles with an average size of around 10 – 12 nm (Figure 13c). Since the shape, elution behaviour and estimated size of particles from the first peak were in perfect agreement with data published on Nanodiscs so far, we concluded that these particles indeed were Nanodiscs. The second peak is likely to be formed of non-lipidated Apo-A1 (see discussion).

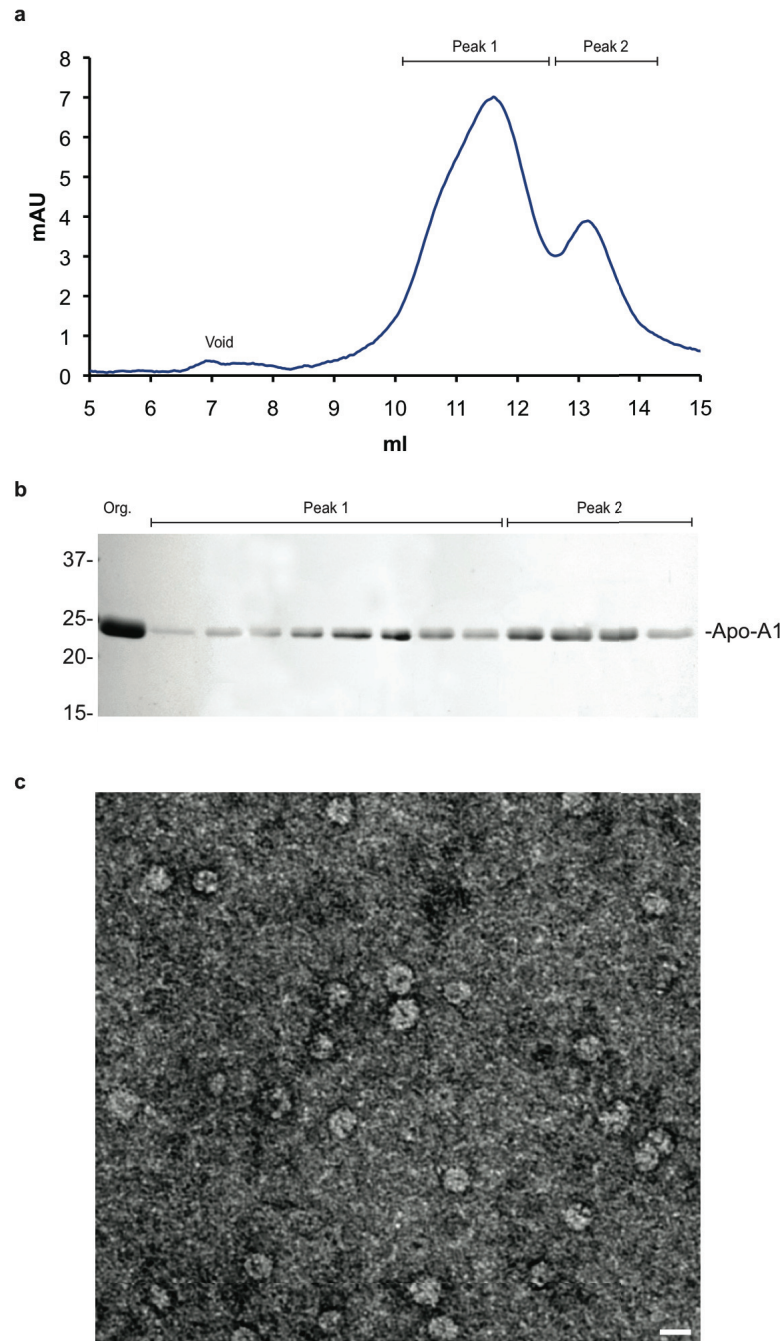


Figure 13: Reconstitution of Nanodiscs. (a) Typical protein elution profile obtained after size-exclusion chromatography of a Nanodisc preparation. (b) The fractions corresponding to elution volume 10–15 ml in (A) were analyzed by SDS-PAGE, followed by Coomassie blue staining of the gel. (c) Negative stain of particles eluted in Peak 1, displaying a discoidal shape with an apparent size of 10 nm, The scale bar represents 10 nm.

Further experiments assessing the usability of Nanodiscs were performed. These involved several freeze (-20° C, -80 °C) and thawing steps of concentrated Nanodiscs, followed by quality control with size-exclusion chromatography and negative-stain EM-data (data not shown). Nanodiscs appear to be robust regarding freezing and thawing, indicating that they display water-soluble model-membranes that, regarding experimental set-ups, can be treated like a soluble protein.

3.4 Incorporation of SecYEG into Nanodiscs

After determining the conditions for the self-assembly of Nanodiscs, the next step was the reconstitution of SecYEG into Nanodiscs. Noteworthy, the protocol for the self-assembly of NdE could be used without major changes, i.e. 600 µg Apo-A1, 150 µg SecYEG and 300 µg lipids were mixed (mass-ratio 4:1:2), reconstitution buffer added and incubated at 37 °C for 1h. After detergent removal with biobeads, the mixture was subjected to size-exclusion chromatography, leading to two distinct peaks at 11 ml and 13.5 ml. According to their elution behaviour, the stokes diameters of the particles eluting in the first peak corresponded to a size of estimated 12 nm, whereas the size of particles eluting in the second peak remained at a size of 8 nm (Figure 14a).

SDS-PAGE analysis revealed that SecYEG was only found in particles eluting in the first peak (Figure 14b). Accordingly, the membrane protein complex associated with Apo-A1 in such way to form water-soluble Nanodiscs with incorporated SecYEG (Nd-SecYEG). As can be deduced from the SDS-PAGE analysis, particles from fractions of the first peak contain a mixture of both Nd-E and Nd-SecYEG, since the intensity of the bands from Apo-A1 is much higher than the intensities of the SecY and SecE/G bands, respectively (Figure 14b). The ratio of Nd-E/Nd-SecYEG obtained by standard preparations ranged from 4:1 to 1:1 (data not shown). Negative-stain data of particles eluting in the first peak displayed discoidal particles with an average size of 10-12 nm, similar to negative-stain data of Nd-E (Figure 14c). The limited resolution of the negative-stain images does not allow for the tracing of incorporated SecYEG.

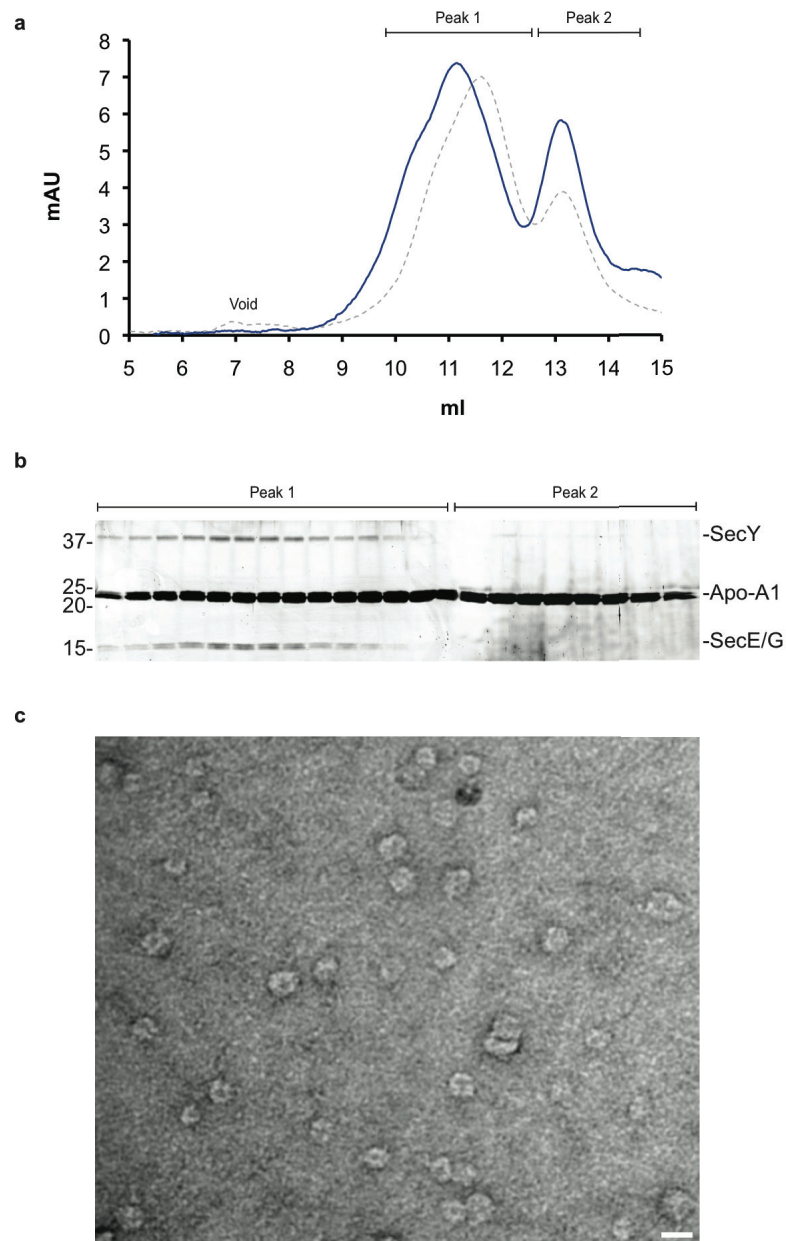


Figure 14: Reconstitution of the SecYEG complex into Nanodiscs | (a) Typical protein elution profile obtained after size-exclusion chromatography of a SecYEG–Nanodisc preparation. (b) The fractions corresponding to elution volume 10–16 ml in (a) were analyzed by SDS–PAGE, followed by Coomassie blue staining of the gel. (c) Negative stain of particles eluted in Peak 1, displaying a discoidal shape with an apparent size of 10 nm, The scale bar represents 10 nm.

3.5 Binding studies of Nanodiscs

Targeting of a ribosome carrying a hydrophobic signal sequence of a membrane protein to the membrane occurs upon binding of SRP to both the signal sequence and the ribosome. Subsequently, the ribosome-nascent-chain (RNC)–SRP complex is directed to the membrane upon interaction with its receptor FtsY. FtsY can be found in a soluble and in a membrane-bound state. In order to address the membrane properties of the Nanodiscs, *in-vitro* binding assays were performed. These involved the binding of FtsY to lipid-only Nanodiscs (Nd-E) and to SecYEG embedded in Nanodiscs (Nd-SecYEG), since it has been shown that FtsY also binds to the SecYEG complex (Angelini et al., 2006; Angelini et al., 2005). For these studies, a truncated FtsY mutant lacking the so-called A-domain (FtsY-NG+1) was used, since its smaller molecular size (34 kDa) compared to the wild-type version of FtsY (54 kDa) was more suitable for the set-up of the binding assay using size-exclusion chromatography. The FtsY-NG+1 mutant is functional *in vivo* (Eitan and Bibi, 2004).

3.5.1 Binding of FtsY to Nd-E

FtsY was bound *in vitro* to Nd-E and the putative complex mixture was subjected to an analytical size-exclusion chromatography followed by SDS-PAGE and Western-Blot analysis of the fractions. For these experiments, FtsY was incubated with GMPPnP, since it had been shown that in the presence of the nonhydrolysable GTP analogue GMPPnP, a significantly larger portion of FtsY was bound to membranes (Angelini et al., 2006). Prior to the binding assay, the elution behaviour of FtsY and Nd-E were evaluated on Superose6-column (Figure 15a)

Nd-E elutes at 1.6 ml. In contrast, due to its smaller size of 34 kDa, FtsY-NG+1 elutes later and appears as a separate peak at 1.9 ml elution volume. For the initial binding, Nd-E was incubated at 37 °C with a three-fold excess of FtsY-NG+1 (see Material and Methods), the binding mixture was loaded onto the column and two distinct peaks were apparent, corresponding to fractions containing Nd-E (1.6 ml) and FtsY-NG+1 (1.9 ml). It has to be noted that the resolution of the column was too low to separate a complex of Nd-E/FtsY-NG+1 from Nd-E.

To determine a possible co-elution and thus complex formation of Nd-E/FtsY-NG+1, fractions from the corresponding Nd-E and FtsY-NG+1 peaks were further analyzed

by Western Blotting (Figure 15b). Stunningly, FtsY indeed co-eluted with Nd-E in similar amounts, which suggests the binding of FtsY-NG+1 to Nd-E and results in the formation of a complex. This indicates that Nanodiscs exhibit membrane-like features that are capable of forming a complex with the membrane-associated protein FtsY.

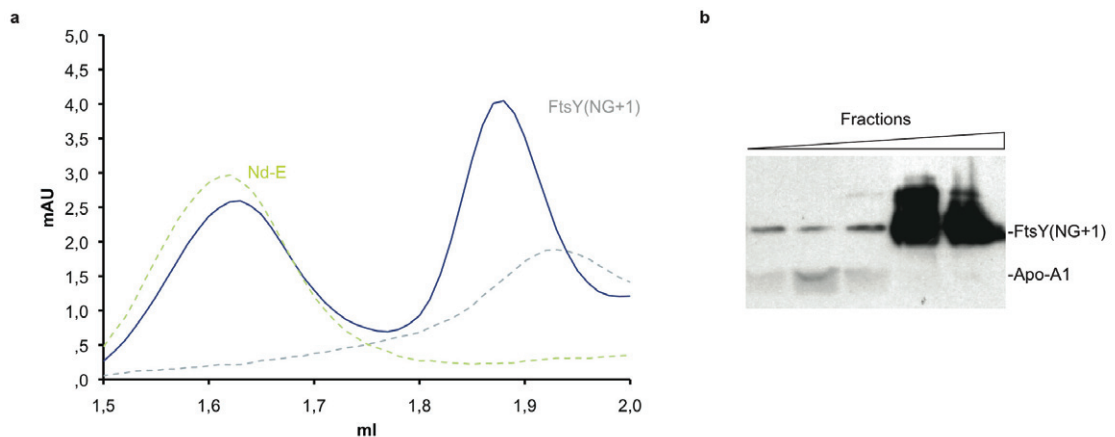


Figure 15: Binding of FtsY(NG+1) to lipid Nanodiscs | (a) Size-exclusion chromatography of a mixture of Nanodiscs (green) and FtsY(NG+1) (grey), mixture in blue. (b) Western blot of subsequent fractions of the size-exclusion chromatography shown in (a), using anti-His antibody.

3.5.2 Binding of FtsY to Nd-SecYEG

In addition to its interaction with the membrane, FtsY also binds to SecYEG (Angelini et al., 2006; Angelini et al., 2005). To test whether SecYEG embedded in Nanodiscs also displays a binding site for FtsY, binding assays using FtsY-NG+1 and Nd-SecYEG were performed as described before.

Again, two peaks were apparent which correspond to fractions containing Nd-SecYEG (1.6 ml) and FtsY-NG+1 (1.9 ml) (Figure 16a). Fractions from the corresponding Nd-SecYEG and FtsYNG+1 peaks were further analyzed by Western Blotting (Figure 16b). As far as interpretation from a WB allows, it appears as if the binding of FtsY to Nd-SecYEG was even enhanced compared to its interaction with Nd-E, indicating a binding of FtsY to both the membrane surface and the SecYEG complex.

While binding of FtsY(NG+1) to Nd-E is based on protein-lipid interactions, the enhanced binding of FtsY(NG+1) to Nd-SecYEG is most likely due to both protein-lipid and protein-protein interactions.

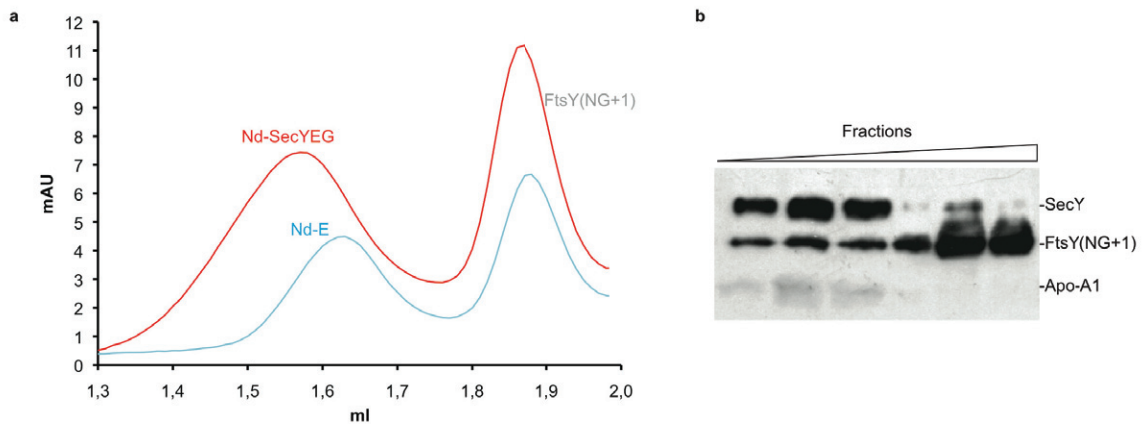


Figure 16: Binding of FtsY(NG+1) to Nd-SecYEG | (a) Size-exclusion chromatography of a mixture of Nd-SecYEG and FtsY(NG+1) mixture in red, compared with the elution absorption profile of the mixture of lipid nanodiscs and FtsY(NG+1) in blue. (b) Western blot of subsequent fractions of the size-exclusion chromatography shown in (a), using anti-His antibody.

3.6 Purification of ribosome-nascent-chain complexes

To investigate the interaction of a translating ribosome with the membrane-embedded SecYEG complex, *E. coli* ribosomes carrying an elongation arrested nascent chain had to be purified. Previously, it has been shown that the nascent membrane protein FtsQ contains an N-terminal signal-anchor transmembrane helix that inserts co-translationally into the membrane and remains in contact with SecY and lipids after insertion (Urbanus et al., 2001). Thus, this well characterized type-II membrane protein was used to purify RNCs. Hereby, mRNA that encodes for the N-terminal 102 residues of FtsQ including the signal anchor sequence and 16 additional C-terminal amino acids, preceded by an HA-tag for WB detection and a His-tag for affinity purification (Figure 17, and Appendix) was used. By using a truncated message, ribosomes were stalled at the end of the mRNA with peptidyl-tRNA in the P-site.

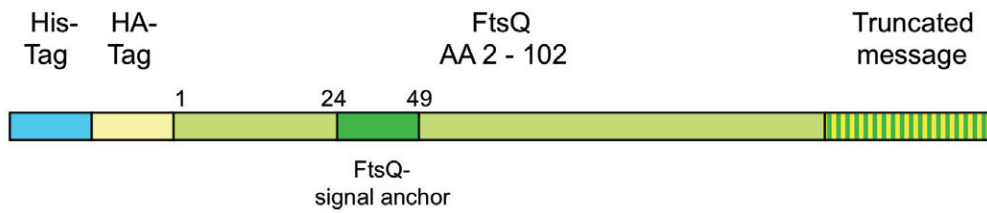


Figure 17: Scheme of the construct for the elongation arrested nascent chain of a FtsQ derivative.

RNCs were purified as described in Material and Methods. Briefly, RNCs were isolated by ultracentrifugation through a sucrose cushion, followed by affinity-purification using metal-affinity chromatography and an additional ultracentrifugation step. The purification steps were analyzed by TCA-precipitation of relative equal amounts of the corresponding fractions followed by Western Blotting (Figure 18). By comparing the intensity of the signal for peptidyl-t-RNA (i.e. RNCs) before purification (R) and after purification (E), an enrichment of RNCs is visible. A standard RNC preparation led to 43 pmol of RNCs (450 nM).

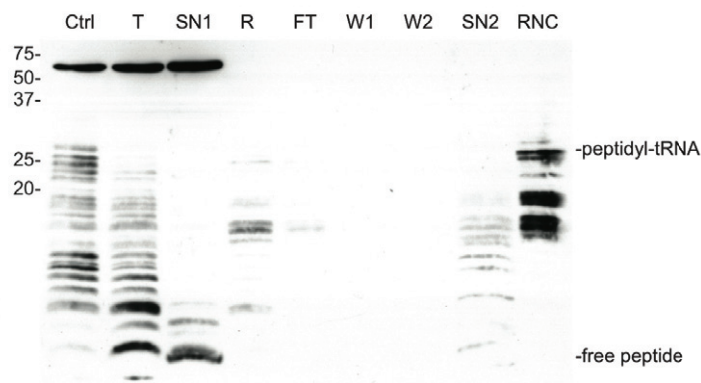


Figure 18: RNC purification | Western Blot of TCA-precipitated samples of the RNC purification procedure, with the negative control of solely the translation extract (ctrl), the translation reaction (T), supernatant of the first centrifugation step (SN1), the ribosomal pellet (R), the flow-through of the purification on a Talon-Matrix (FT), low-salt washing (W1), high salt washing (W2), the supernatant of the second centrifugation step (SN2) and the resulting RNC pellet (RNC).

3.7 Binding assays of RNCs

In order to investigate the behaviour of Nanodiscs and SecYEG embedded in Nanodiscs with respect to co-translational membrane targeting, several reconstitution assays with ribosomes, RNCs and factors involved in co-translational targeting such as FtsY and SRP were performed. So far, co-translational targeting studies that involve model membranes have been carried out using proteoliposomes (Grudnik et al., 2009). In an initial experiment, empty 70S ribosomes were reconstituted with an excess of Nd-SecYEG. Binding of empty ribosomes to the monomeric SecYEG complex in the membrane is not detectable (Figure 19a). Subsequently, nascent FtsQ-carrying RNCs were reconstituted (i) with an excess of Nd-SecYEG and (ii) with an excess of Nd-E and used in binding assays to test whether the RNC-Nanodisc interaction was dependent on SecYEG. Stable binding of RNCs was observed only in the presence of Nd-SecYEG (Figure 19b), indicating that neither the ribosome nor the SA domain of the nascent FtsQ could interact with, or insert into the lipid bilayer in a SecYEG-independent manner.

Taken together, the presence of both the nascent chain and of SecYEG embedded in the Nanodisc are required for a proper interaction of ribosomes with the model membrane.

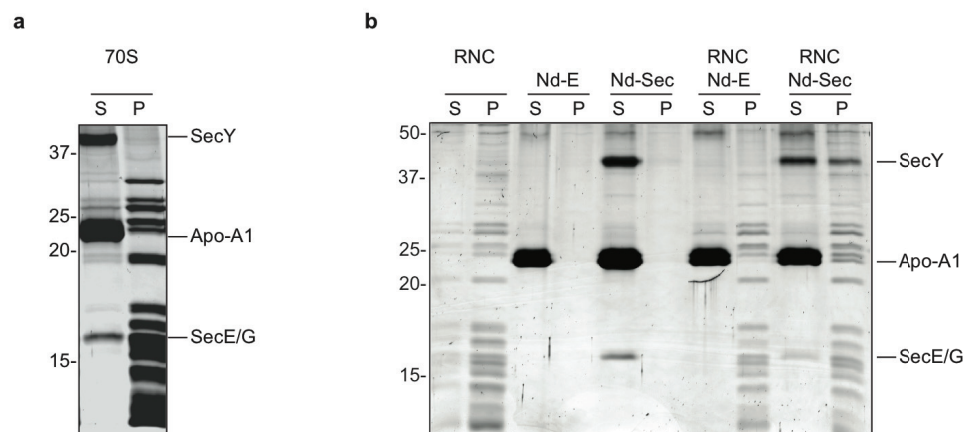


Figure 19: Reconstitution assays | (a) Binding assay using purified 70S ribosomes (inactive) with an excess of Nd-SecYEG. Supernatant (S) and pellet (P) fractions were analyzed by SDS-polyacrylamide gel electrophoresis and SYPRO orange staining. (b) Binding assay using purified RNCs carrying the nascent FtsQ chain with an excess of Nd-E and Nd-SecYEG, respectively.

3.8 Targeting complex formation

According to the initial experiments where a binding of FtsY to Nd-E and to Nd-SecYEG was observed, further investigations should shed new light on the interaction of putative targeting complexes in the presence of a Nanodisc.

At the outset, targeting of RNCs to the membrane was investigated. Hereby, RNCs carrying a nascent chain with the first 102 residues representing the N-terminus of the membrane protein FtsQ, were incubated with SRP in the absence or presence of the non-hydrolysable GTP-analogue GMPPnP, GTP and GDP for 10 min at 37 °C. Simultaneously, Nd-E mimicking the bacterial plasma membrane and FtsY were also incubated in the same manner. Subsequently, RNC with SRP and Nd-E with FtsY were combined and incubated for 15 min at 37 °C, followed by incubation on ice for 30 min.

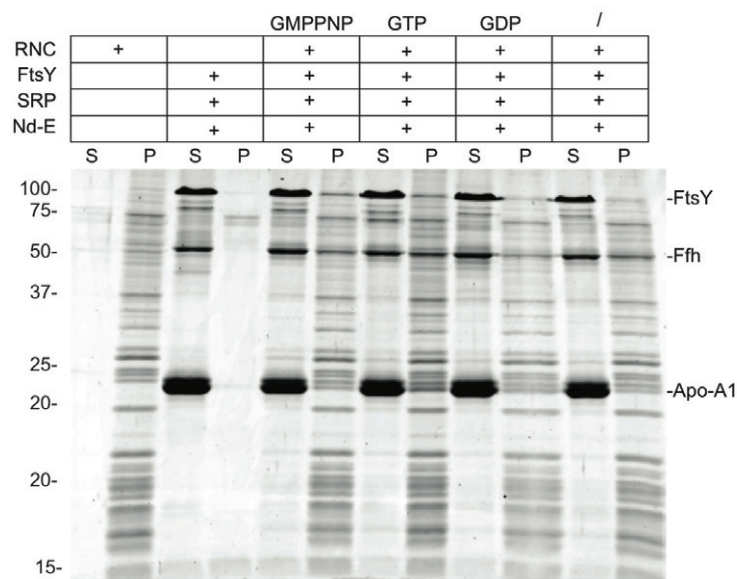


Figure 20: Targeting complex formation | Binding assays using purified RNCs carrying the nascent FtsQ chain were incubated with FtsY, SRP and Nd-E in the presence of GMPPnP, GTP, GDP or without nucleotides.

In the presence of GMPPnP, equimolar amounts of SRP, FtsY and Nd-E bind to the RNCs, indicating that all components of the targeting machinery form a stable complex that mimic a targeting complex in the presence of a membrane (Figure 20, lane 3). Exchanging the non-hydrolysable GTP-analogue with GTP does not lead to a change in the binding pattern and apparently still leads to the formation of a targeting complex (Figure 20, lane 4). In contrast, in the presence of GDP or in the absence of

guanine nucleotides, the binding of SRP and Nd-E to RNCs remains unchanged whereas the binding of the bacterial SRP-receptor FtsY to the complex was almost abolished (Figure 20, lane 5,6). These experiments indicate the formation of a complex of RNCs, SRP, FtsY and the membrane in a GTP-dependent manner.

In consecutive experiments, binding of RNCs and empty ribosomes, SRP, FtsY and the membrane in the presence of guanine nucleotides and SecYEG was assayed. The conditions for binding were as described before. In the presence of the non-hydrolysable GTP-analogue GMPPnP, all components bound in equimolar amounts to the RNCs (Figure 21, lane 4). Interestingly, hardly any binding of FtsY could be observed in the presence of GTP, whereas the binding of SRP and Nd-SecYEG to RNCs did not seem to be affected (Figure 21, lane 5). Furthermore, binding of SPR, FtsY and Nd-SecYEG to empty ribosomes in the presence of GMPPnP was weak when compared with the binding pattern of RNCs (Figure 21, lane 6).

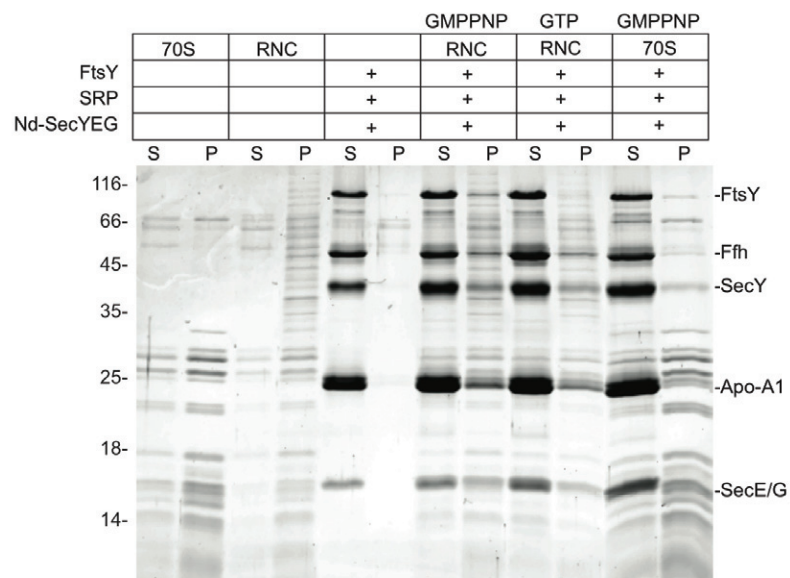


Figure 21: Tertiary complex formation | Binding assays using purified RNCs carrying the nascent FtsQ chain as well as empty 70S ribosomes were incubated with FtsY, SRP and Nd-SecYEG in the presence of GMPPnP and GTP.

3.9 Reconstitution of a RNC-Nd-SecYEG complex

Stable binding of RNCs was observed only in the presence of Nd-SecYEG (Fig. 19b), indicating that neither the ribosome nor the SA domain of the nascent FtsQ could interact with, or insert into the lipid bilayer in a SecYEG-independent manner. This indicates that the reconstituted complexes indeed represented RNC-Nd-SecYEG complexes. Negative-stain data of the reconstituted complex displayed the typical appearance of 70S ribosomes (Figure 22).

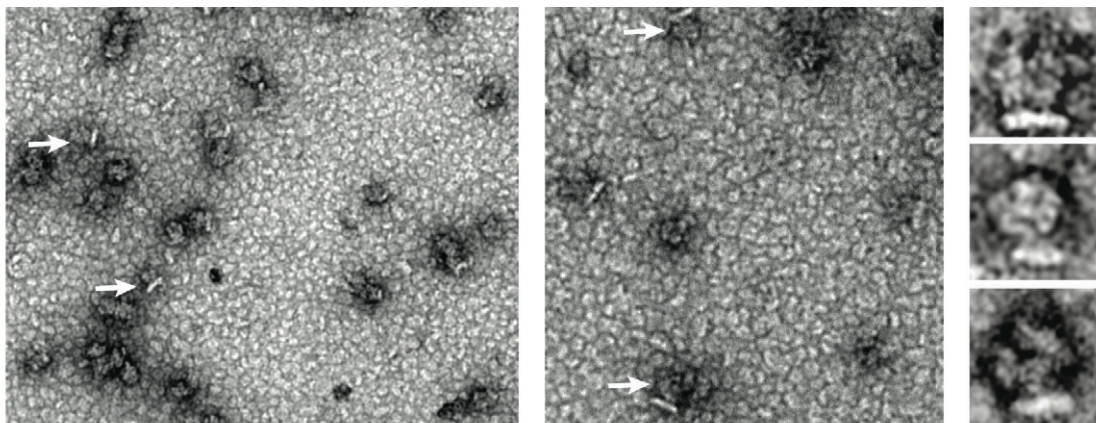


Figure 22: Negative stain of the reconstituted 70S-RNC-Nd-SecYEG complex | 70S-RNCs were incubated with an excess of Nd-SecYEG. 70S-RNC-Nd-SecYEG complexes are indicated with arrows. Nd-SecYEG appears as an extra density at the ribosomal exit-site with a planar shape (shown in increasing magnifications from left to right).

Some of these display an extra density, which appears as a disc-like structure viewed from the side (Figure 22). Furthermore, the surface of the grid is covered with Nanodiscs. Initial reconstructions of cryo-EM samples displayed a Nanodisc-like structure beneath the ribosomal exit site at low resolution (data not shown). Yet, it was impossible to obtain higher resolution data since the large amount of unbound Nanodiscs on the grids led to a high background signal in the reconstructions.

Thus, removing unbound Nanodiscs from the reconstituted complex was a prerequisite for high-resolution data collection. After the reconstitution, the sample was spun through a sucrose cushion. Unbound Nanodiscs remained in the supernatant (Figure 23a), whereas RNCs with bound Nd-SecYEG were found in the pellet (Figure 23b).

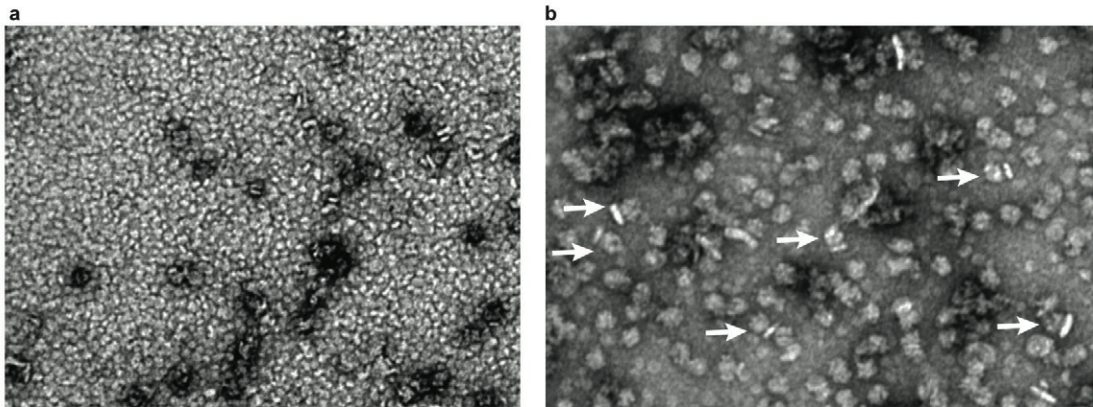


Figure 23: Sample preparation for the reconstitution of the 70S RNC-Nd-SecYEG complex | (a) Negative stain of the supernatant of a reconstitution mixture of RNCs and Nd-SecYEG. Unbound Nanodiscs cover the whole surface of the grid. (b) Negative stain of the pellet fraction of the reconstitution mixture. Only RNC-bound Nd-SecYEG is visible.

After automated particle picking followed by visual inspection, a dataset of 520,000 particles was processed with the SPIDER software package and classified into a subset according to Nd-SecYEG presence. 85,664 particles from the *E. coli* RNC-Nd-SecYEG dataset were used for the final CTF-corrected reconstruction with the resolution of 7.1 Å based on the Fourier shell correlation with a cutoff value of 0.5 (Figure 24).

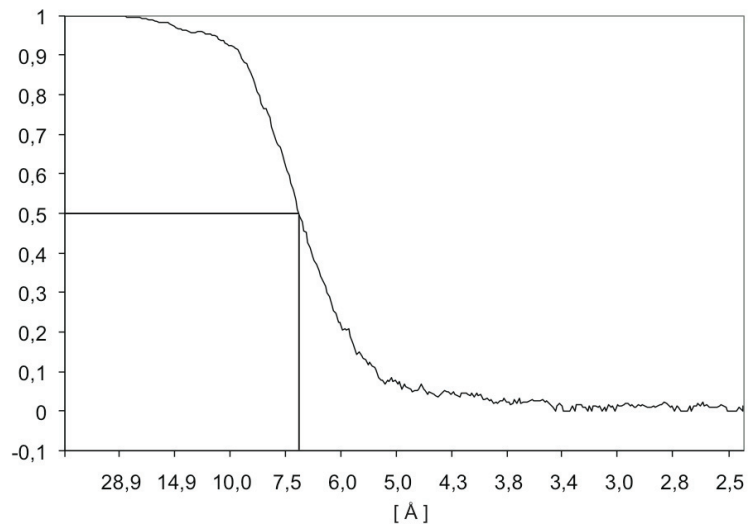


Figure 24: Resolution | Fourier shell correlation (FSC) curve for the cryo-EM reconstruction of the *E. coli* 70S-RNC-Nd-SecYEG complex with a resolution of 7.1 Å using the FSC-0.5-criterion.

3.10 Cryo-EM reconstruction of the 70S-RNC-Nd-SecYEG complex

The cryo-EM reconstruction of this complex shows the appearance of a programmed 70S ribosome at 7.1 Å resolution with an additional disc-like density beneath the ribosomal exit site (Figure 25). This density had a diameter of 10-12 nm and a height of about 4.3 nm, tethered by several contacts to the ribosome.

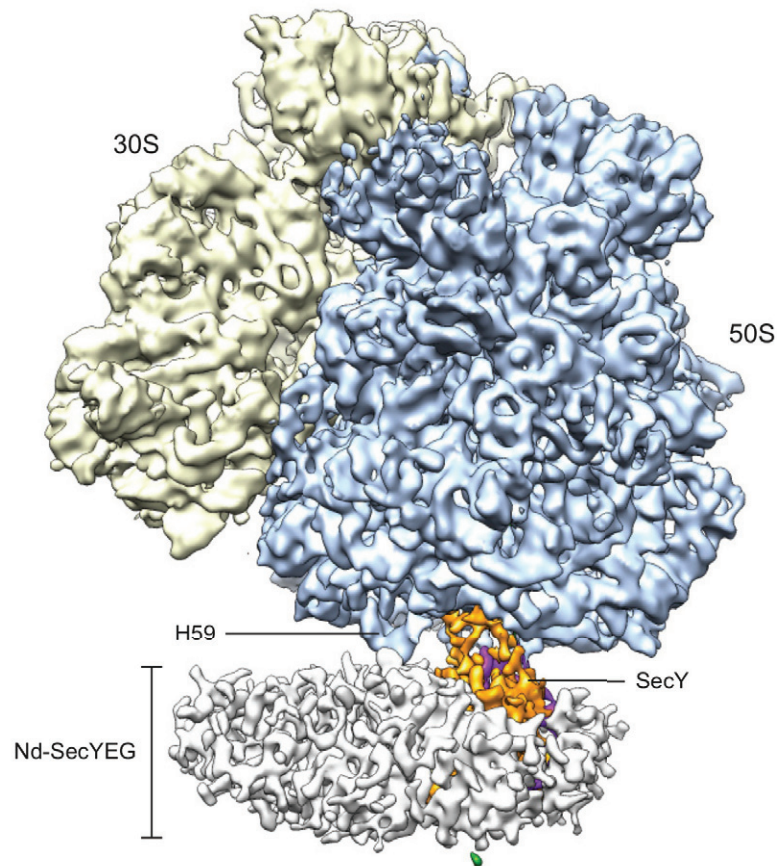


Figure 25: Cryo-EM reconstruction of the active 70S-RNC-Nd-SecYEG complex at 7.1 Å resolution | The ribosomal 30S subunit is shown in yellow, the 50S subunit blue, SecY orange, SecE purple, Nanodisc white.

The appearance of a clear tRNA density in the P-site confirmed the presence of the nascent FtsQ chain as peptidyl-tRNA. It was possible to visualize the density of the nascent chain within the ribosomal exit tunnel reaching from the peptidyl-transferase center (PTC) into the Nd-SecYEG density (Figure 26). The ribosome contacted the Nd-SecYEG density via several connections, yet, leaving a gap on one side of about 15-25 Å between the ribosome and the Nd-SecYEG.

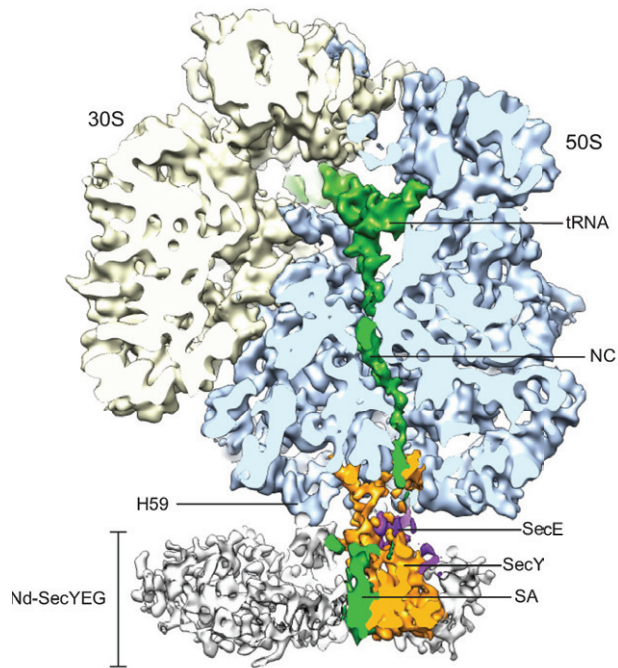


Figure 26: Following the nascent chain from PTC into the membrane | Density as in (b), but cut perpendicularly to the plane of the membrane along the polypeptide exit tunnel, colours as in b with P-site tRNA and nascent polypeptide chain green.

To interpret the cryo-EM map on a molecular level, we docked crystal structures and molecular models into the density and applied molecular dynamics flexible fitting (MDFF), resulting in a complete molecular model for the 70S-RNC-Nd-SecYEG complex (Figure 27).

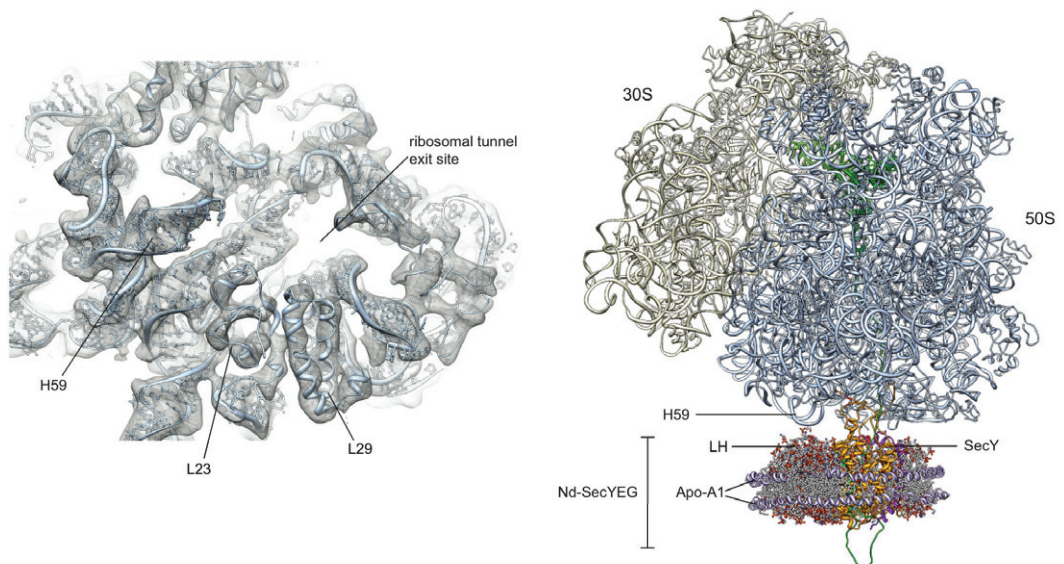


Figure 27: All-atom model of the active 70S-RNC-Nd-SecYEG complex | View and colours as in (b), proteins and RNA in ribbon representation and phospholipids in ball and stick representation with phospholipid headgroups in red/orange and acyl chains white, Apo-A1 in light purple.

3.11 Structure of the Nanodisc

The region of the map representing the Nanodisc was expected to consist of a lipid bilayer with an upper and lower membrane leaflet stabilized by two belt-like Apo-A1 Δ 1-43 molecules surrounding it. The observed density indeed shows the characteristic dimension of a lipid bilayer with a thickness of about 43 Å (Figure 28a).

Strong electron density for the phospholipid headgroups was present that could be distinguished from the very weak density for the region occupied by the acyl chains of the fatty acids (Figure 28a,b). The outer ring of the Nanodisc, suggested to be composed of two parallel copies of Apo-A1 Δ 1-43, also displays a stronger density than the lipid acyl chains. However, the density did not allow for the resolution of the protein belts. Additional fragmented density outside the main disc may be a result of the presence of non-lipidated N-terminal regions of Apo-A1 Δ 1-43, respectively. Since Apo-A1 may rotate freely around the innermost core density of the Nanodiscs, these densities are radially distributed around the Nanodisc.

Within the bilayer, rod-like structures were detected directly beneath the ribosomal tunnel exit, apparently representing the TM helices of the SecYEG complex (Figure 28). The observation shows that the overall dimensions of the membrane protein containing Nanodisc resemble those of a small circular lipid bilayer which can be subjected to structure analysis at sub-nanometer resolution.

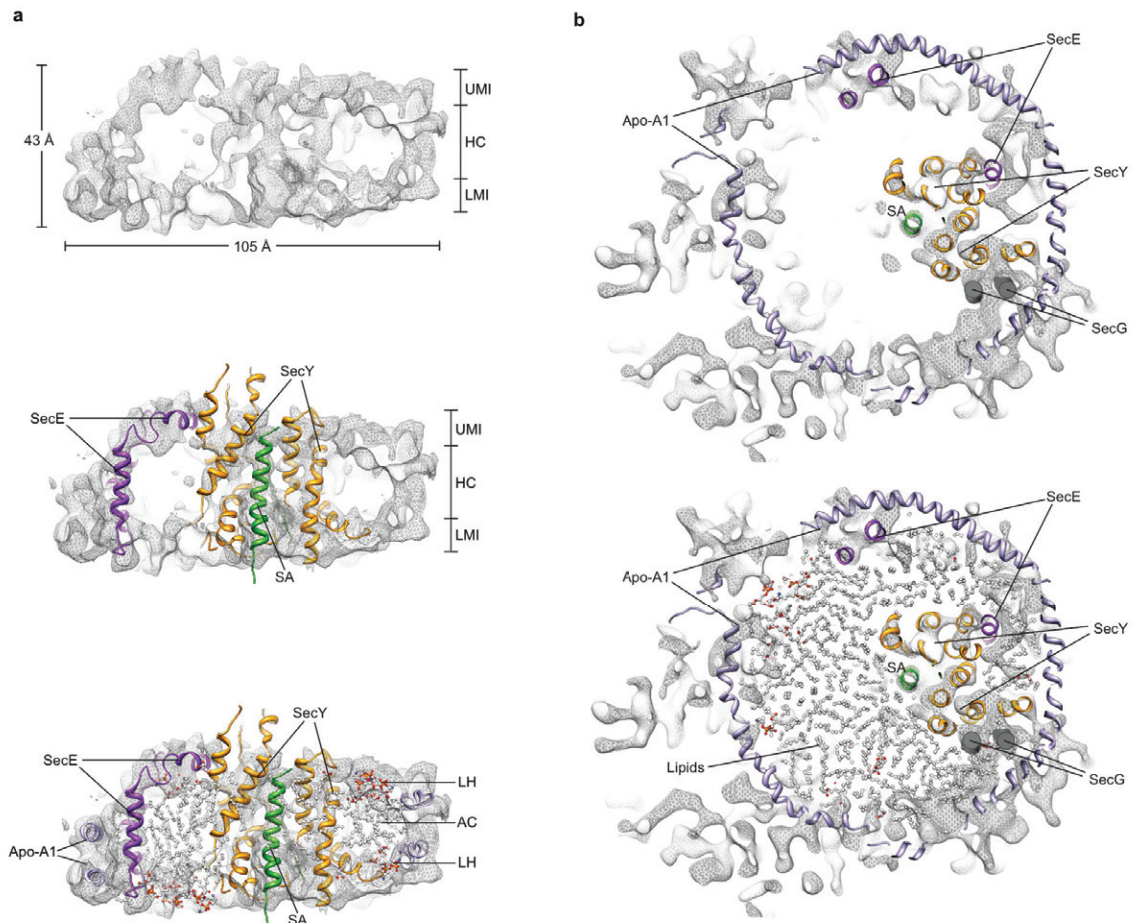


Figure 28: Structure of the Nanodisc | (a) Top: Side view cut perpendicular to the plane of the membrane of the isolated electron density of the Nanodisc-SecYEG complex (Nd-SecYEG) to show the lateral gate of SecY. The electron density is represented as a transparent grey mesh. Two layers of density are visible (upper membrane interface, UMI, and lower membrane interface, LMI), separated by a region of lower density (hydrophobic core, HC), containing rod-like features. Dimensions are indicated. Middle: Same view, with the ribbon representation of the fitted model of a SecY (orange), SecE (purple) and the signal anchor sequence (green). Bottom: Same view, with the fitted Nanodisc-model containing lipids in ball and stick representation. Phospholipid headgroups are red (oxygen) and orange (phosphate), acyl chains white (carbon-hydrogen groups). (b) Top: Horizontal section, sliced within the plane of the membrane within the hydrophobic core of the lipid bilayer. Rod-like features are visible in the interior of the Nanodisc and account for density of a monomeric SecYEG complex. Bottom: Horizontal section with fitted lipids.

3.12 Canonical binding mode

A multitude of contacts between the ribosome and the Nd-SecYEG density (Figure 29) were observed. The most prominent density was close to H59, where even at low resolution a strong contact was observed. In addition, L24 also established a strong contact with the Nd-SecYEG density. At higher resolution, the previously observed interactions between L8/9 and H50 were identified, and, to a lesser extent, L6/7 reaching into the ribosomal exit tunnel (Figure 29a). The positions of L8/9 and L6/7 and the ribosome are in good agreement with recently published structures of the ribosome-Sec-complexes (Becker et al., 2009; Menetret et al., 2007; Menetret et al., 2008).

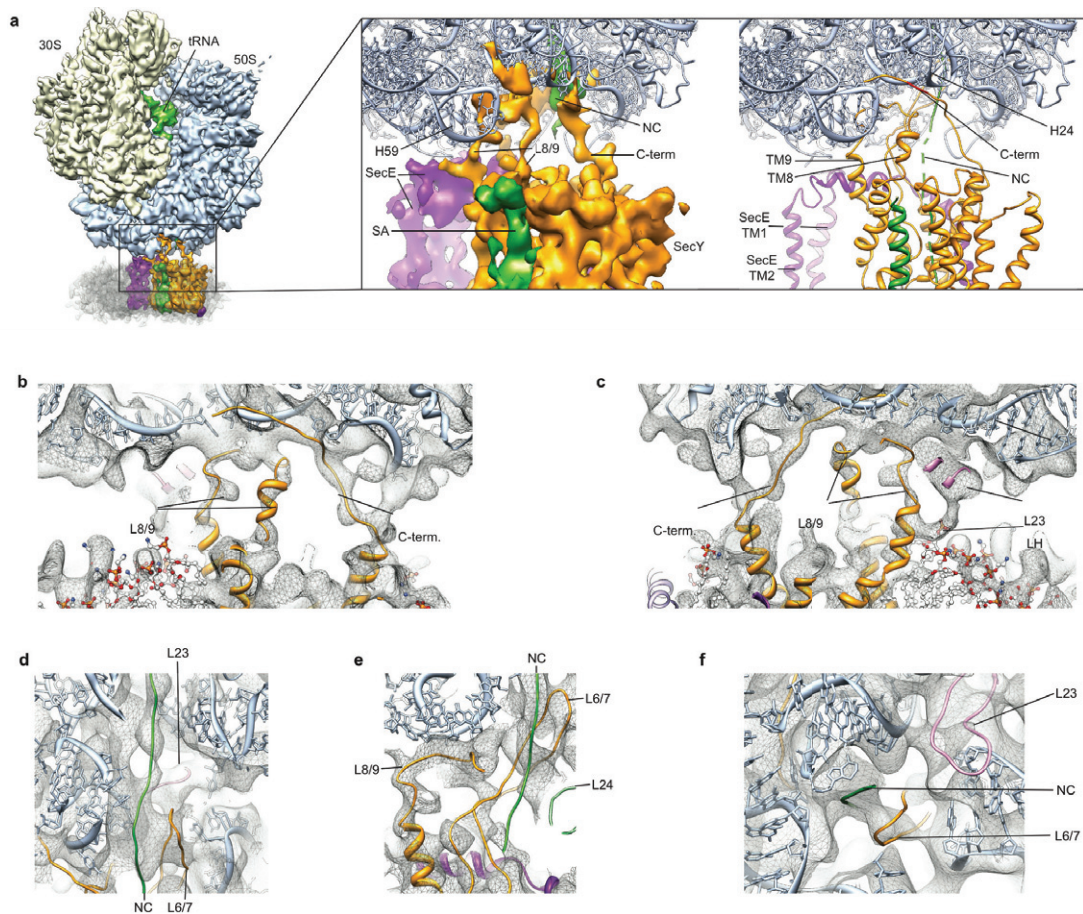


Figure 29: Canonical Sec-binding site | (a) Cryo-EM reconstruction of the active 70S-RNC-Nd-SecYEG complex. Insert: View of the molecular model of the 50S subunit and electron density for SecYE (left) and molecular model for SecYE (right). (b) Close-up of the map showing the interaction of L8/9 (orange) with the prokaryotic 70S RNC. (c) as in (b), but rotated around 180°. (d-f) Close-up of the density showing the interaction of L6/7 with the nascent chain in the ribosomal exit tunnel with the fitted models for SecY, 50S subunit and the nascent chain.

3.13 Model for the *E. coli* SecYE complex

Based on the previously observed contacts of the cytosolic loops L8/9 and L6/7 of SecY/Sec61 to the ribosome (Becker et al., 2009; Menetret et al., 2007; Menetret et al., 2008) (Figure 29), homology models of the *E. coli* SecYE complex were fitted into the density. Since α -helical secondary structures were resolved within the membrane environment, rigid body fits were performed by aligning the model according to known ribosomal connections based on L8/9 and L6/7 of SecY and on characteristic secondary features of densities representing TM helices 6,8,9.

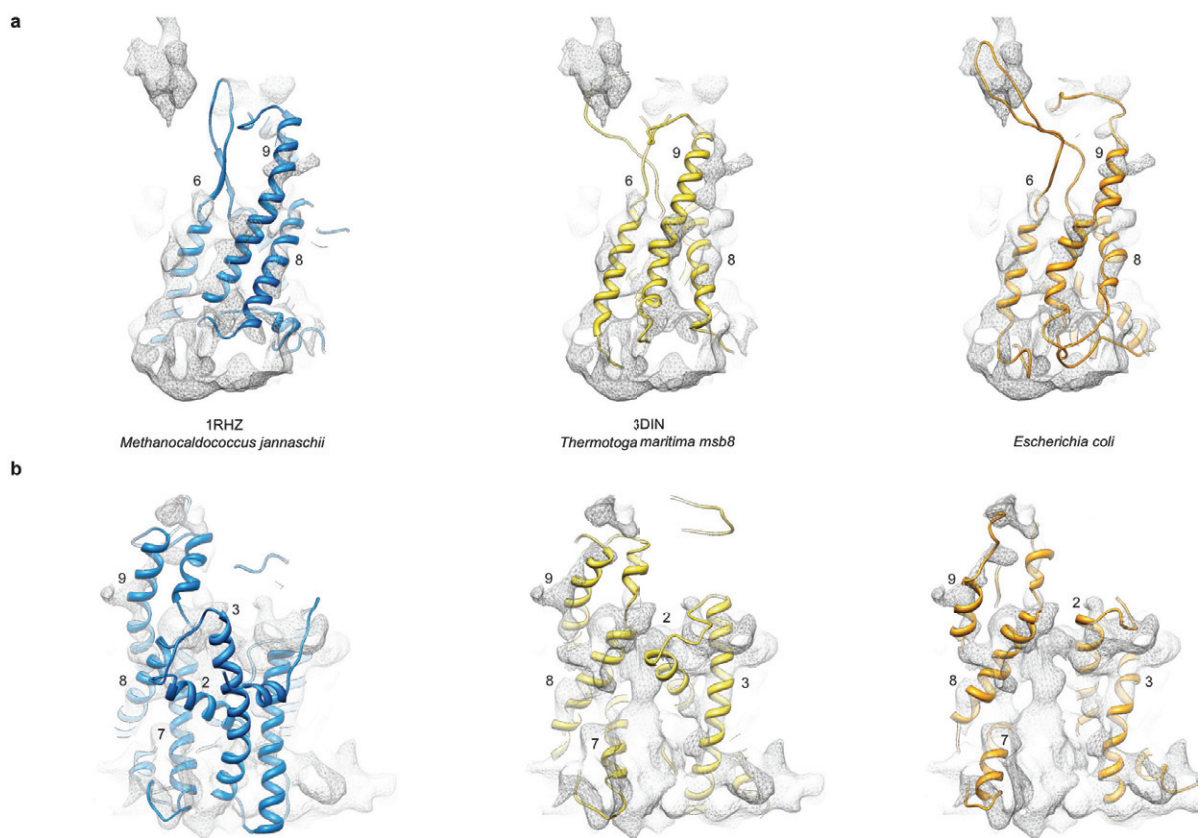


Figure 30: Fitting of SecY structures into the cryo-EM density and comparison with the 2D crystal structure of the *E. coli* SecYEG complex | (a) Close-up of the SecY density, side view cut perpendicular to the plane of the membrane to show SecY TM helices 6, 8, 9 with fitted X-ray structures of SecY *M. jannaschii* (blue, left), *T. maritima* (yellow, middle) and the *E. coli* model (orange, right). b, Close-up of the SecY density, side view cut perpendicular to the plane of the membrane to show the lateral gate with SecY TM helices 2, 3, 7, 8, 9 with fitted X-ray structures of SecY *M. jannaschii* (blue, left), *T. maritima* (yellow, middle) and our current *E. coli* model (orange, right).

The homology model based on the inactive, closed SecY from *M. jannaschii* did not fit properly into density, especially TM helices 2 and 3 were far out of density. In contrast, by using the structure of the SecYE in the SecYE-SecA complex as a template, the C-terminal half of SecY fitted remarkably well and only small adjustments of the N-terminal TM helices of SecY were necessary. According to the open structure of the PCC with shifts in both N- and C-terminal region, their position is also slightly shifted outwards with respect to the inactive model. Noteworthy, a shift of the amphipathic helix has also been observed in the pre-open structure of SecY upon binding of SecA (Zimmer et al. 2009).

The N-terminal TM helices of SecE were placed into two additional rod-like densities the position of which is in agreement with the 2D crystal structure of the SecYEG complex. According to the open structure of the PCC with shifts in both N- and C-terminal region, their position is also slightly shifted outwards with respect to the inactive model (Figure 31).

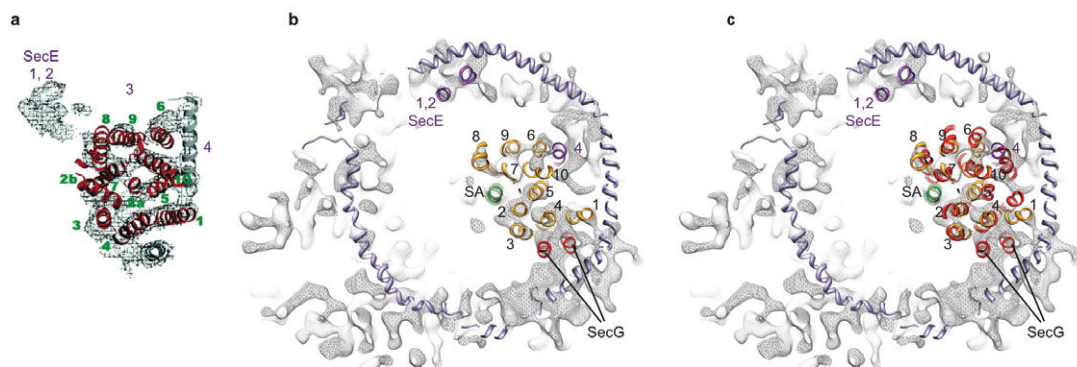


Figure 31: Position of SecE TM helices 1,2 | (a) Cytosolic view of the electron density projection map of the 2D crystal structure of the *E. coli* SecYEG complex with the fitted X-ray structure of the SecYE β from *M. jannaschii* (Collinson, 2005). SecY TM helices in red and labeled in green, SecE C-terminal helix in grey. The position of the two additional N-terminal helices of *E. coli* SecE is labeled in purple, Sec β in grey. (b) Cytosolic view of the electron density map of the cryo-EM structure of the open *E. coli* SecYEG complex. SecY TM helices in orange, SecE TM helices in purple, signal anchor (SA) in green. Note the slightly outward shifted position of the SecE N-terminal density compared to its position in the 2D-crystal map. The position of the SecG TM helices (red) is according to an alignment of the X-ray structure of the SecYEG complex from *T. maritima* on our *E. coli* model. (c) as in (b), with the aligned X-ray structure of the SecYEG complex from *T. maritima* (red) on our *E. coli* model.

Although some density was observed in the region where SecG was expected, its exact position could not unambiguously be identified, indicating a higher degree of flexibility. Notably, the fitted model left a rod-like density in the proposed lateral gate of SecY unaccounted for, that was interpreted as the inserted SA helix of FtsQ (Figure 32).

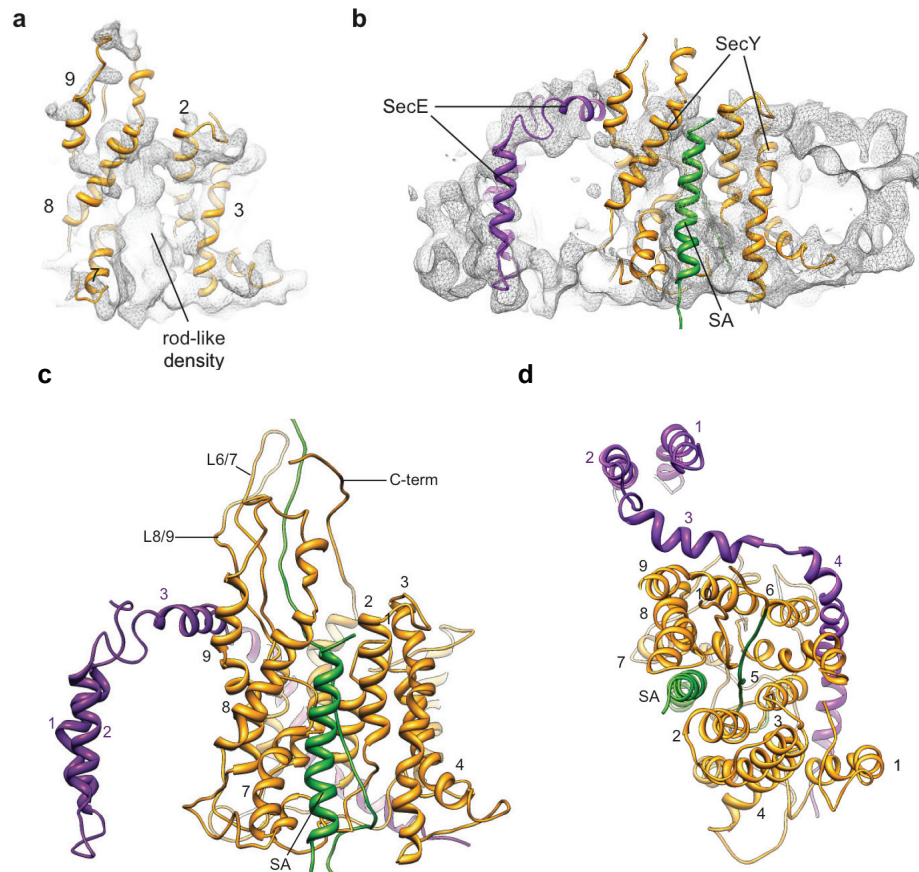


Figure 32: Structure of the open SecYE complex with a signal anchor (SA, green) within the lateral gate | (a) Close-up of the SecY density, side view cut perpendicular to the plane of the membrane to show the lateral gate with SecY TM helices 2, 3, 7, 8, 9 and the additional rod-like density within the lateral gate. (b) Model of SecYE within the Nanodisc density with the fitted SA-helix in green. (c) view of the lateral gate perpendicular to plane of the membrane. (d) As (c), but viewed from the cytoplasmic side.

To determine the quality of the fit, a statistical evaluation based on cross-correlation calculations of the fitted models was performed, with the fitted models according to Figure 30. The results show that the final model fits best when compared to the crystal

structures (1RHZ and 3DIN) as well as the initial model and one in which SecYE is rotated by 180 degrees (Table 2).

Indeed, a correlation coefficient of 0.71 for the final model of SecYE/signal anchor was obtained, compared to 0.47 and 0.41 for SecYE of 3DIN and 1RHZ, respectively.

Table 2: Cross-correlation for different SecYE-structures

Structure	Cross-correlation coeff.
SecYE/SA (initial)	0.60
SecYE/SA (final)	0.71
SecYE/SA (rotated 180°)	0.41
1RHZ (SecYE only)	0.41
3DIN (SecYE only)	0.47

In order to address the question of the quality of the fit, Figure 33 shows the fitted model in the density with several perspectives.

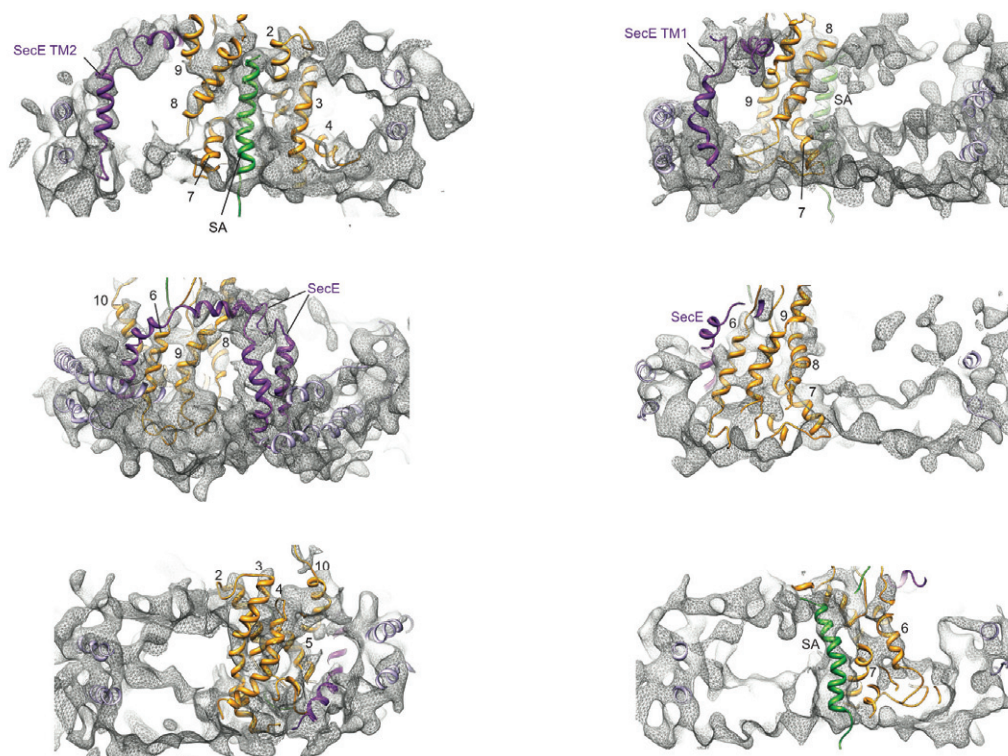


Figure 33: Close-ups of the Nanodisc-density | Different views with the fitted models of SecY (orange), SecE (purple), the signal anchor (green) and the electron density represented in grey mesh.

To further validate the quality of the structure, a series of consecutive sections is shown (Figure 34), sliced within the plane of the membrane in the hydrophobic core of the Nanodiscs. Notably, the electron density of the original map is indeed very similar to a map generated from the fitted Nd-SecYEG model. Interestingly, also in the model-derived map, charged lipid headgroups contribute to the electron density and are visible within the slices. The likely position of the SecG TM helices in the density is according to the X-ray of the SecYEG complex from *T. maritima* (Zimmer et al., 2009).

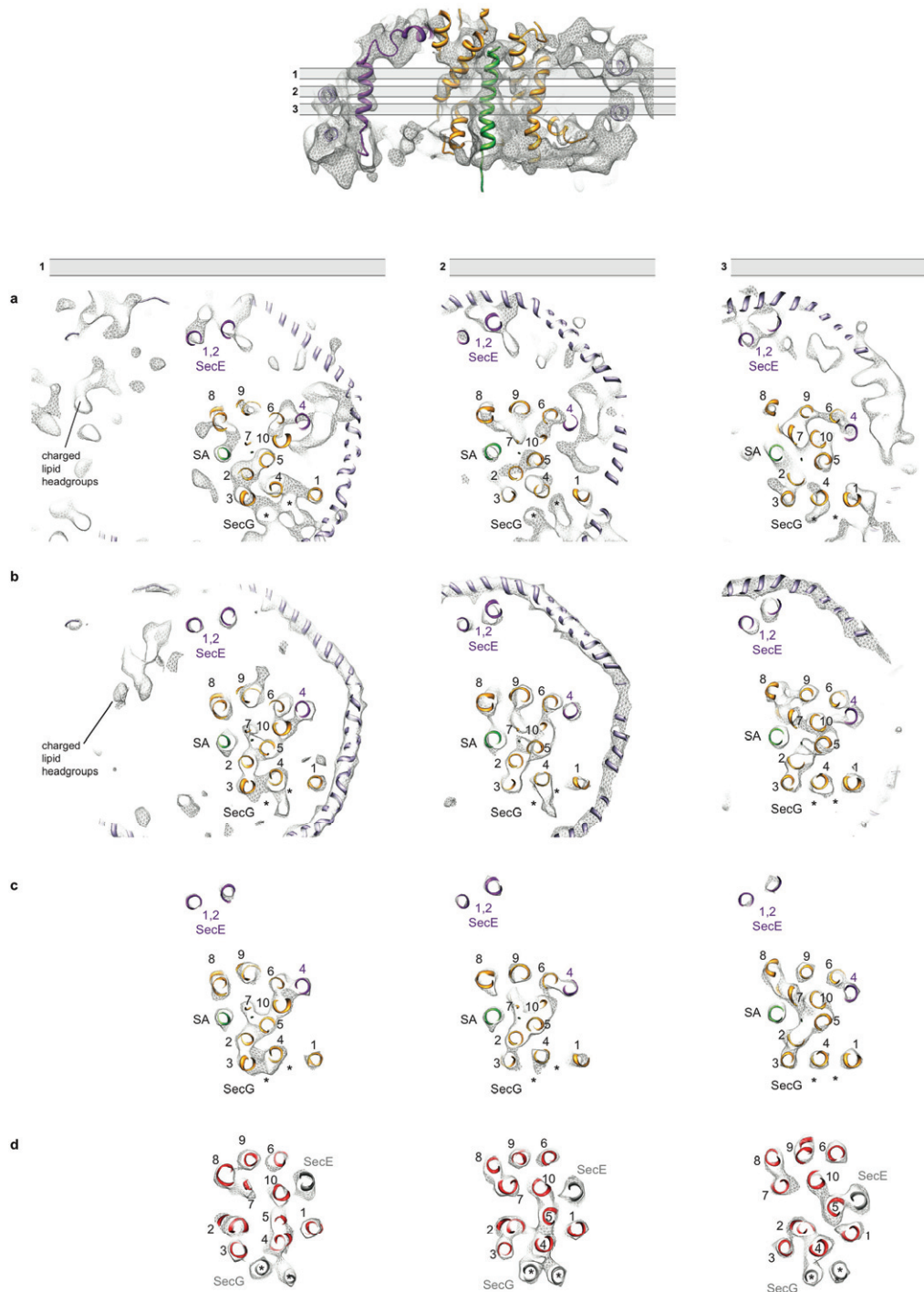


Figure 34: Horizontal sections of Nd-SecYEG and corresponding models | Sections sliced within the plane of the membrane (1, upper; 2, middle; 3, lower). a, Sections through the experimental map at 7-8 Å with the fitted model for Nd-SecYEG/ SA. Charged lipid headgroups and the likely position of SecG are indicated. b, Sections through a density based on the molecular model for SecYE/SA within the Nanodisc at 7-8 Å. Density from charged lipid headgroups is indicated. c, Sections through a density based on the molecular model for SecYE/SA without the Nanodisc (no lipids) at 7-8 Å. d, Sections through a density based on the X-ray structure of the SecYEG complex from *T. maritima* at 7-8 Å.

3.14 Ribosome-SecYE contacts

A multitude of contacts were identified between the ribosome and SecYE as well as lipids. The cytoplasmic loops L8/9 and L6/7 of SecY reached into the ribosomal exit tunnel and contacted ribosomal RNA (rRNA) helices H50/53/59 and H6/24/50, respectively (Figure 29, Figure 35). Furthermore, both loops also contacted the ribosomal protein L23 in different regions.

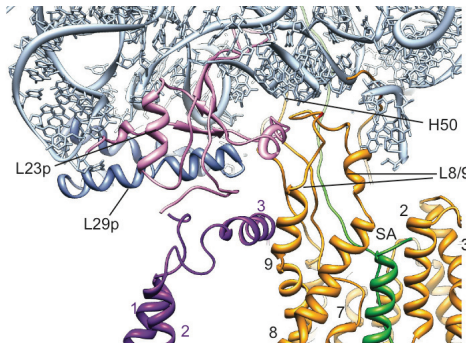


Figure 35: Close-up of the interaction area of universal ribosomal adaptor site and SecYE.

An additional contact was likely to represent the C-terminus of SecY, contacting ribosomal protein L24 and rRNA helices H24/50 (Figure 29). In addition to SecY, SecE contributes to the interaction of the PCC with the ribosome (Figure 35). Several contacts between the N-terminus as well as the amphipathic helix of SecE and the ribosomal adaptor site proteins L23 and L29 were observed. A stretch of conserved residues in the amphipathic helix of SecE appeared to be involved in contacting both SecY and L23/L29.

3.15 Ribosome-lipid interactions

Interestingly, the Nd-SecYEG-bound ribosome did not only interact with the PCC but also with lipids. A strong density between rRNA helix H59 and the disc is very likely to be established by a direct contact to lipid headgroups (Figure 36). In addition, L24 showed a strong contact with the Nd-SecYEG density that may also involve lipids. After the initial fitting of molecular models, a molecular dynamics simulation of the ribosome-Nd-SecYE-lipid model was performed, containing a lipid bilayer of 75% phosphatidylethanolamine and 25% phosphatidylglycerol, mimicking the composition of the bacterial plasma membrane.

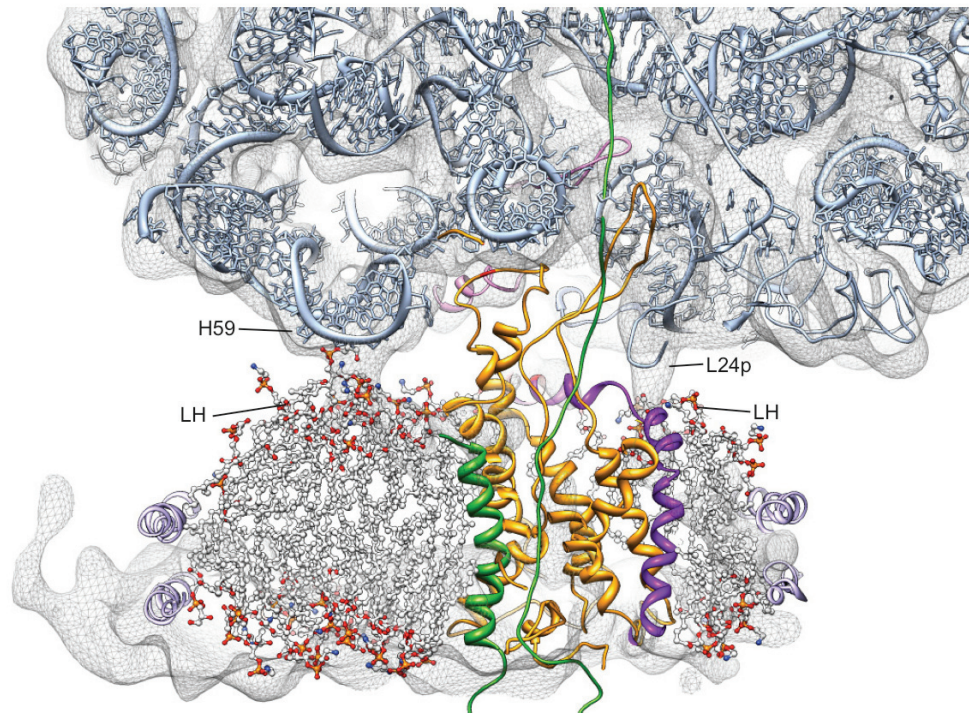


Figure 36: Ribosome-Lipid interactions | Molecular model of the ribosome-SecYE-membrane interface with transparent density filtered at 9-10 Å. Lipid headgroups (LH) contacting the 50S subunit are indicated.

Initially, a flat lipid bilayer was fitted into the Nanodisc density. However, shortly after the start, a stable attraction between lipids and rRNA helix H59 was observed. The resulting density distribution resembled the electron density remarkably well, indicating that H59 indeed is capable of establishing another interaction site between the ribosome and a membrane-PCC-complex (Figure 36). In contrast, the additional interactions between L24 and lipids, which were also in good agreement with our electron density, were intermittent, as L24 prefers to interact with SecY/nascent chain later in the simulation. The direct interaction of the ribosome with the lipid bilayer, in addition to the SecYE contacts, may explain the rigid positioning of the entire disc with respect to the ribosome and the asymmetrical position of the SecY complex in the disc.

3.16 Ribosome-Membrane-SecYE interactions

Taken together, a multitude of contacts between ribosome and the C-terminal half of the PCC as well as lipids result in a robust coordination of the ribosome with respect to the membrane surface (Figure 37). The observed conformation orients the ribosome surface around the tunnel exit almost parallel to the surface of the membrane while leaving a distance of about 20 Å on one side. The position of the lateral gate of SecYEG with respect to the ribosomal-PCC contacts would easily facilitate egress of cytoplasmic domains of nascent peptides alongside the H59 contact away from the main interaction sites.

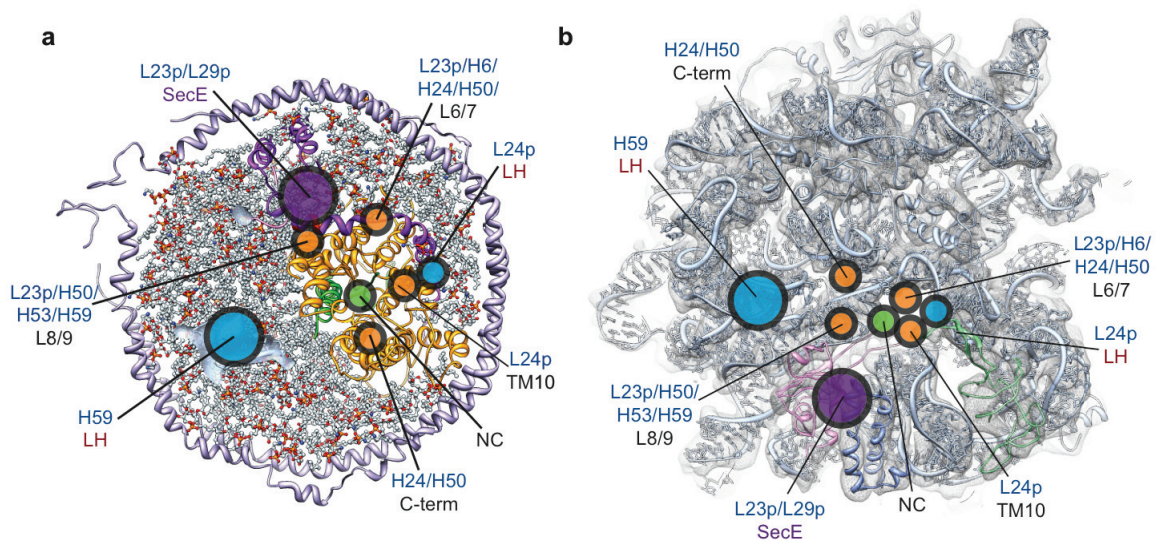


Figure 37: Ribosome-Membrane-SecYE interactions | (a) Cytoplasmic view of the molecular model of the Nd-SecYE complex with contacts to the 50S subunit indicated by circles. (b) View of the ribosomal tunnel exit site, contact sites as in (a)

3.17 Path of the nascent chain within the ribosomal exit tunnel

The resolution of the electron density allowed for the tracing of the nascent polypeptide chain from the PTC through the ribosomal exit tunnel into the cytosolic vestibule of the SecYEG complex (Figure 26). After passing the central constriction of the ribosomal tunnel with an unaltered loop region of L22 (Figure 39), the nascent chain engages in a number of contacts in the lower half of the tunnel involving the ribosomal proteins L23, L24 and SecY (Figure 38, 39) Noteworthy, protein loops participate in all of these contacts and undergo conformational changes when compared to structures of inactive complexes.

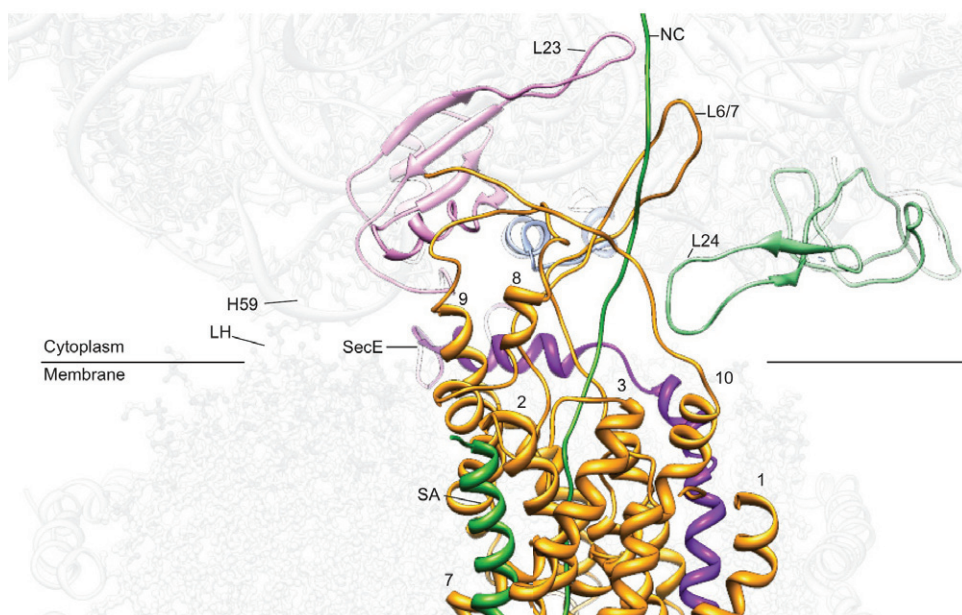


Figure 38: Section through molecular models of the ribosomal exit tunnel and Nd-SecYE | The nascent chain (NC) with the signal anchor (SA) is shown in green. The line indicates the cytoplasm-membrane interface.

The conserved loop of L23 that reaches up the tunnel wall has been suggested to constitute a potential interaction site for nascent proteins (Houben et al., 2005) possibly leading to an inside-outside signalling of the nascent chain (Bornemann et al., 2008). In the density presented in this study, the tip of L23 (Figure 39,40) indeed shifts down when compared to empty ribosomes analyzed by cryo-EM or x-ray crystallography (Figure 39). Compared with the inactive crystal structure (2i2v), the tip of L23p bends 6 Å down. This leads to an interaction of the tip of L23 with the nascent chain at a distance of 19 amino acids from the PTC. In the immediate vicinity,

the nascent chain subsequently contacts the tip of L6/7 of SecY that embraces the nascent chain. In addition, L6/7 also interacts with L23 in that area.

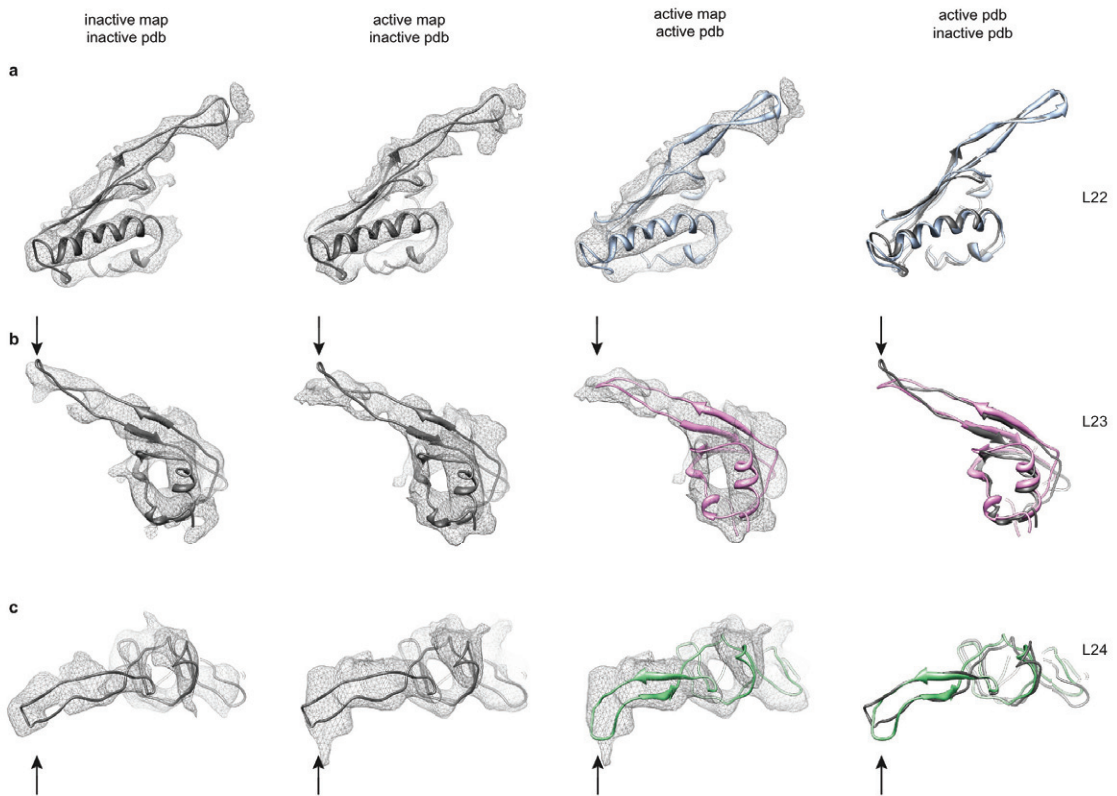


Figure 39: Analysis of ribosomal proteins L22, L23, L24 | Comparison of X-ray structures and cryo-EM densities of an inactive ribosome (PDB: 2I2V) vs. MDFF-models and cryo-EM densities of an active ribosome. (a) Conformation of L22p. Left, isolated density of L22p in an inactive ribosome with the fitted X-ray structure of L22p of an inactive ribosome (dark grey). Middle-left, isolated density of L22p in active ribosome with the fitted X-ray structure of L22p of an inactive ribosome (dark grey). Middle-right, isolated density of L22p in an active ribosome with a MDFF-model of L22p of an active ribosome (light blue). Right, overlay of the X-ray structure of the inactive L22p with the MDFF-model of L22p. (b) Conformation of L23p, side view and comparison of densities as in (a). (c) Conformation of L24p, side view and comparison of densities as in (a).

When finally exiting the ribosomal tunnel, the nascent chain contacts the exposed beta-hairpin of L24 (Figure 40b). This hairpin loop is also bent downwards to probably contact the lipid surface and the C-terminus of SecY. Taken together, the nascent chain is carefully guided by protein loops through the ribosomal tunnel to its site of insertion into the PCC.

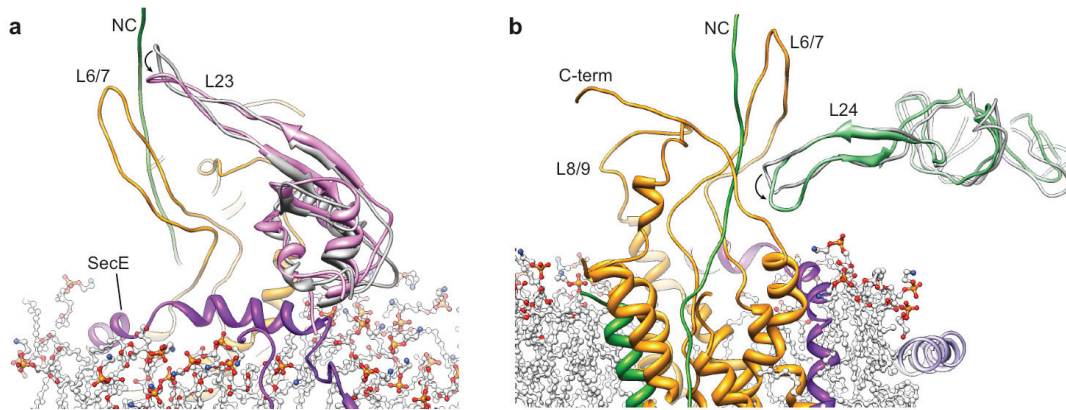


Figure 40: Conformational changes of L23 and L24 | (a) Conformational changes of L23. Comparison of the model of L23 (grey) of an inactive ribosome (PDB: 2i2v) and of L23 (pink) in the presence of a nascent chain (green), SecY (orange), SecE (purple) and lipid headgroups. The intra-tunnel loop of L23 bends towards the nascent chain, close to L6/7 of SecY. (b) Conformational change of the β -hairpin loop of L24. Comparison of the model of L24 (grey) of an inactive ribosome (PDB: 2i2v) and of L24 (green) in the presence of a nascent chain (green), SecY (orange), SecE (purple) and lipid headgroups (LH).

3.18 Conformational changes of SecYE

Due to the limited resolution, it was not possible to trace the path of the complete NC within the PCC. After fitting the TM helices of SecY, the NC model from the cytoplasmic to the periplasmic side was extended through the central pore (Figures 41, 42). In the SecYE model, the central opening in the hydrophobic pore ring has a diameter in the range of 10 Å (Figure 42d). This dimension leaves enough space for an extended polypeptide chain to pass while, at the same, a substantial flow of ions would be prevented in the presence of a translocating peptide.

The NC model was connected with the SA within the proposed lateral gate of the PCC, resulting in the loop-like arrangement expected for a type II membrane protein. Adjusting the SecYE complex from the SecA-activated, pre-open conformation

(Zimmer et al., 2008) of the template to the density resulted in a laterally open conformation. This conformation facilitated the accommodation of the additional SA helix into the lateral gate (Figure 41). Interestingly, mainly the gate helices and the N-terminal half of SecY undergo movements, while the TMs of the C-terminal half superimpose relatively well with the structure of the pre-open state (Figure 41b).

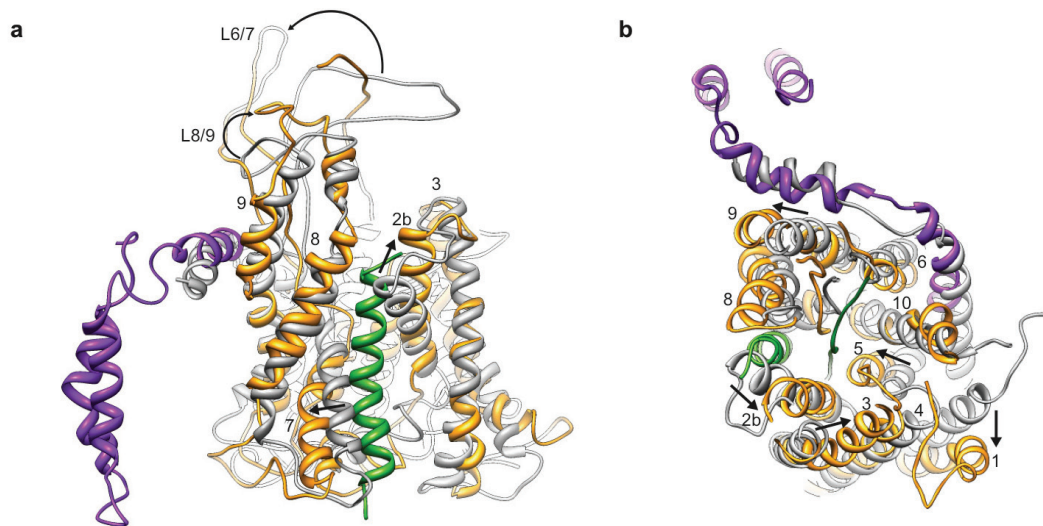


Figure 41: Conformational changes and opening of SecYE. | (a) View of the lateral gate of the PCC. Comparison of the membrane-embedded, open ribosome-bound SecYE (orange, purple) with SecYE from the *T. maritima* SecA- SecYEG complex (grey). Loop movements are indicated with round arrows, helix movements are indicated with small black arrows. SA in green, the NC has been omitted for better clarity. (b) as in (a), but viewed from the cytoplasmic side with the NC in green.

The resulting model provides an overall arrangement that is in agreement with previous biochemical and structural data. The SA is exposed towards the lipid bilayer, yet, it remains tightly enframed by TM2b, TM7 and TM8 that may indeed act as the lateral gate for TM domains for insertion into the membrane.

3.19 Signal anchor helix within the lateral gate

The signal anchor exposes its hydrophobic core towards the lipid bilayer, yet it remains tightly enframed by TM2b/TM8 with the positively charged N-terminus remaining on the cytosolic side by interaction with either negatively charged phospholipid headgroups or the negatively charged phosphate backbone of the nearby RNA helix H59.

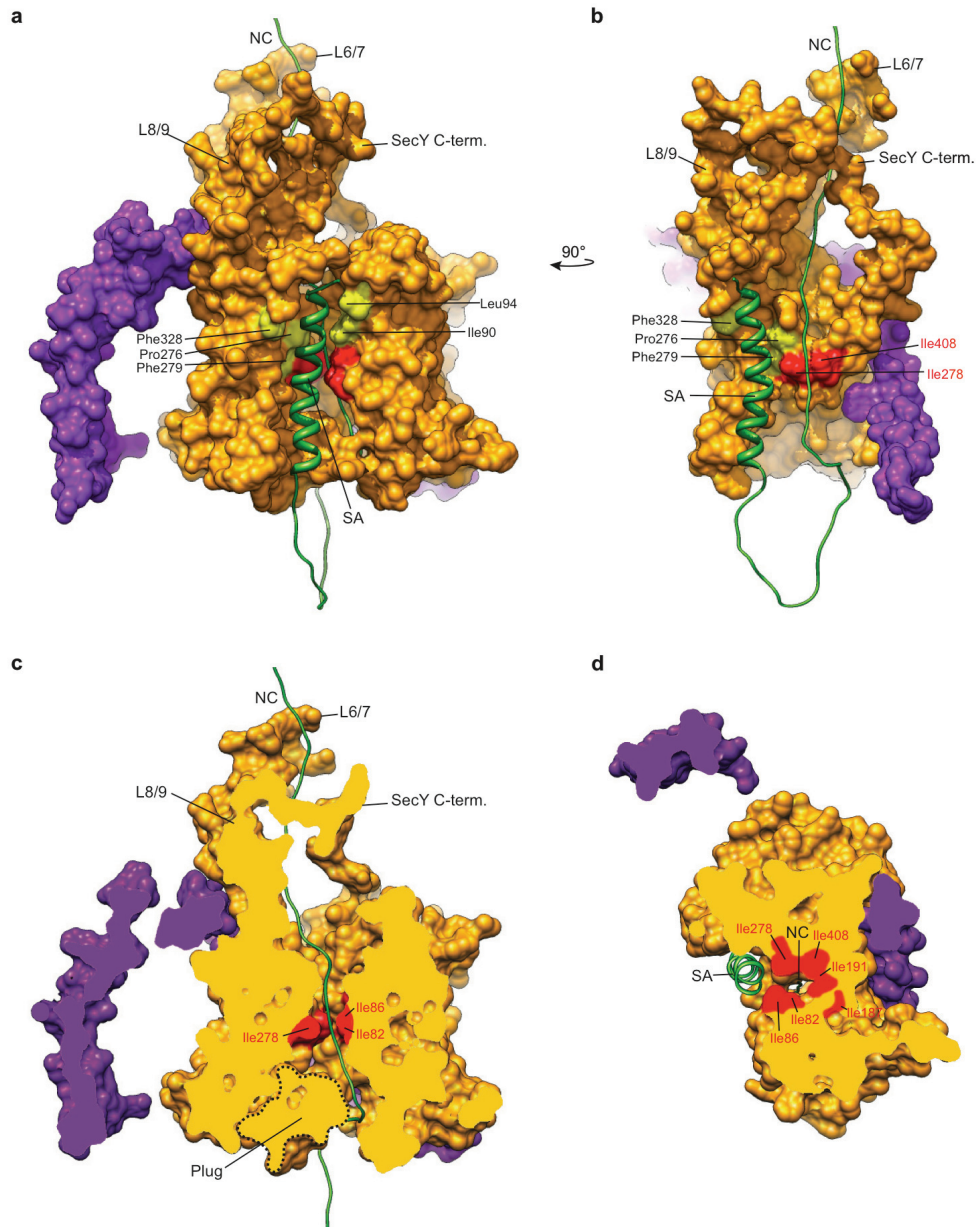


Figure 42: Signal anchor helix within the lateral gate of SecYE | (a) View of the lateral gate of SecYE shown as a surface representation. SecY is shown in orange, SecE in purple, the nascent chain in green. Conserved residues of SecY that contribute to the central hydrophobic pore ring are indicated in red and hydrophobic residues of the hydrophobic crevasse that have been found by mutational analysis to be critical for SecY function are indicated in pale yellow. (b), As in (a) but rotated 90 degrees and shown without the N-terminal half of SecY. (c) As in (a) but cut perpendicular to plane of the membrane, revealing the suggested path of the nascent chain. (d) As in (b) but rotated to view the position of the SA from the cytoplasmic side.

According to the model, the SA is accessible to the acyl chains of the lipid environment, yet phospholipids may not enter the hydrophilic center of the PCC.

Interestingly, TM2b/TM8 are seaming the lateral gate and may thus prevent the influx of phospholipid headgroups into the pore. Furthermore, it looks as if the signal anchor would still be retained by the PCC. The signal anchor helix, retained in the lateral gate of SecY, but at the same time exposed to the lipid environment may represent an intermediate step of the integration of a transmembrane helix into the lipid bilayer.

3.20 Ring fence for the nascent chain

The surface representation of the all-atom model of the complex indicated a semi-seal between the ribosome and the membrane surface. A tight seal is formed on one side of the ribosome from H59 to L23, L29 and L24 with the lipid bilayer and SecE. In contrast, there is a gap of 20 -25 Å on the other side (Figure 43). Yet, the nascent chain is almost completely covered by either the ribosome or SecY and the membrane. Interestingly, the C-terminus of SecY fences the nascent chain on the gap-side of the ribosome-membrane surface in such way that it is almost completely shielded from the hydrophilic cytosol.

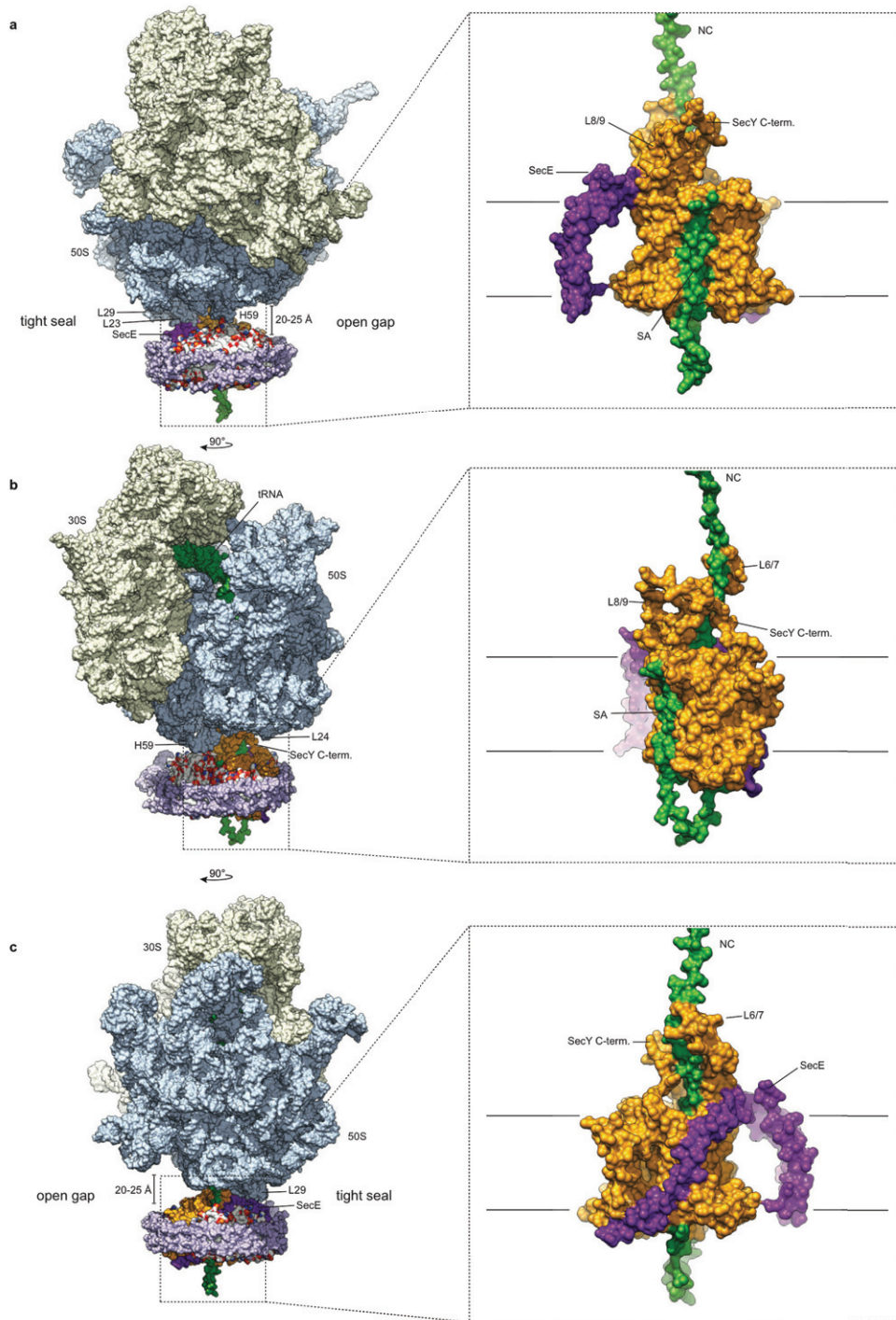


Figure 43: Surface representation of the all-atom model of a 70S-RNC-Nd-SecYEG complex | a, Surface representation of the all-atom model of a 70S-RNC-Nd-SecYE complex, coloured as in Fig. 1. Phospholipid headgroups are red (oxygen) and blue (nitrogen). Right: close-up of the isolated SecYEG complex in the same position within the Nanodisc of the left panel. b, as in (a), but rotated 90° around the y-axis. c, as in (b), but rotated 90° around the y-axis.

3.21 Molecular dynamics simulation

For the molecular interpretation of the cryo-EM map, crystal structures and molecular models were fitted into the density. In collaboration with James C. Gumbart and Klaus Schulten (University of Urbana, Illinois), molecular dynamics flexible fitting (MDFF) was applied to obtain the complete molecular model for the 70S-RNC-Nd-SecYEG complex which was used as a starting point for a 16 ns molecular dynamics (MD) simulation.

In MDFF, the atomic model is simulated using molecular dynamics in the presence of the cryo-EM density map, represented through an additional potential in the simulation. From this potential, forces proportional to the gradient of the cryo-EM density are derived that then drive atoms into high-density regions of the map. In addition, restraints are applied to maintain the secondary structure of protein and RNA molecules, which otherwise would distort or break under the forces required for fitting. Fitting of the 70S proceeded in stages and a total simulation time of 3.5 ns was used to fit the ribosome.

After completion of modeling and MDFF, the resulting ribosome-Nanodisc model was used for further equilibrium simulations. Water and ions were added in an iterative procedure using the program VMD (Humphrey et al., 1996). To reduce simulation complexity and to focus on the interactions between the ribosome and SecYE and Nanodisc, the ribosome and nascent chain were truncated just downstream of the L4/L22 constriction point. Any ribosomal backbone atoms within 5 Å of the truncation point were constrained. At the point of closest approach, SecYE was at least 25 Å away from the truncation point. The simulation of the truncated ribosome-Nanodisc complex included 400,000 atoms.

The equilibration of the system occurred in stages. First, only the lipid tails were allowed to move, permitting them to “melt”, for 0.25 ns. Next, water and sidechains were released for an additional 2.25 ns. For the next 1.5 ns, only the encircling Apo A-1 proteins of the Nanodisc were constrained; the secondary structure of all proteins and RNA was also enforced during this time, and for a further 2 ns. Finally, after 6 ns of total simulation time, all restraints were released. At all times, a constant temperature of 310 K and a constant pressure of 1 atm were maintained.

With respect to the overall conformation of the PCC, the MD simulation revealed a stable behavior of the fitted model (Figure 44), supporting its accuracy. This applied to the ribosomal connections and the conformation of SecYE, as well as to the position of the SA TM domain.

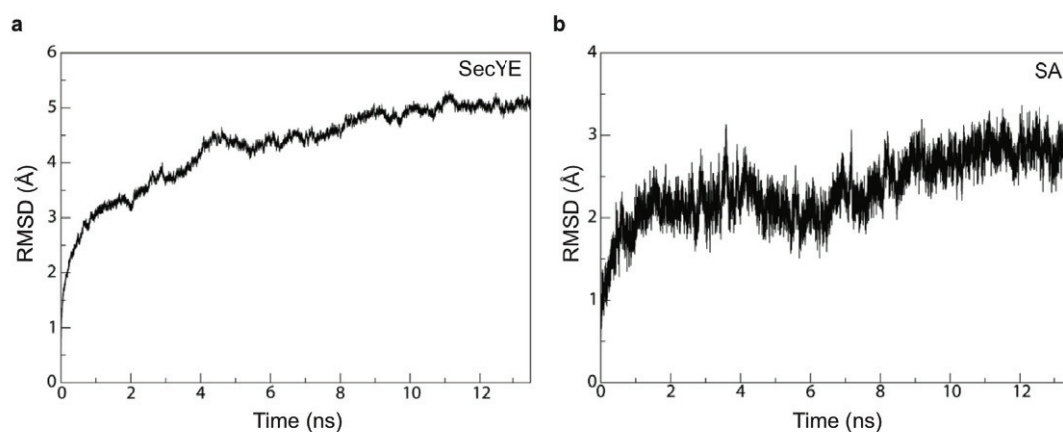


Figure 44: RMSD values of SecYE and of the signal anchor relative to SecYE | The root-mean-square deviation (RMSD) over time is presented for (a) the backbone of SecYE and (b) that of the signal anchor. In both cases, RMSD was calculated after first performing a least-squares fit of SecYE over all frames of the simulation trajectory. Data for the initial 2.5 ns of the simulation in which the proteins were restrained are not shown.

During the MD simulation, also the SA appeared to be stable with respect to SecYE. Notably, between the SA and SecY virtually no hydrogen bonds, but mainly hydrophobic interactions were observed (Figure 45, Appendix). Whereas a substantial number of hydrogen bonds would reduce the TM domain's ability to exit into the bilayer, hydrophobic interactions would be in agreement with partitioning according to the TM domain's hydrophobicity.

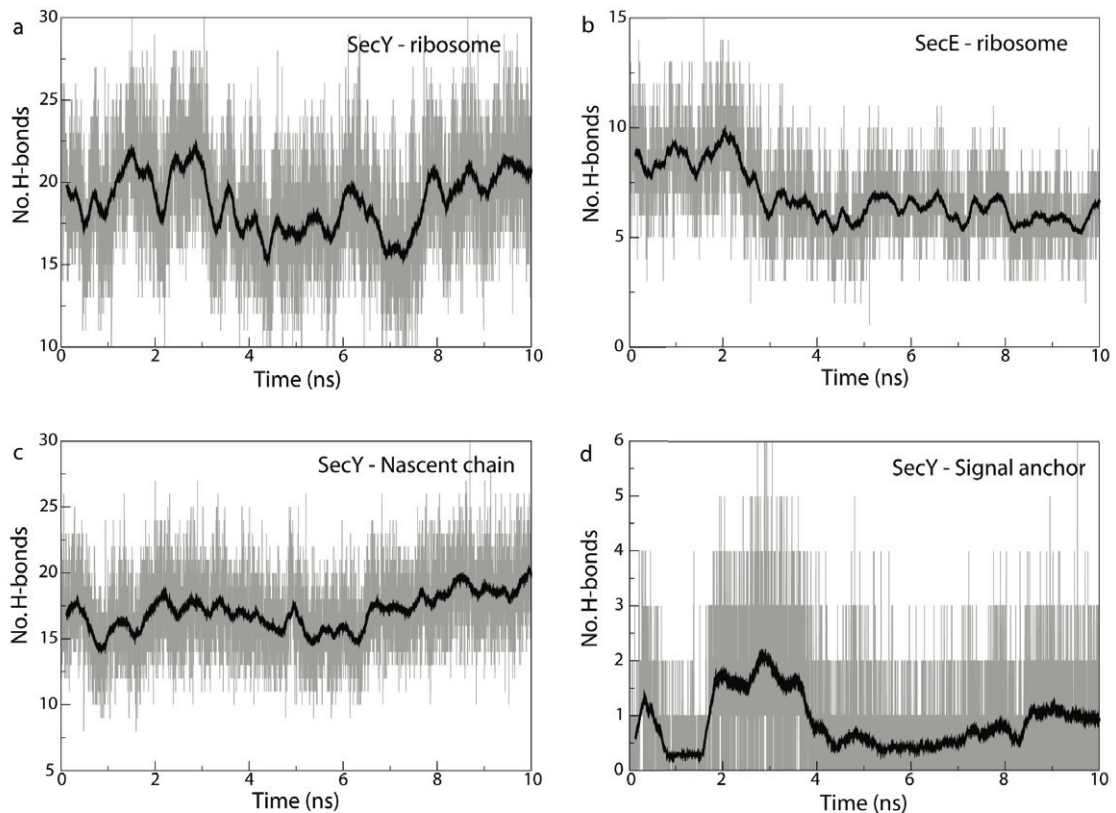


Figure 45: Formation of H-bonds during simulation | Hydrogen bonds formed between different components of the simulation over time are shown. (a,b) H-bonds between the ribosome and (a) SecY and (b) SecE. (c,d) H-bonds between SecY and (c) the nascent chain and (d) the signal anchor. The solid black line denotes a running average of the full data in light grey. Only data from the last 10 ns of the simulation, *i.e.*, the completely unrestrained portion, are shown. H-bonds were counted when the distance between the hydrogen donor and the acceptor was within 3.5 Å and the angle formed by the donor, hydrogen, and acceptor was greater than 145°.

Initially, a flat lipid bilayer was fitted into the Nanodisc density. The bilayer was composed of 75% phosphatidylethanolamine and 25% phosphatidylglycerol in order to mimick the composition of the bacterial plasma membrane. Interestingly, shortly after the start, a stable attraction between lipids and rRNA helix H59 was observed. The resulting density distribution resembled the electron density remarkably well, indicating that H59 indeed is capable of establishing another interaction site between the ribosome and a membrane-PCC-complex (Figure 46). In the course of the simulation, the surface area formed between lipids and H59 varied in a range 100 – 200 Å².

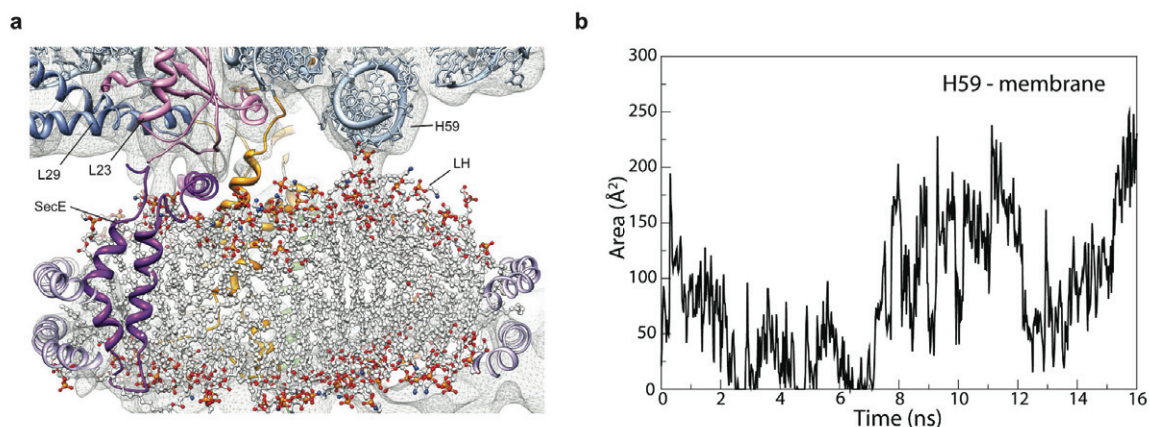


Figure 46: H59 – membrane interaction | (a) Molecular model of the ribosome-SecYE-membrane interface with transparent density filtered at 9-10 Å. Lipid headgroups (LH) contacting the 50S subunit are indicated. (b) Plot of surface area formed between lipids and ribosomal helix H59 during the MD simulation

In contrast, the additional interactions between L24 and lipids, which were also in good agreement with our electron density, were intermittent, as L24 prefers to interact with SecY/nascent chain later in the simulation (Figure 47). In contrast, a strong interaction site was established between the ribosomal protein L23 and the membrane surface. In total, during the simulation the surface area of interaction between the membrane and the entire ribosome varied between 200 – 500 Å².

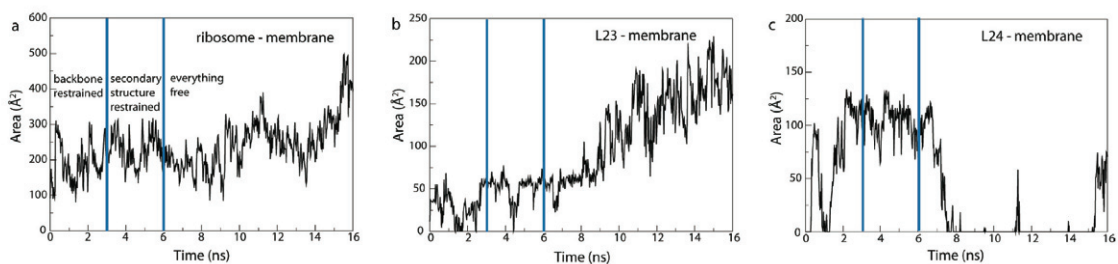


Figure 47: Plot of ribosome-lipid contact area during simulation | Surface area of interaction (measured in Å²) vs. time between the membrane and (a) the entire ribosome, (b) L23, and (c) L24 is shown. The blue lines at 2.5 ns and 6 ns denote the different stages of equilibration

Both, the map and the MD simulation revealed a stable attraction between lipids and rRNA helix H59. Notably, this lipid-H59 interaction resulted in a redistribution of the lipids which affects the immediate vicinity of the suggested TM domain insertion region (Figure 48).

The lateral diffusion of lipids is decreased around H59 and the cytoplasmic leaflet of the membrane is less well ordered. Furthermore, it appears that the positive charges of the lipid headgroups are strongly attracted by the negative charges of RNA helix H59 backbone. The attraction of the charged headgroups induces a certain disorder of the lipid bilayer. Stunningly, a groove within the membrane juxtaposed to the signal anchor helix is formed.

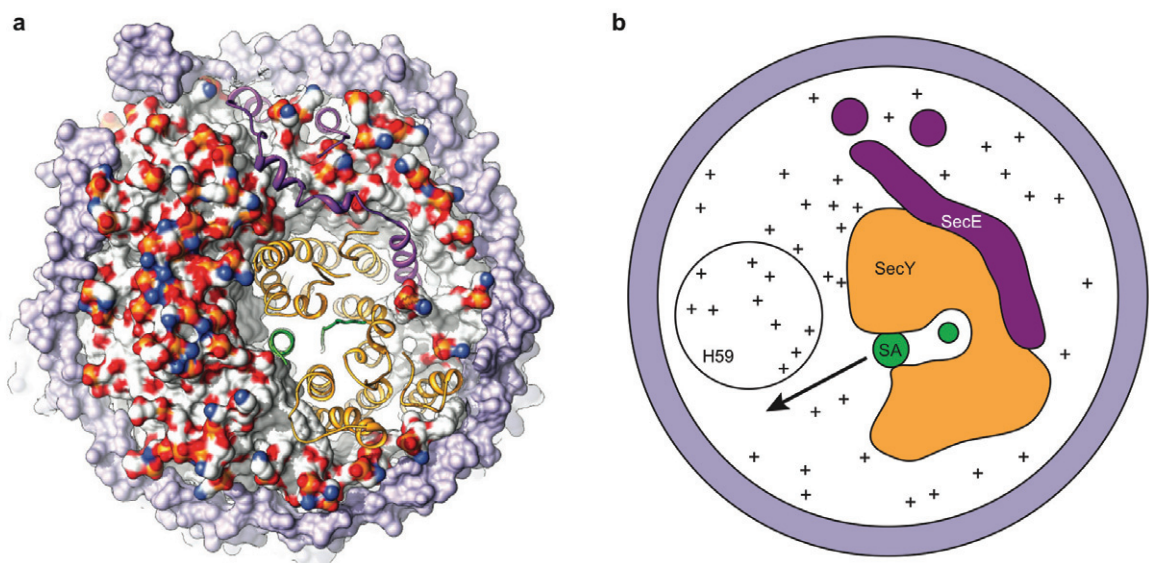


Figure 48: Surface representation of the Nd-SecYE complex seen from the ribosome after 16 ns MD simulation | (a) Apo-A1 is shown in light purple, SecY in orange, SecE in purple, nascent chain in green and the atoms of the lipid head-groups are coloured in orange (phosphate), red (oxygen) and blue (nitrogen), respectively. Note the accumulation of positive charges in the region close to H59 and the disorder of the lipids forming a groove juxtaposed to the signal anchor. (b) Schematic depiction of the view in (a) using the same colour code and indicating the probable path of the nascent TM domain for integration into the bilayer.

4 Discussion

Structural analysis of membrane proteins proves to be difficult. Most of the structural information of membrane proteins obtained thus far is derived from detergent solubilised complexes. Therefore, the visualization of membrane proteins within a lipid bilayer is one of the core issues of structural biology. Here, a new method to obtain subnanometer resolution of membrane proteins in a membrane environment is presented. By integrating the *E. coli* SecYEG complex into a defined nano-scale phospholipid environment, termed Nanodiscs, it was possible to obtain sub-nanometer resolution and to perform a quasi-molecular interpretation of a membrane protein in its natural lipid bilayer environment. An insertion intermediate of a type II membrane protein using the proposed lateral gate of the SecYEG complex for partitioning into the lipid phase was observed. Molecular dynamics simulations based on the structure revealed stable interactions between ribosomal RNA and the membrane that may contribute to the insertase activity of the PCC. This method provides a new approach to visualize functional membrane proteins in the lipid environment by high resolution single particle cryo-EM.

4.1 Generating Nanodiscs

Several protocols for the generation of nanodiscs had been published (Borch and Hamann, 2009). Yet, depending on the type of lipid and membrane protein, the protocols varied in several aspects: the ratio of the components of the self-assembly mixture, incubation times and temperatures and detergent-removal. Accordingly, a new protocol for the generation of Nanodiscs containing *E. coli* lipids had to be established. Initial experiments for the self-assembly of Nanodiscs led to a great variety of Apo-A1/lipid-particles of heterogeneous sizes (data not shown). It was crucial to reduce the amount of lipids in order to obtain monodisperse Nanodiscs. This is in good agreement with data presented by Bayburt et al. (Bayburt et al., 2002). Here, two types of phospholipids were used to assess the optimum ratio of Apo-A1/lipid for the generation of Nanodiscs. Indeed, it is of utmost importance to define the optimum ratio of Apo-A1/lipid. Below the optimum ratios, nonspecific aggregates of Apo-A1 and lipid are generated, whereas above these ratios, larger aggregates containing Apo-A1 and lipids are formed to a much greater extent. Furthermore, these

experiments indicated that the shape of the peak of the size-exclusion chromatography is also depending on the nature of the lipids used. While Nanodiscs composed of dipalmitoyl phosphatidylcholine (DPPC) eluted as a sharp peak, Nanodiscs composed of 1-palmitoyl-2-oleoyl-phosphatidylcholine (POPC) eluted with a shoulder (Bayburt et al., 2002). Accordingly, Nanodiscs composed of *E. coli* lipids also eluted with a shoulder. The self-assembly of Nanodiscs composed of *E. coli* lipids lead to two distinct peaks during SEC, with the first peak corresponding to Nanodiscs of an estimated particle diameter of 11 nm and the second one corresponding to Apo-A1 particles of an estimated diameter of 8 nm (Figure 13). According to molecular dynamics simulations (Catte et al., 2006), lipid-poor Apo-A1-assembly tend to form twisted ellipsoidal particles of a smaller diameter (Figure 49). Hence, the observed second peak in the SEC of *E. coli* lipid Nanodiscs is likely to be composed of these lipid-poor twisted Apo-A1 particles. These findings strongly support the importance of an optimum Apo-A1/lipid ratio.

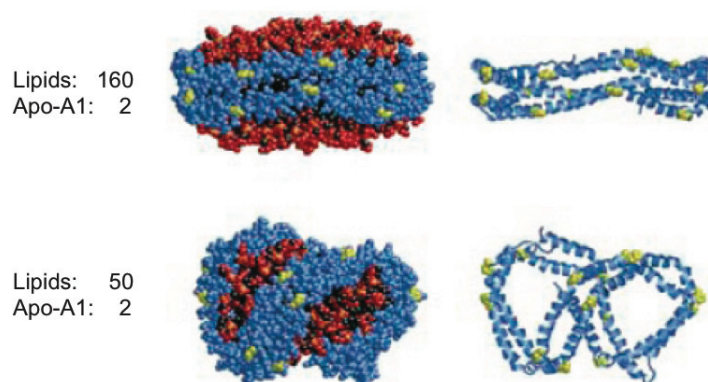


Figure 49: Images of MD simulations of Apo-A1/lipid particles. Two different views are shown as space filling and ribbons representations of each particle containing POPC and ApoA-1 at molar ratios of 160:2 per particle (10.6 nm diameter, upper panel) and 50:2 per particle (7.8 nm diameter, lower panel) Charged portions of the POPC headgroups are space filling in red (oxygen atoms) and orange (phosphorus atoms), and fatty acyl chains are space filling in black. The protein is in blue and prolines are space filling in yellow in both representations (Figure adopted from Catte et al., 2006).

4.2 Incorporation of SecYEG into Nanodiscs

After determining the optimum Apo-A1/lipid ration for the self-assembly of Nanodiscs with *E. coli* lipids, SecYEG was reconstituted into Nanodiscs. Hereby, the protocol for the self-assembly of Nd-E could be used without major changes. In the course of this thesis, Alami *et al.* reported on SecA-interactions with SecYEG incorporated into Nanodiscs (Alami et al., 2007). Interestingly, the size-exclusion chromatography elution profile of Nd-SecYEG generated by Alami et al. was almost identical to data obtained during this thesis. Further biochemical characterization of Nd-SecYEG revealed a monomeric SecYEG within the Nanodiscs. In addition, it was shown that the binding and activity of proteins interacting with SecYEG is dependent on the lipid composition (van Voorst and de Kruijff, 2000). Interestingly, the SecYEG embedded in the Nanodisc was much more thermo-stable when compared to detergent-solubilized SecYEG (Alami et al., 2007), indicating that the lipid bilayer that surrounds the membrane protein indeed provides a superior environment when compared to detergent-micelles.

Taken together, these data show that SecYEG within the Nanodiscs is monomeric, thermostable, functional and, in addition, that the lipid environment is also crucial for SecYEG-interacting factors.

4.3 Membrane and SecYEG interaction of FtsY

The bacterial SRP-receptor FtsY has been shown to interact with both lipids and SecYEG (Grudnik et al., 2009). Based on concerted GTPase activity, the interaction of FtsY with the membrane is crucial for the release of the signal sequence from SRP. It has been shown that the membrane association of FtsY involves two distinct binding sites and that binding to both sites is stabilized by blocking its GTPase activity (Angelini et al., 2006). It was postulated that binding to the membrane requires only the NG-domain of FtsY whereas the A-domain is believed to interact with SecY (Weiche et al., 2008). It was concluded that SecY in that sense may be seen as a transient lipid anchor for FtsY. Recently, Parlitz et al. provided evidence that the conserved autonomous amphipathic alpha-helix at the N-terminal end of the N-domain is the essential lipid binding domain (Parlitz et al., 2007).

In this study, an interaction of FtsY-NG+1 with Nd-E was shown (Figure 15), indicating that FtsY-NG+1 establishes a protein-lipid interaction with Nanodiscs and that Nanodiscs thus exhibit membrane-like features that are capable of forming a complex with the membrane-associated protein FtsY. This is in agreement with data, indicating that the NG-domain alone is sufficient for a proper binding of FtsY to the membrane (Angelini et al., 2006; (Bahari et al., 2007); Parlitz et al, 2007).

Subsequent experiments that involved FtsY-NG+1 and Nd-SecYEG, the binding of FtsY-NG+1 to Nd-SecYEG seemed to be enhanced when compared to binding of FtsY-NG+1 to Nd-E. It remains to be elucidated whether this increased binding to Nd-SecYEG is due to further protein-protein interactions with SecYEG with the NG-domain of FtsY. To date, only the A-domain of FtsY has been suggested to interact with SecY (Angelini et al., 2006).

In conclusion, Nd-E and Nd-SecYEG form a stable interaction with FtsY-NG+1 *in vitro*, indicating that Nanodiscs are indeed capable of mimicking membranes.

4.4 SA-dependent interaction of 70S ribosomes with Nd-SecYEG

Binding of ribosome to the SecYEG complex is mediated by several binding sites located at the ribosomal exit tunnel of the 50S subunit. In this study, several binding assays using membrane-embedded SecYEG and both active and inactive ribosomes were performed. When reconstituted into Nanodiscs, the binding of empty ribosomes to SecYEG was abolished (Figure 19a), whereas binding of translocating ribosomes was not affected. This is in agreement with previous data (Mitra et al., 2005), describing the low binding constant of detergent-solubilized SecYEG to empty ribosomes ($K_d = 2 \mu\text{M}$) in contrast to RNCs (32 nM). This indicates that either conformational changes within the ribosome and SecYEG or an additional interaction with the nascent chain and SecYEG lead to an enhanced binding of ribosomes to the protein-conducting channel. However, Prinz et al. measured the K_d of empty 70S ribosomes to the SecYEG complex reconstituted in proteoliposomes to be at $K_d = 6$ nM (Prinz et al., 2000). In contrast, binding of empty 70S ribosomes to SecYEG in inner membrane vesicles (IMVs) is decreased ($K_d = 17$ nM). Taken together, these results are somewhat contradicting and it remains to be elucidated in which way the experimental setup affects the measurements.

In this study, a monomeric SecYEG complex in a membrane environment is investigated. The fact that empty ribosomes do not bind to Nd-SecYEG might represent a functional state that is closer to the *in-vivo* situation in *E. coli*, since blocking of the SecYEG complex by empty ribosomes would affect both SecA-mediated translocation through the SecYEG complex and hinder targeted active ribosomes accessing free SecYEG in the plasma membrane.

4.4 SecYEG-dependent interaction of RNCs with Nanodiscs

To test whether the interaction of RNCs displaying a hydrophobic signal anchor with Nanodiscs is dependent on SecYEG, nascent FtsQ-carrying RNCs were reconstituted (i) with an excess of Nd-SecYEG and (ii) with an excess of Nd-E. Stable binding of RNCs was observed only in the presence of SecYEG (Figure 19b), indicating that neither the ribosome nor the SA domain of the nascent FtsQ could interact with, or insert into the lipid bilayer in a SecYEG-independent manner. This is in agreement with previous data (Urbanus et al., 2001), providing evidence that the Sec-machinery is required for the membrane insertion of FtsQ. Interestingly, in the same study it has been shown that nascent FtsQ remains in contact to both SecY and lipids, indicating that the signal anchor is in a position with access to the lipid phase on the one side and access to SecY on the other side.

4.5 SecYEG triggers GTP hydrolysis in FtsY

The hydrophobic signal sequence of a membrane protein is recognized by the signal recognition particle (SRP). Upon interaction with the SRP receptor (FtsY in *E. coli*), the whole complex is targeted to the plasma membrane and due to GTP-dependent structural rearrangements of both FtsY and SRP, the nascent chain is transferred from the ribosome to the protein conducting channel.

The binding assays performed in this study are novel in two ways:

- (i) all in-vitro experiments were carried out in the absence of detergent
- (ii) the experiments were performed in the presence of all targeting components including a membrane.

In a recent study (Bradshaw et al., 2009), it was shown that detergent mimics the hydrophobic propensities of signal sequences and thus directly affects the binding of SRP to the ribosome. In which way the presence of detergent affects the whole set of *in vitro* experiments addressing co-translational targeting remains to be elucidated.

Taken together, the experiments presented in this work showed (Figures 20, 21):

- a) In the presence of GTP or the non-hydrolysable GTP-analogue GMPPnP, a simultaneous binding of Nd-E, SRP and FtsY to RNCs is visible.
- b) In the presence of GDP or in the absence of guanine nucleotides, the binding of the bacterial SRP-receptor FtsY to the complex was almost abolished whereas the binding of SRP and Nd-E to RNCs remains unchanged.
- c) In the presence of non-hydrolysable GMPPnP, a simultaneous binding of Nd-SecYEG, SRP and FtsY to RNCs is observed.
- d) In the presence of GTP, the binding of the bacterial SRP-receptor FtsY to the complex was lost whereas the binding of SRP and Nd-SecYEG to RNCs remains unchanged.

The experiments were performed such that the RNCs and SRP were incubated to simulate a SRP-sampling and targeting mode, and independently FtsY and Nd-E/Nd-SecYEG were incubated to generate a membrane-bound FtsY complex. After these separate incubations, all components were mixed and incubated. According to current data regarding co-translational targeting, one can conclude that SRP binds with high affinity to the RNC (Grudnik et al., 2009; Wild et al., 2004). The presence of a signal sequence locks the ribosome-bound SRP in an open conformation and increases the affinities of SRP for both the ribosome and GTP. As a next step, the RNC-SRP complex docks to the receptor and thus, to the membrane (Figure 50). SRP and the SRP receptor form a complex only when the GTPases in both proteins are in the GTP-bound state. In the absence of SecYEG, both SRP and FtsY remain bound to the membrane and RNCs (Figure 50). In contrast, when both SecYEG and GTP are present, FtsY appears to dissociate, indicating that the presence of SecYEG triggers GTP-hydrolysis and subsequently induces a conformational change within FtsY, such that it is released from the complex. This idea is further supported by the fact that, in the presence of a non-hydrolysable GTP-analogue GMPPnP, FtsY remains bound to the complex (Figure 21).

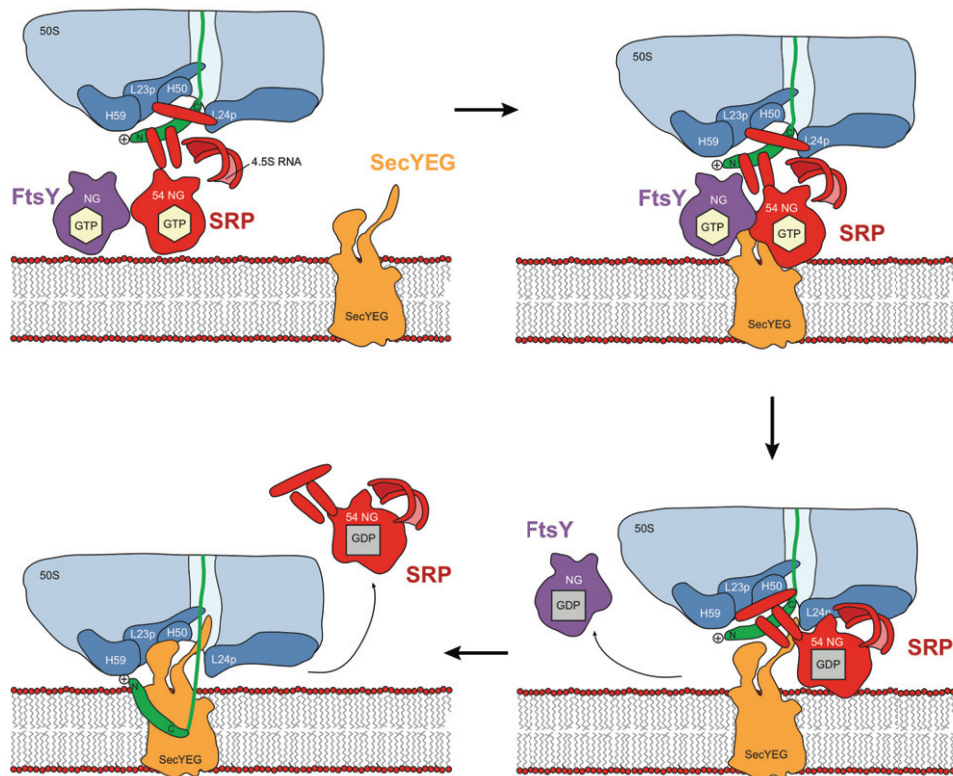


Figure 50: Model for SecYEG-triggered GTP hydrolysis of FtsY | (1) In the cytosol, SRP binds to the nascent SA, FtsY targets the complex to the membrane. (2) The complex interacts with SecYEG, which leads to GTP hydrolysis followed by structural rearrangements of FtsY, leading to the dissociation of FtsY from the targeting complex (3). The nascent SA slides from the hydrophobic M-domain of SRP into the hydrophobic SecYEG/lipid phase (4), while SRP dissociates from the translocating complex.

Taken together, a stable complex of RNCs, SRP, FtsY and the membrane can be formed in the presence of a membrane and GTP. Based on the binding assays presented in this study, it is tempting to speculate that if SecYEG is present, FtsY might undergo a conformational change upon GTP hydrolysis and is released from the complex. Thus, SecYEG would trigger GTP hydrolysis in FtsY (Figure 50).

It remains to be elucidated at which point SRP is released from the targeting complex at the membrane.

4.6 Visualization of transmembrane helices within the lipid bilayer

The cryo-EM density of the reconstituted 70S-RNC-Nd-SecYEG complex revealed a disk-like density beneath the ribosomal tunnel exit, representing the Nanodisc density. It displays the lipid bilayer, with an apparent upper and lower membrane leaflet composed of phospholipid headgroups with a strong electron density (Figure 28a).

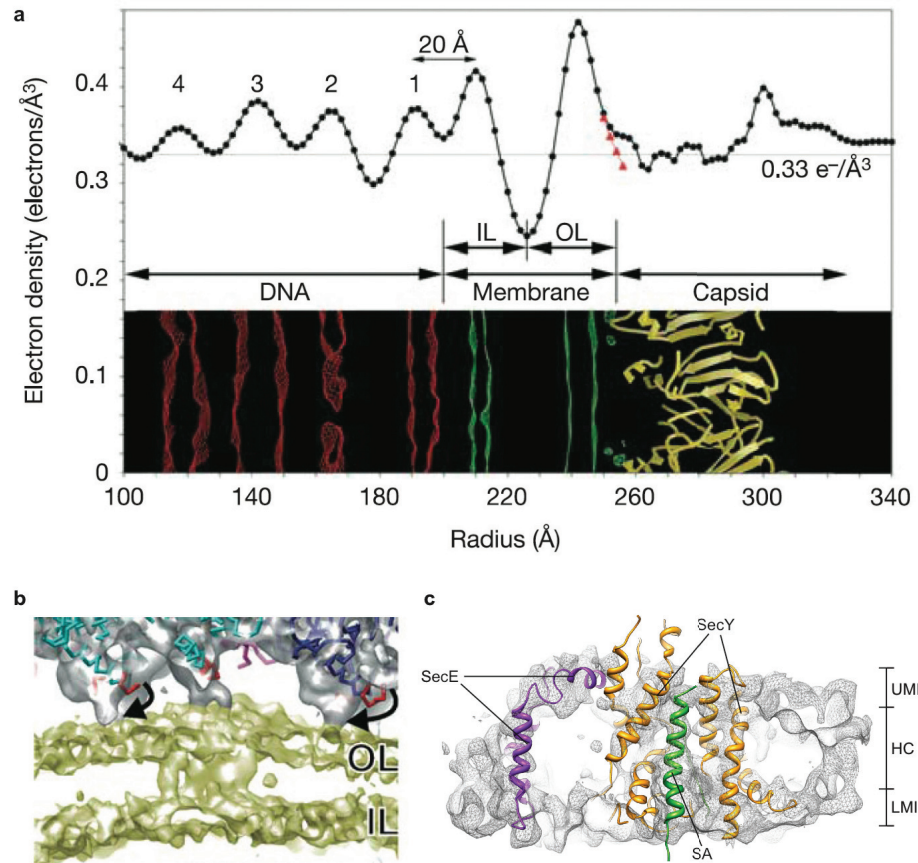


Figure 51: Structures of membrane bilayers | a, Electron density profile (black, circles) of the X-ray structure of the bacteriophage PRD1. Distances are measured from the particle centre along the icosahedral three-fold axis. IL and OL mark the boundaries for the inner and outer leaflets, respectively. DNA layers are numbered 1 to 4 (adapted from Cockburn et al., 2004). b, Transmembrane helices in bacteriophage Bam35. Isosurface representation with membrane density in gold and capsid in gray (adapted from Laurinmäki et al., 2005). c, Side view cut perpendicular to the plane of the membrane of the isolated electron density of the Nanodisc-SecYEG complex to show the TM helices of the lateral gate of SecY. The electron density is represented as a transparent grey mesh. Two layers of density are visible (upper membrane interface, UMI, and lower membrane interface, LMI), separated by a region of lower density (hydrophobic core, HC), containing rod-like features with the ribbon representation of the fitted model of a SecY (orange), SecE (purple) and the signal anchor sequence (green).

In contrast, the electron density for the hydrophobic core sandwiched between the leaflets is not visible, since the acyl chains of the lipids are composed of low-contrast atoms carbon and hydrogen. This distribution resembles that observed in membrane-containing viruses (Cockburn et al., 2004; Laurinmaki et al., 2005) and in liposomes (Tilley et al., 2005) (Figure 51). Interestingly, the cryo-EM reconstruction of the bacteriophage Bam35 showed a clearly visible membrane with outer and inner leaflet, punctuated by bundles of transmembrane helices (Figure 51b). Although the resolution of the virus-density was determined to be at 7.3 Å (FSC 0.5 criterion), the helices within the membrane are not resolved and thus indistinguishable. This indicates that the resolution within the lipid bilayer is worse than 10 Å, since secondary structure information is only available at resolutions in the sub-nanometre range. In contrast, the reconstruction of the 70S-RNC-Nd-SecYEG complex at 7.1 Å resolution (FSC 0.5 criterion) revealed secondary structure information within the lipid bilayer of the Nanodisc with resolved helices, allowing for the fitting of the TM helices of the SecYEG complex (Figure 51c).

4.7 Structure of nascent discoidal HDL

The dimensions of the electron density representing the Nanodisc are in good agreement with a molecular model for nascent discoidal HDL, determined using hydrogen-deuterium exchange mass spectrometry (Wu et al., 2007). The diameter perpendicular to plane of the membrane is 10 nm, whereas the height of the lipid bilayer measures 5 nm (Figure 28). Extra density is visible at the outside of the innermost core density for the Nanodisc. At the very N- and C-terminal regions, Apo-A1 Δ 1-43 contains little stretches of non-lipidated and unstructured protein, resulting in a blob like structure outside the hydrophobic inner radius of the core Nanodisc density. Since Apo-A1 Δ 1-43 may rotate freely around the axis/innermost core density of the Nanodiscs, these blobs are radially distributed around the Nanodisc.

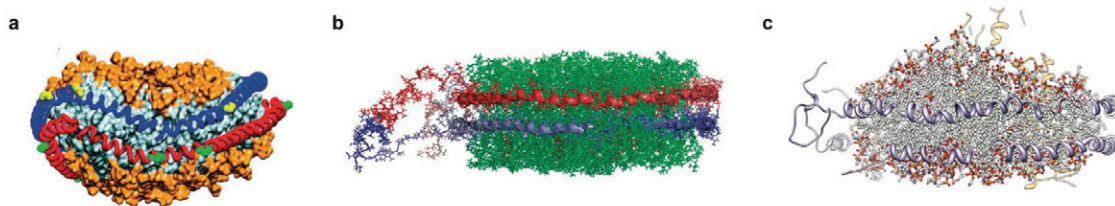


Figure 52: Side view of Nanodisc-models | (a) Nanodiscs model for Apo-A1 by Shih et al. (2005). The Nanodisc is constructed of two Apo-A1 proteins and 160 DPPC lipids. The Apo-A1 proteins are depicted in tube representation in blue and red. Prolines are highlighted in sphere representation in yellow and green. DPPC lipids are shown in MSMS surface representation. The lipid headgroups are shown in orange and the tail groups in gray. (b) Side view view of the solar-flares model of discoidal HDL, shown with antiparallel stacked double-belt Apo-A1 architecture. One Apo-A1 chain (red) encircles the discoidal HDL particle counterclockwise, while a second Apo-A1 chain (dark blue) encircles it clockwise. Green, phospholipids; orange, cholesterol molecules (Wu et al. 2007). (c) Model for Nd-SecYEG with two Apo-A1 proteins in light purple, similar to (b).

In its overall dimensions, the structure of Nd-SecYEG presented here displays a high degree of similarity with the model for nascent discoidal HDL published by Wu et al. as well as models for discoidal Apo-A1 with a lipid-protein ratio of 160:2 presented by Catte et al. as shown in Fig. 48. In contrast, Shih et al. presented a twisted model of Nanodiscs by using Apo-A1 Δ 1-43 (Figure 52a). Here, the Nanodisc displays a severe deformation of both the scaffold protein and lipid bilayer. An explanation has been given in which this is due to insufficient lipid packing density for the length (number of amino acid residues) of Apo-A1 Δ 1-43 surrounding the Nanodisc (Shih et al., 2005). This results in an out-of-plane deformation and a significant flexibility of the Apo-A1 Δ 1-43 scaffold, which do not align well with each other, suggesting that the full 200-residues of Apo-A1 Δ 1-43 do not bind optimally around a lipid bilayer of this size. Although the density of the Nanodisc presented in this work presented here did not allow for the resolution of the protein belts, one can conclude that the reconstruction aligns best with the Nanodisc models presented by Catte et al. and Wu et al. (Figure 52b).

4.7 The ribosome-membrane junction

Previous fluorescence-quenching experiments suggested a tight seal formed between the ribosome and the PCC within the membrane with a large channel (40-60 Å wide) (Crowley et al., 1994; Crowley et al., 1993; Hamman et al., 1997). Yet, a continuous seal around the ribosome-PCC connection would not allow the egress of cytosolic domains of integral membrane proteins. In addition to that, all cryo-EM reconstructions of ribosome-PCC complexes, even at low resolution, revealed a gap between the PCC and the ribosome.

It has to be noted that all complexes reconstructed so far were obtained by detergent-solubilized complexes. Thus, it might be that the presence of the detergent micelle might not allow for the formation of a tight seal and artificially generates a gap. Only one low-resolution (30 Å) reconstruction of a ribosome-PCC complex in a proteoliposome-environment has been obtained so far (Menetret et al., 2000).

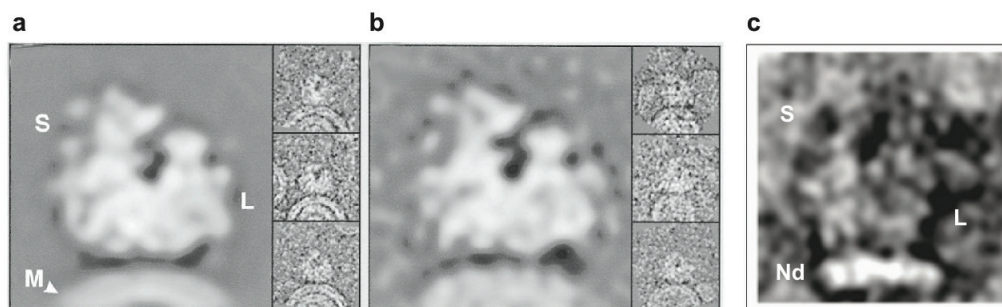


Figure 53: Interaction of Ribosomes with Membranes | (a) Three images of yeast ribosomes associated with channels in vesicles are shown on the right (protein and lipid are white). A projection map of the final 3D reconstruction is shown on the left. The small (S) and large (L) ribosomal subunits are labeled, and the membrane is indicated (M). (b) Three images of canine ribosomes associated with channel complexes in native membranes (K-RM) are shown on the right. A projection map of the final 3D reconstruction is shown on the left (adapted from Menetret et al., 2000). (c) Negative stain image of a 70S RNC complex bound to Nanodisc-SecYEG. Small (S), large subunit (L) and the Nanodisc (Nd) are indicated.

Interestingly, this reconstruction did not reveal a single connection between the ribosome and the PCC/liposome, in contrast, the ribosome seemed to be floating on the proteoliposome and thus exhibiting a massive gap (Figure 53a,b, Figure 54a). However, negative stain images of 70S ribosomes bound to Nanodisc-SecYEG complexes reveal a tight binding between the membrane and the ribosome and several connections (Figure 52c, Figure 53b).

A reconstruction of yeast ribosomes bound to proteoliposomes containing purified yeast Sec61p complex at 30 Å reveals a gap, similar to that observed of between detergent-solubilized Sec-complexes and ribosomes in the same publication (Figure 54). This led to the conclusion that a gap is an intrinsic feature of native ribosome-channel-membrane junctions.

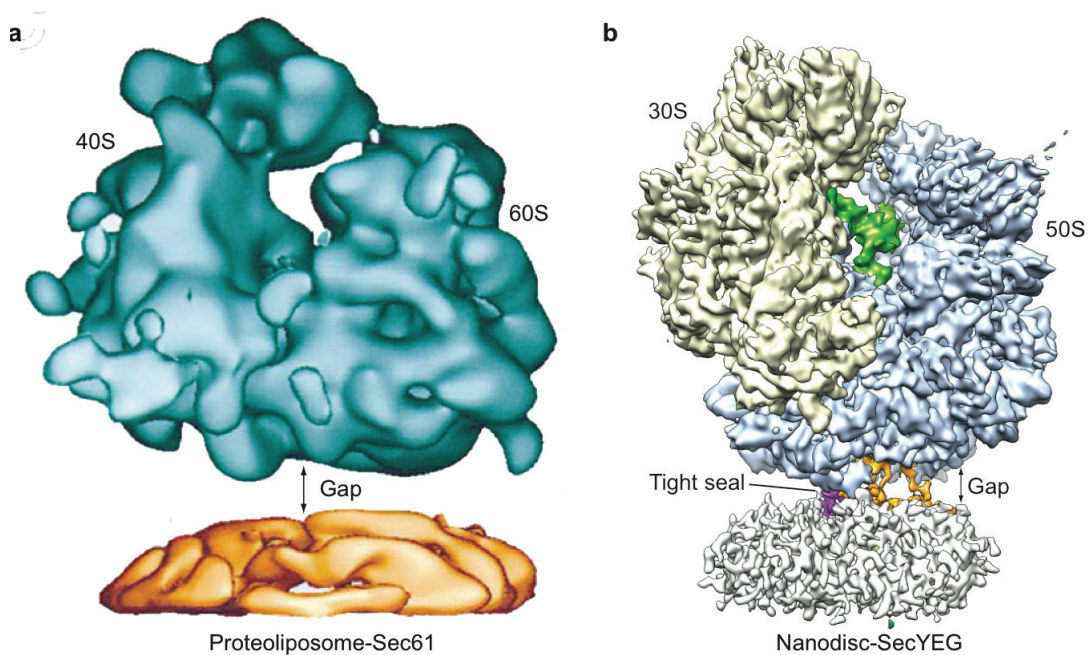


Figure 54: Cryo-EM reconstructions of ribosome-membrane interactions | (a) A 3D surface for the yeast ribosome-vesicle map at 30 Å is shown in the frontal view. A gap is seen between the ribosome (green) and the membrane (gold). The double arrow indicates the large gap (adapted from Menetret et al., 2000). (b) The cryo-EM reconstruction of the active 70S-RNC-Nd-SecYEG complex at 7.1 Å resolution. The ribosomal 30S subunit is shown in yellow, the 50S subunit blue, SecY orange, SecE purple, Nanodisc white. The tight seal on side is indicated, the folding cavity or gap is indicated with a double arrow

Yet, the cryo-EM reconstruction of a 70S-RNC complex bound to Nanodisc-SecYEG at 7.1 Å resolution revealed a semi-seal between the ribosome and the membrane-PCC complex, mainly composed by the interaction of ribosomal proteins L23, L24, L29 and 23S RNA on the one hand and SecE and lipids on the other hand. Thus, there is a tight connection on one half of the ribosomal exit tunnel, whereas on the other half of the ribosomal exit tunnel, a large cavity between the ribosome and the Nd-SecYEG beneath proteins L22 is observed.

With a gap of about 15-25 Å between the ribosome and the Nd-SecYEG, this cavity suffices to provide the space required for folding or egress of cytosolic domains of

membrane proteins or for recruitment of co-factors involved in folding events such as SecA. Interestingly, the cavity is in an area where the cytosolic loops of SecG are expected to reside. SecG is believed to interact with SecA in cotranslational translocation (Matsumoto et al., 1998; Nishiyama and Tokuda, 2009). In general, it can be stated that high-resolution data is needed to precisely define the interactions between the membrane-PCC and the ribosome.

4.8 The canonical binding mode of ribosome-PCC complexes

At higher resolution it is possible to identify the previously observed interactions between L8/9 and H50/53/59 and, to a lesser extent, L6/7 reaching into the ribosomal exit tunnel (Figure 29). The positions of L8/9 and L6/7 and the ribosome are in good agreement with recently published structures of the ribosome-Sec-complexes (Menetret et al., 2007, 2008; Becker et al., 2009). Notably, the binding mode observed here in the presence of a signal sequence and a lipid bilayer is very similar to the mode found in inactive complexes and in detergent solution (Menetret et al., 2007, 2008; Becker et al., 2009) (Figure 55). Thus, this interaction appears to represent the canonical binding mode of the Sec-complex to the universal ribosomal adaptor site for both prokaryotic and eukaryotic complexes.

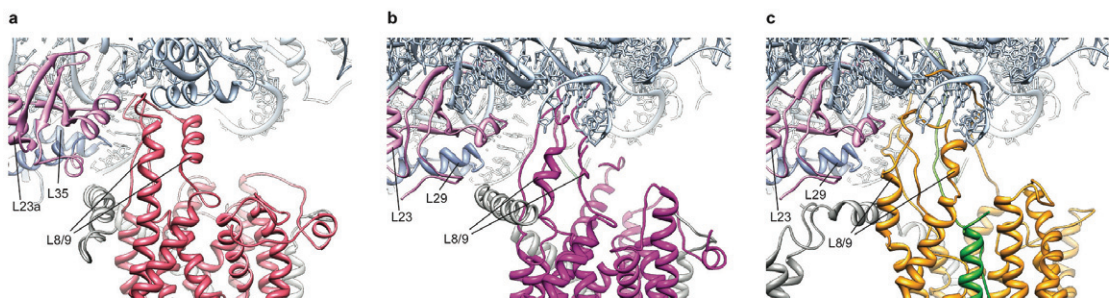


Figure 55: Canonical binding of PCCs to ribosomes | (a) Close-up on the interaction of cytosolic loop L8/9 of the mammalian Sec61 complex (red, PDB: 2WWB) with the eukaryotic 80S ribosome. (b) Close-up on the interaction of cytosolic loop L8/9 of a mixed model of the archeal SecYE complex with L6/7 and L8/9 replaced by a model of the corresponding *E. coli* SecY loops (purple, PDB: 3B00). (c) Close-up on the interaction of cytosolic loop L8/9 of the *E. coli* SecYEG complex (orange) with the prokaryotic 70S RNC and an inserted signal anchor

An additional contact represents the C-terminus of SecY, contacting ribosomal protein L24 and rRNA helices H24/50 (Figure 29). A contribution of the SecY C-terminus to ribosome binding is in agreement with recent findings for both the bacterial (Gumbart et al., 2009) and the eukaryotic system (Becker et al., 2009), as well as mutational studies revealing translocation defects of C-terminally truncated SecY (Chiba et al., 2002). SecE also contributes to the interaction of the PCC with the ribosome (Figure 35) consistent with previous data (Becker et al., 2009; Gumbart et al., 2009; Menetret et al., 2007; Menetret et al., 2008). Both the N-terminus as well as the amphipathic helix of SecE contact the ribosomal adaptor site proteins L23 and L29, respectively. A stretch of conserved residues in the amphipathic helix of SecE (Murphy and Beckwith, 1994) is involved in contacting both SecY and L23/L29. While in agreement with several previous studies (Becker et al., 2009; Kalies et al., 2008; Menetret et al., 2007; Menetret et al., 2008), (Gumbart et al., 2009), these findings are difficult to reconcile with the interpretation by Mitra et al. (Mitra et al., 2005) (Figure 56).

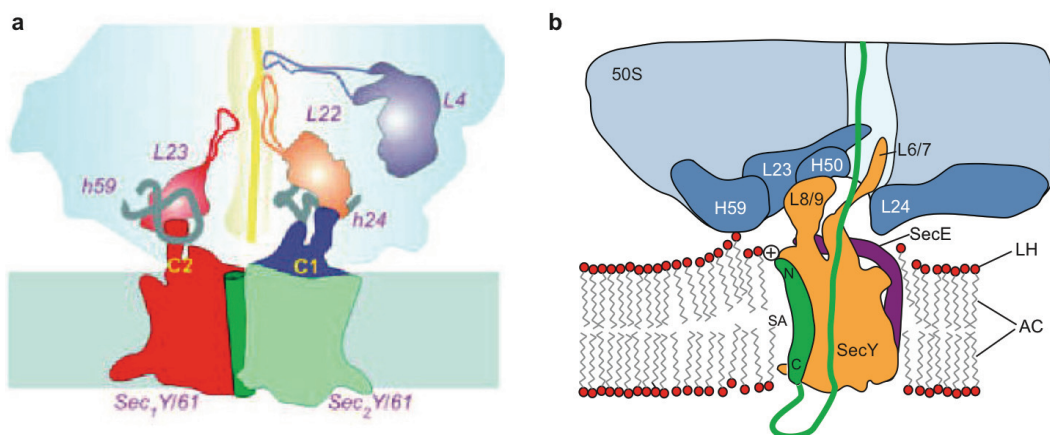


Figure 56: Conflicting models of Sec binding to the ribosome | (a) Schematized version of the PCC-interpretation by Mitra et al. (2005) with the polypeptide exit site of the ribosome in the front view. In this model, the PCC is made up of a dimer of SecYEG complexes (red and green, respectively), arranged in a front-to-front orientation (lateral gates facing each other). (b) Schematized version of the recent PCC-interpretations of the PCC made up of a monomeric Sec-complex (orange) bound to the ribosome.

4.9 L6/7 acts as a sensor within the tunnel

The loop between SecY TM helices 6 and 7, L6/7 reaches into the ribosomal exit tunnel and contacts ribosomal RNA helices H6/24/50, respectively (Figure 29). In addition, L6/7 contacts the nascent chain in various positions, with the upper tip also contacting the tip loop of ribosomal protein L23. The tip of L6/7 of SecY embraces the nascent chain.

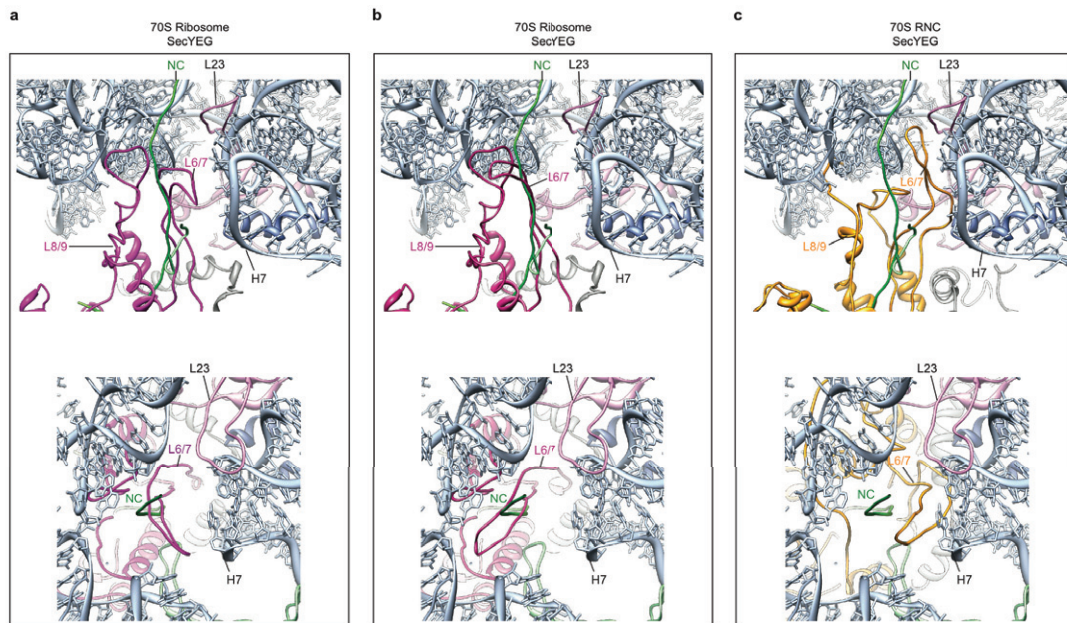


Figure 57: Comparison of L6/7 conformation within the ribosomal tunnel | Close-up of a section through the ribosomal exit tunnel with fitted models of L6/7 of SecY. (a) A model for an inactive, monomeric SecY bound to a non-translating ribosome (purple, PDB: 3BO0) was fitted according to the position of ribosomal RNA and superimposed to our model of the translating ribosome with the nascent chain (green). In that position, L6/7 of the inactive SecY would prevent the exit of the nascent chain. Upper panel: side view, lower panel: view from the inside of the ribosomal tunnel towards the ribosomal exit b, as in (a), but with a model for an inactive, monomeric SecY with an alternate L6/7 conformation binding to a non-translating ribosome (ruby, PDB: 3BO1). Also in this position, the exit of the nascent chain is hindered by L6/7 of the inactive SecY. c, view as in (a). The model for the translating ribosome bound to an open SecY (orange) within a membrane environment. L6/7 reaches up along the wall of the ribosomal tunnel and contacts both, the nascent chain and L23. The position of L6/7 within the ribosomal exit tunnel of the hybrid complex allows the exit of the nascent chain

This may indicate a putative role of L6/7 as a sensor for the presence and/or the nature of the nascent chain inside the ribosomal tunnel. Hereby, mainly residues Lys250 – Arg256 might function as a putative external sensor inside the ribosomal tunnel wall,

interacting with both the ribosome (L23, H6/24/50) and the nascent chain. Recently, it has been shown that Arg255 and Arg256 are crucial for stable binding of 70S ribosomes to SecYEG (Menetret et al., 2007). Interestingly, when interacting with an empty ribosome, a different conformation of L6/7 of SecY was observed to occlude the tunnel (Menetret et al., 2007) (Figure 57a,b). This might be of functional relevance after termination and re-initiation of translation when a newly arriving nascent chain could regulate dissociation of the PCC from the ribosome by interfering with the L6/7.

4.10 Conformational changes of L23 and L24

Upon progression from the PTC into the membrane bilayer, the nascent chain contacts several ribosomal proteins (Seidelt et al., 2009), the PCC and the lipid bilayer. It has been proposed that the conserved loop of L23, reaching into the tunnel wall, might constitute a potential binding site for nascent proteins (Houben et al., 2005) and subsequently altering its conformation, leading to an inside-outside signalling of the nascent chain (Bornemann et al., 2008). Inspection of the ribosomal exit tunnel revealed a conformational change of the tip of L23 (Figure 39,40) when compared to electron densities of unprogrammed ribosomes and in comparison of published crystal structures (2i2v). Compared with the inactive crystal structure (2i2v), the tip of L23 bends 6 Å down, leading to an interaction of L23 His70 with the nascent chain at a distance of 19 aa from the PTC. Taken together, a three-way-junction in the area at the tip of L23, including L23, the nascent chain and L6/7 may lead to an enhanced communication of in- and external ribosomal proteins and thus enable an inside-outside communication between the ribosome and putative binding partners and the membrane surface.

When exiting the ribosomal tunnel, the nascent chain contacts another three-way junction of the complex: the tip of L24 and both the C-terminus and possibly L6/7 of SecY (Figure 39,40). The β -hairpin loop of L24 is bent downwards towards the lipid surface and the C-terminus of SecY. Accordingly, the tip of a homologous L24 has been observed to bend down upon interaction with the *D. radiodurans* trigger factor (TF) in complex with the *D. radiodurans* large ribosomal subunit (Schlunzen et al., 2005). Here, a model was proposed in which the nascent polypeptide chain exiting the

tunnel passes the tip of the extension of L24 and enters into the hydrophobic crevice in the binding domain of the trigger factor. This is in agreement with data presented in this study, where a close interaction between the tip of L24 and the NC is structurally observed.

4.11 Open structure of SecYEG and path of the nascent chain

After fitting of the TM helices of SecY, a strong density within the proposed lateral gate of the PCC was accounted for the signal anchor. To fit an extra helix into the lateral gate, we had to slightly adjust SecY from the SecA-activated, pre-open structure into an open structure (Zimmer et al., 2008) (Figure 41). The transformation from an inactive state (*M. janaschii*, van den Berg et al., 2004) to a pre-open state (*T. maritima*) included mainly TM helices of the C-terminal half (Zimmer et al., 2008), which, in the presence of the translocating ribosome are stably bound to the ribosome. Now, to convert into an open state, the N-terminal half of SecY opens up. This is in agreement with the model for lateral gate opening, which was proposed by van den Berg et al. (2004; see introduction, Figure 5c,d) and in agreement with recent data indicating that the lateral gate has to open up for the insertion during protein translocation (du Plessis et al., 2009). According to the open structure of the PCC with shifts in both N- and C-terminal region, the position of the two N-terminal helices of SecE is also slightly shifted outwards with respect to the inactive model. Noteworthy, a shift of the amphipathic helix has also been observed in the pre-open structure of SecY upon binding of SecA (Zimmer et al., 2008).

Taken together, one may conclude that the conversion from a closed into an active state requires two major events: (i) binding of a translocation partner leads to a shifting of the C-terminal half (as observed with SecA) and (ii) the presence of a nascent chain/signal anchor leads to a shifting of the N-terminal half (Figure 58).

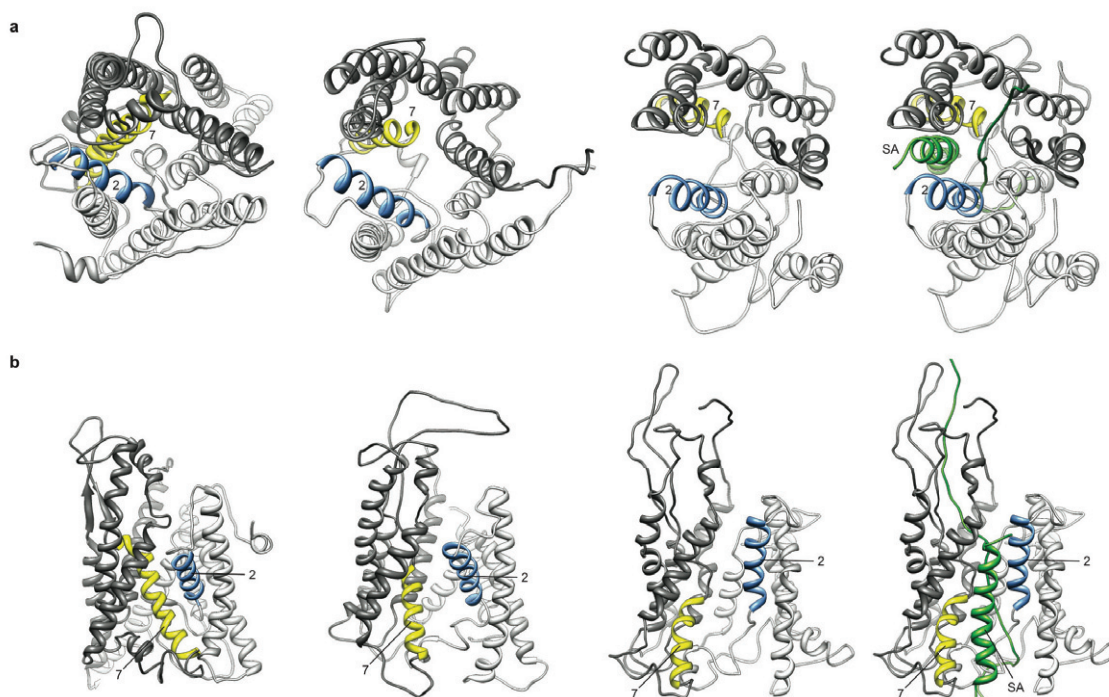


Figure 58: Opening of SecY | (a) Comparison of SecY structures in different conformations, viewed from the cytoplasmic side. Left, structure of the closed, detergent-solubilised SecY from *M. janaschii* (PDB: 1RHZ). Middle left, structure of the pre-open, detergent-solubilised SecY from *T. maritima*. Middle right, model of the open, membrane-embedded SecY from *E. coli*. Right, model of the open, membrane-embedded SecY from *E. coli* with a SA helix within the lateral gate. (b) as in (a), but view of the lateral gate.

4.12 Path of the nascent FtsQ within SecY

Extra density reaching from the exit of the ribosomal tunnel into the center of the PCC was interpreted as the nascent chain. Due to limited resolution, the path of the NC within the PCC could not be traced in a whole. In order to obtain a complete model for the MD simulation, the NC model was extended from the cytoplasmic to the periplasmic side through the central pore (Bauer and Rapoport, 2009; Osborne and Rapoport, 2007) and connected with the SA within the proposed lateral gate of the PCC, resulting in the loop-like arrangement expected for a type II membrane protein. In this model, the hydrophobic pore ring has a diameter of 10-12 Å, which is in good agreement with recent data (personal communication by A.J. Driessen). This dimension leaves enough space for an extended polypeptide chain to pass while, at the same time, a substantial flow of ions would be prevented in the presence of a translocating peptide.

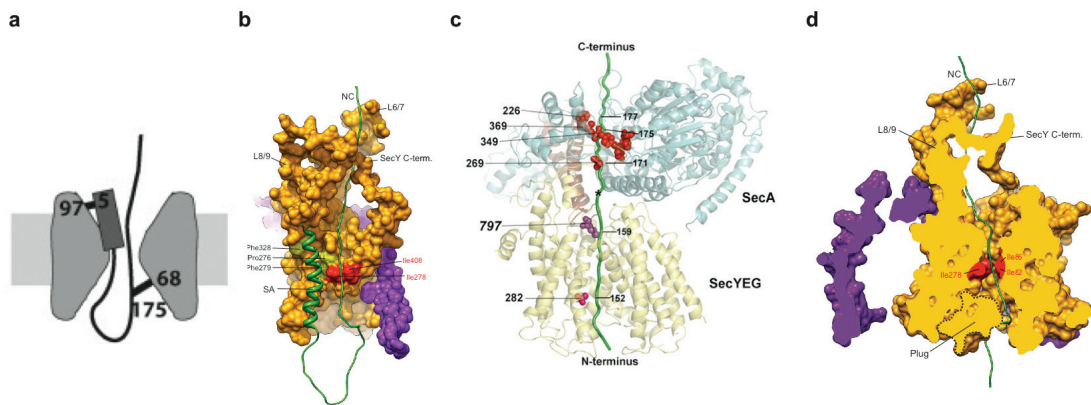


Figure 59: Path of nascent FtsQ within SecY | (a) Scheme of SecY crosslinking to both the signal sequence and mature region of pOA (adapted from Osborne and Rapoport, 2007). (b) Surface representation of the open SecY model (orange) in the presence of the FtsQ signal anchor and the nascent chain within SecY (green), the N-terminal half of SecY is omitted. (c) Interaction sites with a translocating polypeptide mapped onto the *T. maritima* SecA structure (PDB: 3DIN). Side view of the SecA-SecY structure with a modeled translocating pOA-DHFR substrate (pOA is shown in green; the DHFR domain was omitted for clarity). The cross-linking SecY pore residue is shown as pink balls. The star indicates an opening toward the cytosol (adapted from Bauer and Osborne, 2009). (d) Model of SecY, but cut perpendicular to plane of the membrane, revealing the suggested path of the nascent chain.

The resulting model provides a plausible scenario with an overall arrangement that is in agreement with previous biochemical and structural data. This SA position explains chemical cross-link data that indicate, at a similar chain length, close proximity of the SA of FtsQ to both SecY and lipids (Scotti et al., 2000; Urbanus et al., 2001). Upon further chain elongation, complete release of the SA from SecY is likely to be triggered by additional factors such as YidC (Scotti et al., 2000; van der Laan et al., 2001). The position of the SA in the lateral gate is also consistent with contacts to conserved hydrophobic residues of SecY TMs 2, 7 and 8 (Osborne and Rapoport, 2007; Tszukasaki et al., 2008) as well as with contacts to residues that can be cross-linked to the signal sequence of proOmpA (Osborne and Rapoport 2007, Figure 59a). This is further validated by data obtained by crosslinking translocation intermediates of a post-translocational complex of SecA-SecY (Bauer and Rapoport, 2009). Here, a nascent pOA-DHFR polypeptide chain could be cross-linked to the pore residue 282 in SecY (Figure 59c).

4.13 Position of the signal anchor

The MD simulation revealed a stable position of the SA with respect to SecYE (Figure 44) and no hydrogen bonds, but mainly hydrophobic interactions were observed between the SA and SecY (Figure 45). Whereas a substantial number of hydrogen bonds would reduce the TM domain's ability to exit into the bilayer, hydrophobic interactions would be in agreement with partitioning according to the TM domain's hydrophobicity. Although it cannot be excluded that the SA exposes a limited flexibility, the robust density argues in favour of high occupancy in the observed position. Taken together, this indicates that the SA is in a reasonable and meaningful position in the structure. The positively charged N-terminus of the FtsQ SA could remain on the cytosolic side, stabilized by additional interactions with either the phospholipid headgroups or the negatively charged phosphate backbone of the nearby rRNA helix H59. At the same time, the position of the SA would prevent phospholipids from entering the center of the PCC.

Upon an elongation of the nascent FtsQ chain, the signal anchor might move to a combined YidC/lipid environment. As has been reported, the complete translocation of full-length FtsQ requires both SecA and YidC and suggests a crucial role for YidC to mediate TM release into the lipid bilayer (Urbanus et al., 2001). In contrast, it was shown that for the *in vitro* reconstitution of FtsQ into proteoliposomes, YidC is not required for insertion (van der Laan et al., 2004), but could play a kinetic role for the lateral release of the TMS from the translocon. Moreover, it was shown that the initial membrane insertion of the SA of ribosome-bound, nascent FtsQ into SecYEG proteoliposomes occurs independently of the PMF (Scotti et al., 1999; van der Laan et al., 2001), but the insertion of the complete, full-length FtsQ could not be detected under these conditions (van der Laan et al., 2004).

Taken together, our observation of a transmembrane helix, retained in the lateral gate of SecY but at the same time exposed to the lipid environment may represent an intermediate step of the integration of a transmembrane helix into the lipid bilayer. The full integration of FtsQ may require further components such as SecA, YidC and the PMF.

4.13 H59 modulates the lipid bilayer

By applying molecular dynamics flexible fitting to the map, an all-atom model of the active ribosome-Nanodisc-SecYE-complex was generated. The simulation was carried out in a two-stage approach: (i) initial equilibration of water and lipids with maintaining the protein and RNA secondary structure restraints followed by (ii) a complete simulation of the complex.

Initially, a flat lipid bilayer into the Nanodisc density, composed of 75 % POPE and 25 % POPG. Shortly after the equilibration, an attraction of lipids towards H59 could be observed. The resulting appearance resembled remarkably well the electron density, indicating that H59 indeed attracts lipids and thus establishes another binding and interaction site between the ribosome and a membrane-PCC-complex. Note that at this first stage, the electron density was not taken into account and the lipid behaviour is thus independent from EM data. As mentioned before, this lipid-H59 interaction resulted in a redistribution of the lipids that induces a local disorder of the lipid bilayer in the immediate vicinity of the suggested TM domain insertion region (Figure 46). Due to the interaction of positively charged phospholipid headgroups with H59, the lateral diffusion of lipids is decreased in that region. Thus, it is tempting to speculate that this induced disorder may favour membrane insertion of TM domains by decreasing the energy barrier for the TM to access the hydrophobic core of the lipid bilayer through the layer of charged head groups. This is supported by the idea that insertion efficiency is determined by the energetic cost of distorting the bilayer in the vicinity of the TM helix, as predicted by MD simulations (Jaud et al., 2009).

4.14 Double role of H59

Based on the observations of electron density that were further supported by the molecular dynamics simulations of the lipid bilayer, it was concluded that H59 attracts the phospholipid headgroups (mainly POPE) of the upper bilayer surface close to the exit of the lateral gate of the translocon, *i.e.* close to the inserted TM helix. Hereby, H59 might facilitate the transit of the SA from the lateral gate into the lipid bilayer by disordering the lipid bilayer and attracting the charged phospholipid headgroups that are in proximity to the inserted SA. Thus, it might reduce the energy requirements for the transit of the TM helix into the membrane.

The proximity between H59 and the SA is striking. The distance between the N-terminus of the signal anchor and H59 is in the range of only 12-15 Å. In type-II membrane proteins, positively charged amino acids N-terminally precede the SA (von Heijne, 1986) (Figure 3). They are typical and necessary for the correct orientation for type-II membrane proteins. According to the observed proximity of H59 and the SA, it is tempting to assume that the positively charged amino acids flanking the SA may be attracted towards the negatively charged backbone of the close-by H59 RNA.

According to this observation, the position of the SA as part of the 70S-RNC-Nd-SecYEG structure was compared to that of an active ribosome with an SRP-bound FtsQ SA (Halic et al., 2006). Stunningly, also in this structure, the N-terminus of the FtsQ-signal anchor is directed towards H59 and in close proximity (8-12 Å, Figure 60).

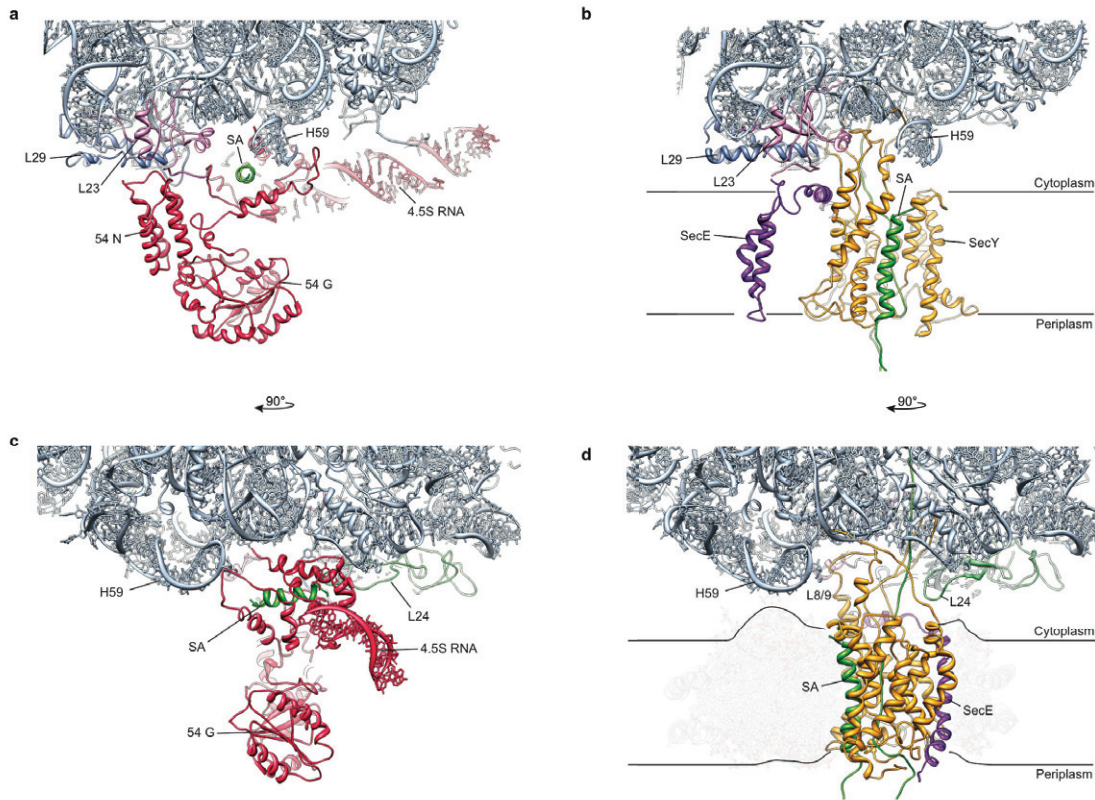


Figure 60: Comparison of the position of the signal anchor with respect to the ribosome in (i) a SRP bound state and (ii) the PCC-inserted state | (a) Close-up of the ribosomal exit site. A molecular model of SRP bound to a translating ribosome with the FtsQ signal anchor (PDB: 2j28). Note the orientation of the signal anchor with respect to ribosomal rRNA H59. (b) Same view as in (a), but now with the molecular model of the PCC-inserted signal anchor. Note the orientation of the signal anchor with respect to H59. (c) As in (a), rotated 90°. (d) As in (b), rotated 90°.

Based on these observations, I would like to suggest a double role for H59 for cotranslational translocation of type-II membrane proteins, according to the positive-inside-rule (van Heijne, 1986) (Figure 61). The signal anchor emerges from the ribosome and glides into the hydrophobic groove of the SRP54 M domain (Grudnik et al., 2009). Here, the positively charged amino acids come into contact with H59 of the ribosome (Figure 61a). The RNC-SRP complex is targeted to the PCC and upon interaction with FtsY, the positively charged amino acids of the SA remain loosely attracted to H59. Upon binding of L8/9 and L6/7 of the PCC to the ribosome, the SA has to shift only slightly and glide downwards into the hydrophobic groove of the lateral gate of the PCC, whereas hydrophilic residues following the SA may be

attracted towards the hydrophilic interior of the channel. After its correct orientation with respect to the lateral gate of the PCC, the phospholipid headgroups of the upper membrane bilayer start to interact with H59 and are thus competing with the positively charged AAs of the SA (Figure 61b). After its correct insertion into the lateral gate of the PCC, the transit of the SA into the lipid bilayer is facilitated by H59-induced distortion within the bilayer close to the SA and H59 (Figure 61c). Thus, H59 plays a double role:

- (i) Orienting the signal anchor with respect to the ribosome and SecY
- (ii) Disordering the lipid bilayer and attracting charged phospholipid headgroups which are in proximity to the inserted SA, thus facilitating the transit of the SA into the membrane.

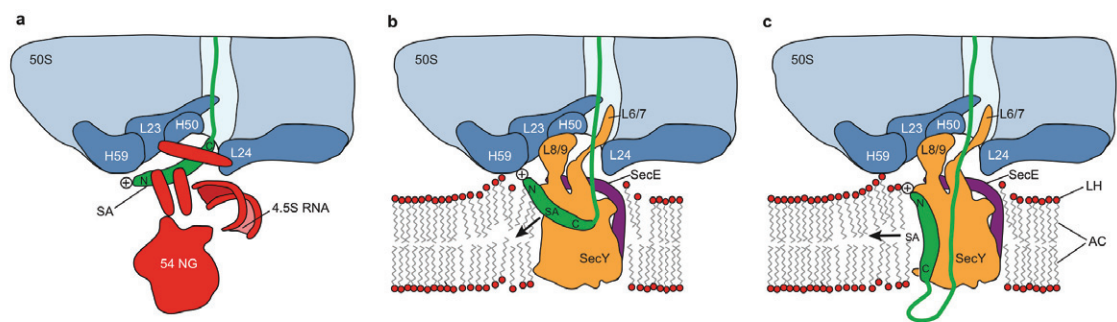


Figure 61: Double role of H59 | (a) Schematic depiction of the bacterial 50S ribosomal subunit (blue) bound to SRP (red) in the presence of a signal anchor sequence as observed before (Halic et al., 2006). The nascent chain with the signal anchor is shown in green. (b) Schematic depiction of a hypothetical TM domain insertion intermediate showing the bacterial 50S ribosomal subunit (blue) bound to the SecYEG complex (orange) in the presence of a signal anchor, accessing the hydrophobic lipid phase through a partially open lateral gate. (c) Schematic depiction of the observed insertion intermediate with the signal anchor TM domain fully inserted into the lateral gate and exposed to the hydrophobic core of the bilayer. Note the proximity of the SA position as observed in the targeting complex (a) and in the insertion intermediate (b,c).

Taken together, the ribosome plays an active role in the process of protein translocation: sensing signal sequences from within the ribosomal tunnel, attracting SRP, orienting the signal anchor and finally altering the conformation of both the PCC and the surrounding membrane to facilitate the incorporation of a TM helix. All components that are involved in the process of protein translocation undergo conformational changes, including the nearby membrane.

It will be interesting to see in which way ribosome-PCC complexes contribute to the folding of cytosolic domains and to what extent cofactors like SecA are involved. Furthermore, it remains to be structurally elucidated how and to what extent other membrane proteins such as YidC are involved in the process of membrane protein insertion.

5. Summary

The ubiquitous SecY/Sec61-complex translocates nascent secretory proteins across cellular membranes and integrates membrane proteins into lipid bilayers. Several structures of this protein-conducting channel have been reported using mostly detergent solubilized Sec-complexes. In this study, a novel approach was carried out: To provide a natural lipid environment, the SecYEG complex was reconstituted into Nanodiscs. Initial biochemical experiments addressing the membrane-mimicking properties of Nanodiscs and their behaviour with respect to co-translational targeting were performed. Moreover, a single-particle cryo-electron microscopy structure of the SecYEG complex in a membrane environment at sub-nanometer resolution, bound to a translating ribosome, was presented. The nascent polypeptide chain could be traced from the peptidyl transferase center into the membrane. Ribosome-PCC as well as ribosome-lipid contacts were identified and structural changes within the PCC were observed. Based on the cryo-EM map, molecular dynamics flexible fitting as well as simulations, a model of a monomeric open PCC with a signal anchor residing in the lateral gate is presented.

For the visualization of the SecYEG complex, the major prerequisite was the generation of “lipid-only” Nanodiscs (Nd-E) and the successful incorporation of SecYEG into these discoidal membranes (Nd-SecYEG). Therefore, the purification of both Apolipoprotein A-1 and SecYEG were established in the laboratory. As a next step, initial experiments were performed to elucidate the conditions for the generation of Nanodiscs containing *E. coli* lipids. Once these conditions had been established, it was crucial to reconstitute the SecYEG complex into Nanodiscs. Subsequently, *in vitro* assays were performed that addressed the membrane-mimicking properties of the Nanodiscs that involved binding of the bacterial SRP receptor FtsY. It could be shown that a truncated version of FtsY binds to both Nd-E and Nd-SecYEG, indicating that Nanodiscs behave similarly to native *E. coli* membranes. To reconstitute a complex of a translating ribosome with Nd-SecYEG, *E. coli* ribosomes carrying an elongation arrested nascent chain of the membrane protein FtsQ were purified and subjected to binding assays. Here, the behaviour of Nanodiscs with respect to co-translational targeting was investigated and it could be shown that empty

ribosomes do not bind to Nd-SecYEG, while FtsQ-RNCs bind to Nanodiscs only in the presence of SecYEG. Thus, both the presence of a nascent chain and of SecYEG embedded in the Nanodisc is required for a proper interaction of ribosomes with these model membranes. In addition, experiments for the formation of co-translational targeting intermediates were performed, indicating that in the presence of GTP or its non-hydrolysable analogue GMPPnP, a stable complex of RNC-SRP-FtsY-Nd-E can be formed. In contrast, only in the presence of GMPPnP a complex of RNC-SRP-FtsY-Nd-SecYEG can be formed, while FtsY seems to dissociate from this complex in the presence of GTP.

In order to obtain high-resolution cryo-EM data, it was crucial to remove unbound Nanodiscs from the reconstituted 70S-RNC-Nd-SecYEG complex. A dataset of 520,000 particles was processed and classified into a subset of 85,664 particles, according to Nd-SecYEG presence. The final reconstruction exhibited a programmed 70S ribosome at 7.1 Å resolution with an additional disc-like density beneath the ribosomal exit site, thus displaying the first structure of a Nanodisc. Furthermore, this was the first single particle cryo-EM structure of a membrane protein embedded in a membrane at sub-nanometer resolution, making it possible to visualize transmembrane helices (TM) within the lipid environment. To interpret the cryo-EM map on a molecular level, crystal structures and molecular models were docked into the density and molecular dynamics flexible fitting procedures were applied. This resulted in a complete molecular model for the 70S-RNC-Nd-SecYEG complex.

Inspection of the ribosomal tunnel revealed a conformational change of the loops of L23 and L24 upon interaction with the nascent chain and L6/7 of SecY. Thus, according to its various conformations when bound to programmed and empty ribosomes, respectively, the tip of L6/7 was suggested to function as a sensor for the presence and/ or the nature of the nascent chain inside the ribosomal tunnel.

Within the Nanodisc, rod-like structures were visible, representing the TM-helices of the SecYEG complex. Fitting of the SecYE-TM-helices resulted in the model of an open SecYE-complex with a strong density within the lateral gate, accounted for by the signal anchor (SA) of FtsQ. In addition to the canonical binding sites of Sec-complexes to ribosomes, a strong connection between the C-terminus of SecY and L24/H24/50 of the ribosome was observed. Furthermore, another strong connection

between rRNA helix 59 and the membrane was observed both in the experimental electron density and in the molecular dynamics simulation. Interestingly, this interaction of H59 and the lipid headgroups resulted in a local disorder of the lipids in vicinity to the lateral gate and the suggested TM insertion region. By interacting with positively charged N-terminal residues of TM domains during co-translational targeting, it was speculated that H59 contributes to the correct orientation of TM domains according to the positive-inside rule.

Taken together, the sub-nanometer resolution cryo-EM structure of the bacterial ribosome-SecYEG complex in a Nanodisc allows for the molecular interpretation of a membrane protein, the SecYEG complex, in its natural lipid bilayer environment. The structure suggests an insertion intermediate of a type II membrane protein using the proposed lateral gate of the SecYEG complex for partitioning into the lipid phase. Molecular dynamics simulations based on the structure reveal stable interactions between ribosomal RNA and the membrane that may contribute to the insertase activity of the PCC. Using nascent polytopic membrane proteins, future studies will address the mechanism of more complex membrane insertion events. This method may provide a general approach to visualize functional membrane proteins in the lipid environment by high-resolution single particle cryo-EM.

6. References

- Ajees, A.A., Anantharamaiah, G.M., Mishra, V.K., Hussain, M.M., and Murthy, H.M. (2006). Crystal structure of human apolipoprotein A-I: insights into its protective effect against cardiovascular diseases. *Proc Natl Acad Sci U S A* *103*, 2126-2131.
- Akimaru, J., Matsuyama, S., Tokuda, H., and Mizushima, S. (1991). Reconstitution of a protein translocation system containing purified SecY, SecE, and SecA from *Escherichia coli*. *Proc Natl Acad Sci U S A* *88*, 6545-6549.
- Alami, M., Dalal, K., Lelj-Garolla, B., Sligar, S.G., and Duong, F. (2007). Nanodiscs unravel the interaction between the SecYEG channel and its cytosolic partner SecA. *EMBO J* *26*, 1995-2004.
- Angelini, S., Boy, D., Schiltz, E., and Koch, H.G. (2006). Membrane binding of the bacterial signal recognition particle receptor involves two distinct binding sites. *J Cell Biol* *174*, 715-724.
- Angelini, S., Deitermann, S., and Koch, H.G. (2005). FtsY, the bacterial signal-recognition particle receptor, interacts functionally and physically with the SecYEG translocon. *EMBO Rep* *6*, 476-481.
- Bahari, L., Parlitz, R., Eitan, A., Stjepanovic, G., Bochkareva, E.S., Sinning, I., and Bibi, E. (2007). Membrane targeting of ribosomes and their release require distinct and separable functions of FtsY. *J Biol Chem* *282*, 32168-32175.
- Bauer, B.W., and Rapoport, T.A. (2009). Mapping polypeptide interactions of the SecA ATPase during translocation. *Proc Natl Acad Sci U S A*.
- Bayburt, T.H., Grinkova, Y.V., and Sligar, S.G. (2002). Self-Assembly of Discoidal Phospholipid Bilayer Nanoparticles with Membrane Scaffold Proteins. *Nano Letters* *2*, 853-856.
- Becker, T., Bhushan, S., Jarasch, A., Armache, J.P., Funes, S., Jossinet, F., Gumbart, J., Mielke, T., Berninghausen, O., Schulten, K., *et al.* (2009). Structure of Monomeric Yeast and Mammalian Sec61 Complexes Interacting with the Translating Ribosome. *Science*.
- Beckmann, R., Bubeck, D., Grassucci, R., Penczek, P., Verschoor, A., Blobel, G., and Frank, J. (1997). Alignment of conduits for the nascent polypeptide chain in the ribosome-Sec61 complex. *Science* *278*, 2123-2126.
- Beckmann, R., Spahn, C.M., Eswar, N., Helmers, J., Penczek, P.A., Sali, A., Frank, J., and Blobel, G. (2001). Architecture of the protein-conducting channel associated with the translating 80S ribosome. *Cell* *107*, 361-372.
- Berk, V., Zhang, W., Pai, R.D., and Cate, J.H. (2006). Structural basis for mRNA and tRNA positioning on the ribosome. *Proc Natl Acad Sci U S A* *103*, 15830-15834.

- Bogdanov, M., Sun, J., Kaback, H.R., and Dowhan, W. (1996). A phospholipid acts as a chaperone in assembly of a membrane transport protein. *J Biol Chem* *271*, 11615-11618.
- Bogdanov, M., Xie, J., and Dowhan, W. (2009). Lipid-protein interactions drive membrane protein topogenesis in accordance with the positive inside rule. *J Biol Chem* *284*, 9637-9641.
- Borch, J., and Hamann, T. (2009). The nanodisc: a novel tool for membrane protein studies. *Biol Chem* *390*, 805-814.
- Borhani, D.W., Rogers, D.P., Engler, J.A., and Brouillette, C.G. (1997). Crystal structure of truncated human apolipoprotein A-I suggests a lipid-bound conformation. *Proc Natl Acad Sci U S A* *94*, 12291-12296.
- Bornemann, T., Jockel, J., Rodnina, M.V., and Wintermeyer, W. (2008). Signal sequence-independent membrane targeting of ribosomes containing short nascent peptides within the exit tunnel. *Nat Struct Mol Biol* *15*, 494-499.
- Bostina, M., Mohsin, B., Kühlbrandt, W., and Collinson, I. (2005). Atomic model of the *E. coli* membrane-bound protein translocation complex SecYEG. *J Mol Biol* *352*, 1035-1043.
- Bradshaw, N., Neher, S.B., Booth, D.S., and Walter, P. (2009). Signal sequences activate the catalytic switch of SRP RNA. *Science* *323*, 127-130.
- Braig, D., Bar, C., Thumfart, J.O., and Koch, H.G. (2009). Two cooperating helices constitute the lipid-binding domain of the bacterial SRP receptor. *J Mol Biol* *390*, 401-413.
- Breyton, C., Haase, W., Rapoport, T.A., Kühlbrandt, W., and Collinson, I. (2002). Three-dimensional structure of the bacterial protein-translocation complex SecYEG. *Nature* *418*, 662-665.
- Breyton, C., Tribet, C., Olive, J., Dubacq, J.P., and Popot, J.L. (1997). Dimer to monomer conversion of the cytochrome b6 f complex. Causes and consequences. *J Biol Chem* *272*, 21892-21900.
- Brundage, L., Hendrick, J.P., Schiebel, E., Driessen, A.J., and Wickner, W. (1990). The purified *E. coli* integral membrane protein SecY/E is sufficient for reconstitution of SecA-dependent precursor protein translocation. *Cell* *62*, 649-657.
- Catte, A., Patterson, J.C., Jones, M.K., Jerome, W.G., Bashtovyy, D., Su, Z., Gu, F., Chen, J., Aliste, M.P., Harvey, S.C., *et al.* (2006). Novel changes in discoidal high density lipoprotein morphology: a molecular dynamics study. *Biophys J* *90*, 4345-4360.
- Chen, J.Z., and Grigorieff, N. (2007). SIGNATURE: a single-particle selection system for molecular electron microscopy. *J Struct Biol* *157*, 168-173.

- Chiba, K., Mori, H., and Ito, K. (2002). Roles of the C-terminal end of SecY in protein translocation and viability of *Escherichia coli*. *J Bacteriol* *184*, 2243-2250.
- Cockburn, J.J., Abrescia, N.G., Grimes, J.M., Sutton, G.C., Diprose, J.M., Benevides, J.M., Thomas, G.J., Jr., Bamford, J.K., Bamford, D.H., and Stuart, D.I. (2004). Membrane structure and interactions with protein and DNA in bacteriophage PRD1. *Nature* *432*, 122-125.
- Collinson, I. (2005). The structure of the bacterial protein translocation complex SecYEG. *Biochem Soc Trans* *33*, 1225-1230.
- Crowley, K.S., Liao, S., Worrell, V.E., Reinhart, G.D., and Johnson, A.E. (1994). Secretory proteins move through the endoplasmic reticulum membrane via an aqueous, gated pore. *Cell* *78*, 461-471.
- Crowley, K.S., Reinhart, G.D., and Johnson, A.E. (1993). The signal sequence moves through a ribosomal tunnel into a noncytoplasmic aqueous environment at the ER membrane early in translocation. *Cell* *73*, 1101-1115.
- Dalbey, R.E., and Chen, M. (2004). Sec-translocase mediated membrane protein biogenesis. *Biochim Biophys Acta* *1694*, 37-53.
- de Keyzer, J., van der Does, C., and Driessen, A.J. (2003). The bacterial translocase: a dynamic protein channel complex. *Cell Mol Life Sci* *60*, 2034-2052.
- de Leeuw, E., te Kaat, K., Moser, C., Menestrina, G., Demel, R., de Kruijff, B., Oudega, B., Luirink, J., and Sinning, I. (2000). Anionic phospholipids are involved in membrane association of FtsY and stimulate its GTPase activity. *EMBO J* *19*, 531-541.
- Denisov, I.G., McLean, M.A., Shaw, A.W., Grinkova, Y.V., and Sligar, S.G. (2005). Thermotropic phase transition in soluble nanoscale lipid bilayers. *J Phys Chem B* *109*, 15580-15588.
- Driessen, A.J., and Nouwen, N. (2008). Protein translocation across the bacterial cytoplasmic membrane. *Annu Rev Biochem* *77*, 643-667.
- du Plessis, D.J., Berrelkamp, G., Nouwen, N., and Driessen, A.J. (2009). The lateral gate of SecYEG opens during protein translocation. *J Biol Chem* *284*, 15805-15814.
- Eitan, A., and Bibi, E. (2004). The core *Escherichia coli* signal recognition particle receptor contains only the N and G domains of FtsY. *J Bacteriol* *186*, 2492-2494.
- Emsley, P., and Cowtan, K. (2004). Coot: model-building tools for molecular graphics. *Acta Crystallogr D Biol Crystallogr* *60*, 2126-2132.
- Foloppe, N., Mackerell, A., and Jr (2000). All-atom empirical force field for nucleic acids: I. Parameter optimization based on small molecule and condensed phase macromolecular target data. *Journal of Computational Chemistry* *21*, 86-104.

- Frank, J., Radermacher, M., Penczek, P., Zhu, J., Li, Y., Ladjadj, M., and Leith, A. (1996). SPIDER and WEB: processing and visualization of images in 3D electron microscopy and related fields. *J Struct Biol* *116*, 190-199.
- Gorlich, D., and Rapoport, T.A. (1993). Protein translocation into proteoliposomes reconstituted from purified components of the endoplasmic reticulum membrane. *Cell* *75*, 615-630.
- Grudnik, P., Bange, G., and Sinning, I. (2009). Protein targeting by the signal recognition particle. *Biol Chem* *390*, 775-782.
- Gumbart, J., Trabuco, L.G., Schreiner, E., Villa, E., and Schulten, K. (2009). Regulation of the protein-conducting channel by a bound ribosome. *Structure* *17*, 1453-1464.
- Halic, M., and Beckmann, R. (2005). The signal recognition particle and its interactions during protein targeting. *Curr Opin Struct Biol* *15*, 116-125.
- Halic, M., Blau, M., Becker, T., Mielke, T., Pool, M., Wild, K., Sinning, I., and Beckmann, R. (2006). Following the signal sequence from ribosomal tunnel exit to signal recognition particle. *Nature* *444*, 507-511.
- Hamman, B.D., Chen, J.C., Johnson, E.E., and Johnson, A.E. (1997). The aqueous pore through the translocon has a diameter of 40-60 Å during cotranslational protein translocation at the ER membrane. *Cell* *89*, 535-544.
- Houben, E.N., Zarivach, R., Oudega, B., and Luirink, J. (2005). Early encounters of a nascent membrane protein: specificity and timing of contacts inside and outside the ribosome. *J Cell Biol* *170*, 27-35.
- Humphrey, W., Dalke, A., and Schulten, K. (1996). VMD: visual molecular dynamics. *J Mol Graph* *14*, 33-38, 27-38.
- Jaud, S., Fernandez-Vidal, M., Nilsson, I., Meindl-Beinker, N.M., Hubner, N.C., Tobias, D.J., von Heijne, G., and White, S.H. (2009). Insertion of short transmembrane helices by the Sec61 translocon. *Proc Natl Acad Sci U S A* *106*, 11588-11593.
- Kalies, K.U., Stokes, V., and Hartmann, E. (2008). A single Sec61-complex functions as a protein-conducting channel. *Biochim Biophys Acta* *1783*, 2375-2383.
- Katayama, H., Wang, J., Tama, F., Chollet, L., Gogol, E.P., Collier, R.J., and Fisher, M.T. (2010). Three-dimensional structure of the anthrax toxin pore inserted into lipid nanodiscs and lipid vesicles. *Proc Natl Acad Sci U S A*.
- Laemmli, U.K. (1970). Cleavage of structural proteins during the assembly of the head of bacteriophage T4. *Nature* *227*, 680-685.

- Laurinmaki, P.A., Huiskonen, J.T., Bamford, D.H., and Butcher, S.J. (2005). Membrane proteins modulate the bilayer curvature in the bacterial virus Bam35. *Structure* *13*, 1819-1828.
- Lerch-Bader, M., Lundin, C., Kim, H., Nilsson, I., and von Heijne, G. (2008). Contribution of positively charged flanking residues to the insertion of transmembrane helices into the endoplasmic reticulum. *Proc Natl Acad Sci U S A* *105*, 4127-4132.
- Luirink, J., von Heijne, G., Houben, E., and de Gier, J.W. (2005). Biogenesis of inner membrane proteins in *Escherichia coli*. *Annu Rev Microbiol* *59*, 329-355.
- MacKerell, A.D., Bashford, D., Bellott, Dunbrack, R.L., Evanseck, J.D., Field, M.J., Fischer, S., Gao, J., Guo, H., Ha, S., *et al.* (1998). All-Atom Empirical Potential for Molecular Modeling and Dynamics Studies of Proteins, \ddagger . *The Journal of Physical Chemistry B* *102*, 3586-3616.
- Mackerell, A.D., Jr., Feig, M., and Brooks, C.L., 3rd (2004). Extending the treatment of backbone energetics in protein force fields: limitations of gas-phase quantum mechanics in reproducing protein conformational distributions in molecular dynamics simulations. *J Comput Chem* *25*, 1400-1415.
- Marsh, D. (2008). Protein modulation of lipids, and vice-versa, in membranes. *Biochim Biophys Acta* *1778*, 1545-1575.
- Martoglio, B., Hofmann, M.W., Brunner, J., and Dobberstein, B. (1995). The protein-conducting channel in the membrane of the endoplasmic reticulum is open laterally toward the lipid bilayer. *Cell* *81*, 207-214.
- Matsumoto, G., Mori, H., and Ito, K. (1998). Roles of SecE in ATP- and SecA-dependent protein translocation. *Proc Natl Acad Sci U S A* *95*, 13567-13572.
- Menetret, J., Neuhof, A., Morgan, D.G., Plath, K., Radermacher, M., Rapoport, T.A., and Akey, C.W. (2000). The structure of ribosome-channel complexes engaged in protein translocation. *Mol Cell* *6*, 1219-1232.
- Menetret, J.-F., Schaletzky, J., Clemons, Osborne, A., Skanland, S., Denison, C., Gygi, S., Kirkpatrick, D., Park, E., Ludtke, S., *et al.* (2007). Ribosome Binding of a Single Copy of the SecY Complex: Implications for Protein Translocation. *Molecular Cell* *28*, 1083-1092.
- Menetret, J.F., Hegde, R.S., Aguiar, M., Gygi, S.P., Park, E., Rapoport, T.A., and Akey, C.W. (2008). Single copies of Sec61 and TRAP associate with a nontranslating mammalian ribosome. *Structure* *16*, 1126-1137.
- Mindell, J.A., and Grigorieff, N. (2003). Accurate determination of local defocus and specimen tilt in electron microscopy. *J Struct Biol* *142*, 334-347.

Mitra, K., Schaffitzel, C., Shaikh, T., Tama, F., Jenni, S., Brooks, C.L., 3rd, Ban, N., and Frank, J. (2005). Structure of the *E. coli* protein-conducting channel bound to a translating ribosome. *Nature* *438*, 318-324.

Murphy, C.K., and Beckwith, J. (1994). Residues essential for the function of SecE, a membrane component of the *Escherichia coli* secretion apparatus, are located in a conserved cytoplasmic region. *Proc Natl Acad Sci U S A* *91*, 2557-2561.

Nath, A., Atkins, W.M., and Sligar, S.G. (2007). Applications of phospholipid bilayer nanodiscs in the study of membranes and membrane proteins. *Biochemistry* *46*, 2059-2069.

Ng, D.T., Brown, J.D., and Walter, P. (1996). Signal sequences specify the targeting route to the endoplasmic reticulum membrane. *J Cell Biol* *134*, 269-278.

Nishiyama, K., Ikegami, A., Moser, M., Schiltz, E., Tokuda, H., and Muller, M. (2006). A derivative of lipid A is involved in signal recognition particle/SecYEG-dependent and -independent membrane integrations. *J Biol Chem* *281*, 35667-35676.

Nishiyama, K., and Tokuda, H. (2009). Development of a functional in vitro integration system for an integral membrane protein, SecG. *Biochem Biophys Res Commun* *390*, 920-924.

Osborne, A.R., and Rapoport, T.A. (2007). Protein translocation is mediated by oligomers of the SecY complex with one SecY copy forming the channel. *Cell* *129*, 97-110.

Panzner, S., Dreier, L., Hartmann, E., Kostka, S., and Rapoport, T.A. (1995). Posttranslational protein transport in yeast reconstituted with a purified complex of Sec proteins and Kar2p. *Cell* *81*, 561-570.

Parlitz, R., Eitan, A., Stjepanovic, G., Bahari, L., Bange, G., Bibi, E., and Sinning, I. (2007). *Escherichia coli* signal recognition particle receptor FtsY contains an essential and autonomous membrane-binding amphipathic helix. *J Biol Chem* *282*, 32176-32184.

Patargias, G., Bond, P.J., Deol, S.S., and Sansom, M.S. (2005). Molecular dynamics simulations of GlpF in a micelle vs in a bilayer: conformational dynamics of a membrane protein as a function of environment. *J Phys Chem B* *109*, 575-582.

Pettersen, E.F., Goddard, T.D., Huang, C.C., Couch, G.S., Greenblatt, D.M., Meng, E.C., and Ferrin, T.E. (2004). UCSF Chimera--a visualization system for exploratory research and analysis. *J Comput Chem* *25*, 1605-1612.

Phillips, J.C., Braun, R., Wang, W., Gumbart, J., Tajkhorshid, E., Villa, E., Chipot, C., Skeel, R.D., Kale, L., and Schulten, K. (2005). Scalable molecular dynamics with NAMD. *J Comput Chem* *26*, 1781-1802.

- Prinz, A., Behrens, C., Rapoport, T.A., Hartmann, E., and Kalies, K.U. (2000). Evolutionarily conserved binding of ribosomes to the translocation channel via the large ribosomal RNA. *Embo J* 19, 1900-1906.
- Rapoport, T.A. (2007). Protein translocation across the eukaryotic endoplasmic reticulum and bacterial plasma membranes. *Nature* 450, 663-669.
- Raunser, S., and Walz, T. (2009). Electron crystallography as a technique to study the structure on membrane proteins in a lipidic environment. *Annu Rev Biophys* 38, 89-105.
- Reichow, S.L., and Gonen, T. (2009). Lipid-protein interactions probed by electron crystallography. *Curr Opin Struct Biol* 19, 560-565.
- Sambrook, and Russell (2001). *Molecular Cloning: A Laboratory Manual* (3rd ed.). Cold Spring Harbor Laboratory Press.
- Sansom, M.S., Bond, P.J., Deol, S.S., Grottesi, A., Haider, S., and Sands, Z.A. (2005). Molecular simulations and lipid-protein interactions: potassium channels and other membrane proteins. *Biochem Soc Trans* 33, 916-920.
- Schlunzen, F., Wilson, D.N., Tian, P., Harms, J.M., McInnes, S.J., Hansen, H.A., Albrecht, R., Buerger, J., Wilbanks, S.M., and Fucini, P. (2005). The binding mode of the trigger factor on the ribosome: implications for protein folding and SRP interaction. *Structure* 13, 1685-1694.
- Scotti, P.A., Urbanus, M.L., Brunner, J., de Gier, J.W., von Heijne, G., van der Does, C., Driessen, A.J., Oudega, B., and Luirink, J. (2000). YidC, the Escherichia coli homologue of mitochondrial Oxa1p, is a component of the Sec translocase. *Embo J* 19, 542-549.
- Scotti, P.A., Valent, Q.A., Manting, E.H., Urbanus, M.L., Driessen, A.J., Oudega, B., and Luirink, J. (1999). SecA is not required for signal recognition particle-mediated targeting and initial membrane insertion of a nascent inner membrane protein. *J Biol Chem* 274, 29883-29888.
- Seidelt, B., Innis, C.A., Wilson, D.N., Gartmann, M., Armache, J.P., Villa, E., Trabuco, L.G., Becker, T., Mielke, T., Schulten, K., *et al.* (2009). Structural Insight into Nascent Polypeptide Chain-Mediated Translational Stalling. *Science*.
- Shan, S.O., and Walter, P. (2005). Co-translational protein targeting by the signal recognition particle. *FEBS Lett* 579, 921-926.
- Shih, A.Y., Denisov, I.G., Phillips, J.C., Sligar, S.G., and Schulten, K. (2005). Molecular dynamics simulations of discoidal bilayers assembled from truncated human lipoproteins. *Biophys J* 88, 548-556.
- Simon, S.M., and Blobel, G. (1991). A protein-conducting channel in the endoplasmic reticulum. *Cell* 65, 371-380.

- Soding, J., Biegert, A., and Lupas, A.N. (2005). The HHpred interactive server for protein homology detection and structure prediction. *Nucleic Acids Res* 33, W244-248.
- Tilley, S.J., Orlova, E.V., Gilbert, R.J., Andrew, P.W., and Saibil, H.R. (2005). Structural basis of pore formation by the bacterial toxin pneumolysin. *Cell* 121, 247-256.
- Trabuco, L.G., Villa, E., Mitra, K., Frank, J., and Schulten, K. (2008). Flexible fitting of atomic structures into electron microscopy maps using molecular dynamics. *Structure* 16, 673-683.
- Tsukazaki, T., Mori, H., Fukai, S., Ishitani, R., Mori, T., Dohmae, N., Perederina, A., Sugita, Y., Vassylyev, D.G., Ito, K., *et al.* (2008). Conformational transition of Sec machinery inferred from bacterial SecYE structures. *Nature* 455, 988-991.
- Urbanus, M.L., Scotti, P.A., Froderberg, L., Saaf, A., de Gier, J.W., Brunner, J., Samuelson, J.C., Dalbey, R.E., Oudega, B., and Luirink, J. (2001). Sec-dependent membrane protein insertion: sequential interaction of nascent FtsQ with SecY and YidC. *EMBO Rep* 2, 524-529.
- Van den Berg, B., Clemons, W.M., Jr., Collinson, I., Modis, Y., Hartmann, E., Harrison, S.C., and Rapoport, T.A. (2004). X-ray structure of a protein-conducting channel. *Nature* 427, 36-44. Epub 2003 Dec 2003.
- van der Does, C., de Keyzer, J., van der Laan, M., and Driessen, A.J. (2003). Reconstitution of purified bacterial preprotein translocase in liposomes. *Methods Enzymol* 372, 86-98.
- van der Laan, M., Houben, E.N., Nouwen, N., Luirink, J., and Driessen, A.J. (2001). Reconstitution of Sec-dependent membrane protein insertion: nascent FtsQ interacts with YidC in a SecYEG-dependent manner. *EMBO Rep* 2, 519-523.
- van der Laan, M., Nouwen, N., and Driessen, A.J. (2004). SecYEG proteoliposomes catalyze the Deltaphi-dependent membrane insertion of FtsQ. *J Biol Chem* 279, 1659-1664.
- van der Sluis, E.O., Nouwen, N., and Driessen, A.J. (2002). SecY-SecY and SecY-SecG contacts revealed by site-specific crosslinking. *FEBS Lett* 527, 159-165.
- Van Voorst, F., and De Kruijff, B. (2000). Role of lipids in the translocation of proteins across membranes. *Biochem J* 347 Pt 3, 601-612.
- von Heijne, G. (1986). The distribution of positively charged residues in bacterial inner membrane proteins correlates with the trans-membrane topology. *EMBO J* 5, 3021-3027.
- Wagenknecht, T., Grassucci, R., and Frank, J. (1988). Electron microscopy and computer image averaging of ice-embedded large ribosomal subunits from *Escherichia coli*. *J Mol Biol* 199, 137-147.

- Wang, L., and Sigworth, F.J. (2009). Structure of the BK potassium channel in a lipid membrane from electron cryomicroscopy. *Nature* *461*, 292-295.
- Weiche, B., Burk, J., Angelini, S., Schiltz, E., Thumfart, J.O., and Koch, H.G. (2008). A cleavable N-terminal membrane anchor is involved in membrane binding of the *Escherichia coli* SRP receptor. *J Mol Biol* *377*, 761-773.
- White, S.H., and von Heijne, G. (2008). How translocons select transmembrane helices. *Annu Rev Biophys* *37*, 23-42.
- Wild, K., Halic, M., Sinning, I., and Beckmann, R. (2004). SRP meets the ribosome. *Nat Struct Mol Biol* *11*, 1049-1053.
- Wu, Z., Wagner, M.A., Zheng, L., Parks, J.S., Shy, J.M., 3rd, Smith, J.D., Gogonea, V., and Hazen, S.L. (2007). The refined structure of nascent HDL reveals a key functional domain for particle maturation and dysfunction. *Nat Struct Mol Biol* *14*, 861-868.
- Zimmer, J., Nam, Y., and Rapoport, T.A. (2008). Structure of a complex of the ATPase SecA and the protein-translocation channel. *Nature* *455*, 936-943.

7. Appendix

FtsQ construct:

MHHHHHHYPYDVPDYASQAALNTRNSEEVSSRRNNGTRLGILFLLTVLTTVLVSGWVV
LGMEDAQRLPLSKLVLTGERHYTRNDDIRQSILALGEPGTFMTQDVNIIQTQIEQRLQH
ARLDKPGARHPCWP

FtsQ construct forward primer:

5' – tta tac gac tca cta tag gga aaa gaa aat aag gag gtt cct tca tgc atc atc atc atc att acc
cat acg atg ttc cag att acg ctt cgc agg ctg ctg tga aca cgc gaa aca gcg -3'

FtsQ construct reverse primer:

5' – agg gcc agc acg gat gcc ttg cgc ctg gct tat cca gac ggg cgt gct gct gaa ggc gtt gtt cta tt
gcg -3'

Supplementary Table 1: Ribosome-SecY interactions

SecY residue		Ribosome residue		Interaction
Arg243	SecY L6/7	Gln38	(L29)	H-bond
Arg243	SecY L6/7	Ura62	(23S)	hydrophilic
Arg243	SecY L6/7	Ade63	(23S)	hydrophilic
Val245	SecY L6/7	Gua93	(23S)	H-bond
Val246	SecY L6/7	Ura62	(23S)	H-bond
Val246	SecY L6/7	Ade63	(23S)	hydrophobic
Asn247	SecY L6/7	Ade63	(23S)	H-bond
Tyr248	SecY L6/7	Lys46	(L24)	hydrophobic (weak)
Tyr248	SecY L6/7	Val48	(L24)	hydrophobic
Tyr248	SecY L6/7	Ade482	(23S)	hydrophilic (weak)
Arg251	SecY L6/7	Ade492	(23S)	H-bond
Arg251	SecY L6/7	Gua493	(23S)	H-bond
Gln252	SecY L6/7	Ade507	(23S)	H-bond
Gln253	SecY L6/7	Gua493	(23S)	hydrophilic
Gln253	SecY L6/7	Ade507	(23S)	H-bond
Gln253	SecY L6/7	Ade508	(23S)	hydrophilic
Arg255	SecY L6/7	Cyt1335	(23S)	hydrophilic
Arg256	SecY L6/7	Gln72	(L23)	H-bond
Arg256	SecY L6/7	Ade64	(23S)	H-bond
Tyr258	SecY L6/7	Cyt1335	(23S)	H-bond
Lys348	SecY L8/9	Gua1317	(23S)	H-bond
Lys348	SecY L8/9	Ura1318	(23S)	hydrophilic
Phe352	SecY L8/9	Cyt1335	(23S)	H-bond
Val353	SecY L8/9	Ade1336	(23S)	H-bond
Ile356	SecY L8/9	Ura1316	(23S)	H-bond
Ile356	SecY L8/9	Gua1337	(23S)	H-bond
Ile356	SecY L8/9	Ade1392	(23S)	hydrophobic
Arg357	SecY L8/9	Ura1316	(23S)	H-bond
Arg357	SecY L8/9	Gua1317	(23S)	H-bond
Arg357	SecY L8/9	Ade1392	(23S)	H-bond
Glu360	SecY L8/9	Ade1535	(23S)	H-bond
Tyr365	SecY L8/9	Asp94	(L23)	hydrophilic
Tyr429	SecY C-term.	Ala50	(L24)	hydrophobic
Ser431	SecY C-term.	Cyt490	(23S)	hydrophilic
Lys434	SecY C-term.	Cyt1320	(23S)	H-bond
Asn437	SecY C-term.	Cyt1319	(23S)	H-bond
Asn437	SecY C-term.	Cyt1330	(23S)	hydrophilic
Lys439	SecY C-term.	Gua1317	(23S)	hydrophilic
Lys439	SecY C-term.	Ura1318	(23S)	H-bond
Lys439	SecY C-term.	Gua1331	(23S)	H-bond
Tyr441	SecY C-term.	Gua1317	(23S)	H-bond
Gly442	SecY C-term.	Ura1316	(23S)	H-bond
Arg243	SecY L6/7	Gln38	(L29)	H-bond
Arg243	SecY L6/7	Ura62	(23S)	hydrophilic
Arg243	SecY L6/7	Ade63	(23S)	hydrophilic
Val245	SecY L6/7	Gua93	(23S)	H-bond

Supplementary Table 2: Ribosome-SecE interactions

SecE residue		Ribosome residue		Interaction
Arg12	SecE N-term.	Glu24	(L29)	H-bond
Leu14	SecE N-term.	Leu37	(L29)	hydrophobic
Glu15	SecE N-term.	Asn27	(L29)	hydrophilic
Glu15	SecE N-term.	Gln31	(L29)	hydrophilic
Gly65	SecE amphi.	Glu100	(L23)	H-bond
Lys66	SecE amphi.	Glu52	(L23)	H-bond
Lys66	SecE amphi.	Glu100	(L23)	H-bond
Arg73	SecE amphi.	Glu89	(L23)	H-bond/hydrophilic
Glu74	SecE amphi.	Gln91	(L23)	H-bond
Arg76	SecE amphi.	Phe95	(L23)	H-bond
Thr77	SecE amphi.	Leu93	(L23)	H-bond
Lys81	SecE amphi.	Gln36	(L29)	hydrophilic (weak)
Lys81	SecE amphi.	Asp94	(L23)	H-bond
Trp84	SecE amphi.	Leu37	(L29)	hydrophobic

Supplementary Table 3: NC-ribosome-SecY interactions

NC residue		Ribosome/SecY residue		Interaction
Gln104	NC	Arg84	(L22)	H-bond
Arg102	NC	Cyt1323	(23S)	hydrophilic
Arg102	NC	Ade1322	(23S)	hydrophilic
Arg102	NC	Ade508	(23S)	hydrophilic
Gln101	NC	Ade1322	(23S)	H-bond
Gln101	NC	His70	(L23)	Hydrophilic
Glu100	NC	Ade508	(23S)	H-bond
Glu100	NC	Gln253	SecY L6/7	H-bond
Ile99	NC	Ade1321	(23S)	hydrophobic
Ile99	NC	Ade1321	(23S)	H-bond
Gln98	NC	Ade1321	(23S)	H-bond
Gln98	NC	Ade492	(23S)	hydrophilic
Gln98	NC	Gua491	(23S)	H-bond
Gln96	NC	Ade492	(23S)	H-bond
Gln96	NC	Gua491	(23S)	H-bond
Ile95	NC	Ala432	SecY C-term.	hydrophobic
Ile94	NC	Tyr258	SecY L6/7	hydrophobic
Val92	NC	Ala432	SecY C-term.	hydrophobic
Val92	NC	Ala50	(L24)	hydrophobic
Asp91	NC	Thr263	SecY L6/7	hydrophilic (weak)
Asp91	NC	Arg242	SecY L6/7	hydrophilic
Asp91	NC	Pro49	(L24)	H-bond
Gln90	NC	Glu430	SecY C-term.	hydrophilic
Met88	NC	Pro339	SecY L8/9	hydrophobic
Met88	NC	Leu265	SecY L6/7	hydrophobic
Phe87	NC	Val274	SecY TM7	hydrophobic
Phe87	NC	Asn270	SecY L6/7	H-bond
Phe87	NC	Val234	SecY TM6	hydrophobic
Phe87	NC	Phe233	SecY TM6	hydrophobic

Supplementary Table 4: NC-SecY interactions

NC residue		SecY residue		Interaction
Glu83	NC	Ile275	SecY TM7	H-bond
Gly82	NC	Ile275	SecY TM7	H-bond
Gly82	NC	Asn185	SecY TM5	H-bond
Leu81	NC	Ile90	SecY TM2	hydrophobic
Leu81	NC	Ile275	SecY TM7	hydrophobic
Leu81	NC	Ala277	SecY TM7	H-bond
Leu81	NC	Pro276	SecY TM7	H-bond (weak)
Leu81	NC	Ile86	SecY TM2	hydrophobic
Ala80	NC	Ile278	SecY TM7	hydrophobic
Ala80	NC	Ile86	SecY TM2	H-bond (weak)
Ala80	NC	Ile86	SecY TM2	hydrophobic (weak)
Ala80	NC	Ile82	SecY TM2	hydrophobic
Leu79	NC	Ile408	SecY TM10	hydrophobic
Leu79	NC	Ile278	SecY TM7	H-bond (weak)
Leu79	NC	Ile195	SecY TM5	hydrophobic
Leu79	NC	Ile191	SecY TM5	hydrophobic
Leu79	NC	Tyr85	SecY TM2	hydrophobic
Leu79	NC	Ala79	SecY TM2	hydrophobic
Ile78	NC	Ile82	SecY TM2	hydrophobic
Ile78	NC	Gly81	SecY TM2	H-bond
Ser77	NC	Gly81	SecY TM2	H-bond (weak)
Ser77	NC	Ile77	SecY TM2	H-bond
Ser77	NC	Ser76	SecY TM2	H-bond
Ser77	NC	Arg74	SecY TM2	H-bond (weak)
Gln76	NC	Gly81	SecY TM2	H-bond
Gln76	NC	Arg74	SecY TM2	hydrophilic
Gln76	NC	Ser73	SecY TM2	hydrophilic
Arg75	NC	Arg74	SecY TM2	H-bond (weak)
Ile74	NC	Pro143	SecY TM3	hydrophobic
Ile74	NC	Arg74	SecY TM2	H-bond
Asp73	NC	Ser76	SecY TM2	H-bond
Asp73	NC	Lys51	SecY TM1	H-bond
Asp72	NC	Ser76	SecY TM2	H-bond (weak)
Asn71	NC	Ile77	SecY TM2	H-bond (weak)
Asn71	NC	Gln56	SecY TM1	H-bond

Supplementary Table 5: SA-SecY interactions

SA residue		SecY residue		Interaction
Thr23	SA	Val98	SecY TM2b	H-bond
Thr23	SA	Val336	SecY TM8	H-bond
Leu25	SA	Ile275	SecY TM7	hydrophobic
Ala26	SA	Leu94	SecY TM2b	hydrophobic
Ile28	SA	Phe328	SecY TM8	hydrophobic
Ile28	SA	Tyr332	SecY TM8	hydrophobic
Leu29	SA	Ile90	SecY TM2b	hydrophobic
Leu29	SA	Gln93	SecY TM2b	H-bond
Leu29	SA	Ile275	SecY TM7	hydrophobic
Phe30	SA	Met83	SecY TM2b	hydrophobic
Phe30	SA	Ile86	SecY TM2b	hydrophobic
Phe30	SA	Ile90	SecY TM2b	hydrophobic
Leu32	SA	Ile325	SecY TM8	hydrophobic
Val34	SA	Ile86	SecY TM2b	hydrophobic
Thr36	SA	Ser282	SecY TM7	H-bond
Thr37	SA	Ile82	SecY TM2b	H-bond (weak)
Leu39	SA	Ser282	SecY TM7	H-bond
Leu39	SA	Phe286	SecY TM7	hydrophobic
Val40	SA	Phe64	SecY TM2	hydrophobic
Val40	SA	Phe67	SecY TM2	hydrophobic
Trp43	SA	Phe64	SecY TM2	hydrophobic
Trp43	SA	Phe286	SecY TM7	hydrophobic
Trp43	SA	Phe286	SecY TM7	H-bond
Trp43	SA	Ile290	SecY TM7	hydrophobic
Trp43	SA	Phe294	SecY TM7	hydrophobic
Val44	SA	Phe64	SecY TM2	hydrophobic
Val44	SA	Gly70	SecY TM2	H-bond
Val45	SA	Leu72	SecY TM2	hydrophobic (weak)
Leu46	SA	Phe294	SecY TM7	hydrophobic
Trp48	SA	Asn65	SecY TM2	H-bond
Trp48	SA	Ala71	SecY TM2	hydrophobic
Trp48	SA	Ala71	SecY TM2	H-bond (weak)
Trp48	SA	Leu72	SecY TM2	hydrophobic
Met49	SA	Ile61	SecY TM2	hydrophobic

8. Acknowledgements

Mein erster Dank gilt Prof. Dr. Roland Beckmann, für die interessante Themenstellung, die Betreuung dieser Arbeit, große Forschungsfreiheiten, seine Unterstützung bei der Bewerbung für Stipendien und Konferenzen, für hervorragende Forschungsbedingungen und seinen Enthusiasmus. Für die Begutachtung dieser Arbeit möchte ich mich auch bei Prof. Dr. Karl-Peter Hopfner bedanken.

Einen großen Dank möchte ich auch dem Boehringer Ingelheim Fonds aussprechen, hierbei insbesondere Dr. Claudia Walther, Monika Beutelspacher, Dr. Sabine Achten und Dr. Hermann Fröhlich, sowohl für die finanzielle Unterstützung meiner Arbeit, insbesondere aber auch für die persönliche Betreuung und Weiterbildung.

Besonders bedanken möchte ich mich auch bei Dr. Marco Gartmann, mit ihm gestaltete sich der Laboralltag höchst vergnüglich, überdies hat er das ein oder andere Mal den Cluster gerettet. Auch Dr. Eli van der Sluis gebührt großer Dank, stets hat er ein offenes Ohr gehabt und konnte als Dr. Thunder in vielen biochemischen Fragestellungen weiterhelfen, vor allem aber auch heel erg bedankt voor het corrigeren van mijn scriptie. Dr. Thomas Becker möchte ich für die Einführung in die Kunst des Prozessierens und die vielen guten Ratschläge diesbezüglich danken. Auch Jean-Paul Armache, Birgit Seidelt und Dr. Soledad Funes haben zum Gelingen dieser Arbeit beigetragen.

Für die erfolgreiche Mitarbeit an diesem Projekt möchte ich mich sehr bei Daniela Dirndorfer und Kerstin Anders bedanken. Auch Caroline Haas und Daniel Wacker haben große Hilfe geleistet. Dank gebührt auch Dr. Otto Berninghausen, sowohl was seine Unterstützung in Sachen Mikroskopie anbelangt, insbesondere aber auch für die gemeinsame Entwicklung von großen Theorien. Auch Dr. Daniel Wilson möchte ich für viele anregende Diskussionen danken. Großer Dank gebührt auch Heidi Sieber, Joanna Musial, Charlotte Ungewickell, Timo Weiler und Andrea Gilmozzi, die das

Labor tragen. Für Unterstützung in vielerlei Hinsicht möchte ich mich bei Alexander Jarasch, Dr. Birgitta Beatrix, Andreas Anger, Sibylle Frankenberg und allen Mitgliedern der AG Beckmann und Wilson bedanken.

I would also like to thank Dr. James C. Gumbart and Prof. Dr. Klaus Schulten for the fruitful and productive collaboration regarding the molecular dynamics simulation.

Mein größter Dank gilt Christine, für ihre stetige Unterstützung, Nachsicht und Motivation, und meiner Familie, insbesondere meinen Eltern, die den Grundstein für alles gelegt haben.

9. Curriculum vitae Jens Frauenfeld

Geboren am 28.09.1979 in Mannheim, Staatsangehörigkeit: Deutsch

Ausbildung und Promotion

- 06/2006 - 05/2010 Promotion am GeneCenter der LMU München,
Arbeitsgruppe Prof. Dr. Beckmann
Thema: „The ribosome-SecYEG complex in the membrane environment“
- 08/2005 – 03/2006 Diplomarbeit bei Roche Diagnostics GmbH, Penzberg
Arbeitsgruppe Dr. Erhard Fernholz (Roche) und Dr. Roland Brock (Universität Tübingen)
Thema: Zellfreie Expression und Mutationsstudien einer viralen Reversen Transkriptase
- 07/2004 – 06/2006 Studium der Biochemie (Diplom) an der Universität Tübingen mit den Hauptfächern Biochemie und Organische Chemie
- 09/2003 – 06/2004 Studium der Biochemie an der Université Louis Pasteur und der École Supérieure de Biotechnologie, Strasbourg, Frankreich
- 10/2000 – 06/2003 Studium der Biochemie (Vordiplom) an der Universität Tübingen
- 07/1999 – 06/2000 Zivildienst im Rettungsdienst
- 09/1990 – 06/1999 Ludwig-Frank-Gymnasium, Mannheim
Leistungskurse Mathematik und Chemie

Stipendien und Auszeichnungen

- 11/2009 ROMIUS Förderpreis für Wissenschaft und Forschung (Roche Stiftung)
- 04/2009 Poster-Preis: “Best Science”, <interact2009> Symposium
- 03/2007 – 06/2009 Boehringer-Ingelheim-Stipendium
- 12/2006 Schering-Stipendium
- seit 04/2004 Mentee von Roche Diagnostics bei Mentorin Dr. Dr. Ildiko Amann-Zalan
- seit 01/2002 Stipendiat von e-fellows.net

Konferenzen

- 03/2010 Gordon Research Conference "Protein Transport Across Cell Membranes", Galveston, USA (Poster)
- 09/2009 EMBO course "Image processing for cryo-EM 2009", London (Vortrag)
- 05/2009 Membrane Protein Symposium, Heidelberg (Vortrag)
- 10/2008 EMBO conference "Control of protein targeting and translocation", St. Maxime, Frankreich (Poster)

Publikationen

- 04/2010 "Structure of the ribosome-SecYEG complex in the membrane environment", Frauenfeld et al., (in preparation)
- 03/2007 "Multivalence and spot heterogeneity in microarray-based measurement of binding constants"
Martin Elbs, Michael Hulko, Jens Frauenfeld, Rainer Fischer, Roland Brock
Analytical and Bioanalytical Chemistry 387 (6), 2007